



Durham E-Theses

Some investigations of inorganic and catalytic systems by esca and other spectroscopic

Briggs, David

How to cite:

Briggs, David (1973) *Some investigations of inorganic and catalytic systems by esca and other spectroscopic*, Durham theses, Durham University. Available at Durham E-Theses Online:
<http://etheses.dur.ac.uk/10512/>

Use policy

The full-text may be used and/or reproduced, and given to third parties in any format or medium, without prior permission or charge, for personal research or study, educational, or not-for-profit purposes provided that:

- a full bibliographic reference is made to the original source
- a [link](#) is made to the metadata record in Durham E-Theses
- the full-text is not changed in any way

The full-text must not be sold in any format or medium without the formal permission of the copyright holders.

Please consult the [full Durham E-Theses policy](#) for further details.

Academic Support Office, Durham University, University Office, Old Elvet, Durham DH1 3HP
e-mail: e-theses.admin@dur.ac.uk Tel: +44 0191 334 6107
<http://etheses.dur.ac.uk>

SOME INVESTIGATIONS OF INORGANIC AND CATALYTIC SYSTEMS
BY ESCA AND OTHER SPECTROSCOPIC TECHNIQUES

By

David Briggs B.Sc.

A thesis submitted to the University of Durham
for the degree of Doctor of Philosophy

May 1973



To Jill and
my parents

MEMORANDUM

The work described in this thesis was carried out in the University of Durham, with periods of time at the I.C.I. Corporate Laboratory - Runcorn, between September 1970 and April 1973. It has not been submitted for any other degree and is the original work of the author except where acknowledged by reference.

Part of the work in this thesis has formed the subject matter of the following publications:

- (i) X-ray photoelectron studies of Platinum and Palladium Complexes; Observation of the trans-Influence and Distinction between Terminal and Bridging chlorine.
D.T. Clark, D.B. Adams and D. Briggs, Chem. Comm., 1971, 602.
- (ii) Surface Layer Isomerisation of a Platinum-Olefin Complex observed by X-ray Photoelectron Spectroscopy.
D.T. Clark and D. Briggs, Nature. Phys. Sci., 237, 15 (1972).
- (iii) ESCA Studies of Square-planar Platinum Complexes; Correlations with Nuclear Quadrupole Resonance Studies.
D.T. Clark, D. Briggs and D.B. Adams, J.C.S. (Dalton), 1973, 169.
- (iv) Hydrogenation of Ethylene on Supported Platinum.
D. Briggs and J. Dewing, J. Catalysis, 1973, in press.
- (v) On the Question of Hydrogen Spillover in Ethylene Hydrogenation on Supported Platinum.
D. Briggs, J. Dewing and C.J. Jones, J. Catalysis, 1973, in press.

ACKNOWLEDGEMENTS

To my two supervisors - Dr D.T. Clark of the University of Durham and Dr J. Dewing of the I.C.I. Corporate Laboratory (Runcorn) I extend my sincere gratitude for their unfailing help and enthusiasm. I am indebted to I.C.I. Ltd. for their generous financial support and to S.R.C. for provision of equipment.

I particularly wish to thank the following for their invaluable assistance: Dr's. H.R. Keable and M. Kilner (preparation of organo-nitrogen metal carbonyl complexes and helpful discussion), my colleagues Dr D. Kilcast and Mr D.B. Adams (all of the University of Durham); Dr J.D. Jones (preparation of chloro-olefin/vinyl complexes and helpful discussion), Mrs C.J. Jones (mass spectroscopy), Mr G.T. Monks (i.r. spectroscopy) and Dr's. W.R. Patterson and G.L. Price (for helpful discussions) (all of the I.C.I. Corporate Laboratory - Runcorn).

Thanks are also due to the analytical staff of both the above mentioned institutions and to Mr A.J. Cunningham (I.C.I. Mond Division) for his help with computer programming.

Some of the platinum complexes studied were kindly supplied by Professor F.G.A. Stone and Dr P.L. Goggin of the University of Bristol.

D. Briggs
Durham 1973

ABSTRACT

X-ray photoelectron spectroscopy (ESCA) has been used to study platinum complexes, structural and bonding effects in complexes of the type $(R_3P)_2PtXY$ have been investigated, bridging and terminal chlorines in dimeric complexes, $L_2Pt_2Cl_4$, have been distinguished and a correlation found between Cl2p binding energies and ^{35}Cl n.q.r. frequencies in square-planar Pt-Cl complexes.

At ambient temperature the complex $(Ph_3P)_2Pt(C_2Cl_4)$ has been found to undergo layer isomerisation to $(Ph_3P)_2PtCl(CCl = CCl_2)$. Using infrared spectroscopy, differences between surface and bulk effects have been followed and confirmed for related complexes. Isomerisation could be arrested by studying the olefin complex at $-110^\circ C$.

Some complexes of the methyleneamino ($R_2C:N-$) and aza-allyl/allene (R_2CNR_2) ligands with molybdenum and tungsten carbonyl derivatives have been studied by ESCA to gain further information on their possible bonding modes. A correlation has been found between the metal binding energies and the stretching frequencies of attached carbonyl groups.

In order to acquire information on a Pt/SiO₂ catalyst for eventual ESCA study, background investigations involving kinetic, deuterium addition/exchange and i.r. studies on the H₂-C₂H₄-Pt/SiO₂ system have been performed. Catalyst poisoning has been investigated and eliminated, the reported occurrence of 'hydrogen spillover' has been disproved and the ethylene exchange rate found to be a sensitive

probe of small, but reproducible support effects. The i.r. data obtained goes some way to resolving inconsistencies in the literature.

The same catalyst has been subjected to preliminary ESCA investigation, with especial regard to the state of the metal during preparation and subsequent cleaning treatments. The available vacuum conditions were found to be unsuitable for adsorption studies.

ABBREVIATIONS

BE	Binding Energy
KE	Kinetic Energy
nmr	nuclear magnetic resonance spectroscopy
nqr	nuclear quadrupole resonance spectroscopy
glc	gas-liquid chromatography
m. s.	mass spectroscopy
i. r.	infrared spectroscopy
Me	Methyl, CH_3^-
Et	Ethyl, CH_3CH_2^-
ⁿ Bu	normal Butyl, $\text{CH}_3(\text{CH}_2)_2\text{CH}_2^-$
Ph	Phenyl, C_6H_5^-
vw	very weak
w	weak
m	medium
b	broad

CONTENTS

PART I

	<u>Page</u>
<u>CHAPTER I - Electron Spectroscopy for Chemical Applications (ESCA)</u>	
(i) General Introduction	1
(ii) History and Development	3
(iii) Theory of Electron Spectroscopy	7
(a) Photoionisation Processes	7
(b) Electronic Relaxation Processes	10
(c) Comparison of ESCA and X-ray Spectroscopy	13
(d) Calculation of Binding Energies from ESCA Spectra	14
(e) Relationship Between Energy Levels of Gaseous and Solid Samples	18
(iv) Instrumentation	21
(a) The Source	21
(b) Electron Energy Analysers	24
(c) Detection Systems	28
(d) Data Acquisition	29
(e) Recent Developments	30
(v) Review of ESCA Applications in Inorganic Chemistry	31
<u>CHAPTER II - ESCA Studies of Some Square-Planar Platinum Complexes (I)</u>	
(i) Platinum-Olefin Complexes	37
(a) Introduction	37
(b) Experimental	39

	<u>Page</u>
(c) Results	39
(d) Discussion	40
(e) Satellite Peaks	48
(ii) $(R_3P)_2PtXY$ Complexes	54
(a) Introduction	54
(b) Results and Discussion	54
<u>CHAPTER III - ESCA Studies of Square-Planar Platinum Complexes (II)</u>	
<u>Correlations with N.Q.R. Studies</u>	
(i) N.q.r. Correlations	59
(a) Introduction	59
(b) Experimental	61
(c) Results and Discussion	61
(ii) Zeise's Salt and Related Complexes	68
(a) Introduction	68
(b) Results and Discussion	69
<u>CHAPTER IV - Studies of the Surface Isomerisation of $(Ph_3P)_2Pt(C_2Cl_4)$</u>	
<u>and Related Complexes</u>	
(i) The Surface Isomerisation of $(Ph_3P)_2Pt(C_2Cl_4)$	78
(a) Introduction	78
(b) Experimental	78
(c) Results and Discussion	78
(ii) Surface Isomerisation of $(Ph_3As)_2Pt(C_2Cl_4)$ and $(Ph_3As)_2Pt(C_2HCl_3)$	85
(iii) Attempts to obtain ESCA Spectra of Unisomerised $(Ph_3As)_2Pt(C_2Cl_4)$	91

	<u>Page</u>
(iv) Mechanisms of Isomerisation	94

CHAPTER V - ESCA Studies of Some Transition Metal Carbonyl Complexes
Containing Organo-Nitrogen Ligands

(i) Introduction	97
(ii) Experimental	97
(iii) Results and Discussion	98
(a) Qualitative Discussion	98
(b) Methyleneamino Complexes	102
(c) Aza-allyl/allene Complexes	106

PART II

CHAPTER VI - Some Investigations of the Platinum-Ethylene-Hydrogen System

(i) General Introduction	111
(ii) Kinetic Studies	114
(a) Experimental	114
(b) Description of Experiments and Results	124
(c) Discussion	135
(iii) Mass Spectrometric Studies of Ethylene Deuteration	137
(a) Introduction	137
(b) Experimental	138
(c) Analysis	139
(d) Description of Experiments and Results	140
(e) Discussion	145

	<u>Page</u>
(iv) I.r. Studies of The $C_2H_4-H_2$ -Pt/SiO ₂ System	149
(a) Introduction	149
(b) Experimental	152
(c) Results and Discussion	155
(v) Conclusions	160
<u>CHAPTER VII - ESCA Studies of the Pt/SiO₂ Catalyst</u>	
(i) Introduction	164
(ii) Experimental	165
(iii) Results and Discussion	165
<u>APPENDIX I</u>	172
<u>APPENDIX II</u>	174
<u>REFERENCES</u>	178

All nature is but art, unknown to thee
All chance, direction which thou canst not see,
All discord, harmony not understood,
All partial evil, universal good,
And, spite of pride in erring reason's plight
One truth is clear, whatever is, is right.

Alexander Pope.

PART I

CHAPTER I

ELECTRON SPECTROSCOPY FOR CHEMICAL APPLICATIONS (ESCA)

(i) General Introduction

In electron spectroscopy the BE's of electrons in a molecule are determined by measurement of the energies of electrons ejected by the interactions of the molecule with a monoenergetic beam of exciting radiation. There are essentially three ways to excite electron spectra, namely by X-rays, u.v. light or electrons. There are advantages and also limitations attached to each method.

X-ray excitation has the great advantage that core and valence levels for all atoms can be observed using this radiation (e.g. $MgK\alpha_{1,2} = 1253.6$ eV, $AlK\alpha_{1,2} = 1486.6$ eV) and, furthermore, that not only gases but also solids can be conveniently studied (see below). This technique, particularly utilising soft X-rays, has come to be known as ESCA^{1,2} (Electron Spectroscopy for Chemical Applications) or XPS (X-ray photoelectron spectroscopy).

U.v. excitation has the advantage that much higher resolution can be obtained because of the lower inherent widths of the u.v. lines themselves. The technique is limited to observation of low BE valence and molecular orbitals (exciting energies are usually $He^I = 21.2$ eV and $He^{II} = 40.8$ eV). Until very recently chemical applications of this branch of electron spectroscopy (usually referred to simply as 'photoelectron spectroscopy', PES) have been limited to the study of gases³ although solids have been investigated under uhv conditions for many years by physicists ('photoemission' studies).⁴ The two themes are now converging but will not be further considered here.

Electron excitation, finally, has been extensively used for studying Auger electron spectra (see below) of gases and solids⁵ but cannot, of course, produce ordinary photoelectron spectra. Since the



electron beam can be readily focussed and its energy continuously varied a higher sensitivity can be achieved compared with X-ray excitation but at the cost of a lower signal/background ratio. Although the electron escape depth is not critically dependent on the energy of the exciting radiation the penetration depth for electrons is similar, only a few atomic layers, compared with ca. 10^3 \AA for X-rays. Electron excited Auger spectroscopy is thus ideally suited to surface analysis (especially of metals). The main difficulties are lack of resolution and in interpretation of spectra. There also exists the possibility of using pulse techniques to excite molecules, in situ, by electron bombardment and measure the photoelectron spectra, using lower energy exciting radiation, of the excited states so produced.

Part I of this thesis is concerned with the application of soft X-ray photoelectron spectroscopy (hereafter referred to as ESCA) to studies in inorganic and surface chemistry. The advantages of ESCA for studies in these fields can be summarised as follows:

- a) all elements in the periodic table from Li onwards can be studied with high sensitivity, regardless of any spin properties of the nucleus,
- b) the sample may be a solid, liquid or gas and the technique is essentially non-destructive,
- c) the sample requirement is modest; in favourable cases 1 mgm. of solid, 0.1 μl of liquid, 0.5 cc of gas (at STP) or, in surface work, fractions of a monolayer,
- d) the information obtained is directly related to the electronic structure of a molecule and the theoretical interpretation is relatively straightforward,

- e) information can be obtained on both core and valence levels of molecules,
- f) with commonly used X-ray sources (Mg,Al) the escape depth for photoelectrons is generally in the range 0-50Å, enabling surface effects to be probed.

Since the technique is relatively new to applications in chemistry (the work described herein was carried out with the first available instrument in this country) it is pertinent to discuss the development of ESCA as well as the theory and instrumentation in a little more detail.

(ii) History and Development

The energy distribution of electrons in various elements was first investigated by means of X-ray irradiation of thin foils (producing photoelectrons via the Compton effect) between ~ 1914-25 by Robinson⁶ (in England) and de Broglie⁷ (in France). Energy analysis of the transmitted photoelectrons was performed using a homogeneous magnetic field and the distributions were recorded photographically - a magnetic electron spectrograph. Although the anode material emits a continuous spectrum (bremsstrahlung) there are also characteristic X-ray lines which provide the principle exciting energy (e.g. $K\alpha_{1,2}$ from Mg or Al). Thus electron distributions were obtained which were characterised by long tails with edges at the high energy end. Measurement of these edge positions gave a determination of the energies of the photoelectrons ejected from different atomic shells and hence their binding energies from a knowledge of the energy of the exciting X-ray lines. However, the edge positions were not well defined because the electrons

emerging from the sample (foil) underwent collision processes leading to energy loss (energy absorption by the sample).

Similar data is obtainable from X-ray spectroscopy (absorption and emission); consequently at this stage of research photoelectron spectroscopy was in competition with X-ray spectroscopic methods. The precise relationship between these spectroscopies is discussed below (Section (iii)). In X-ray absorption the primary X-ray beam passes through a thin foil and the absorption spectrum is obtained with an X-ray spectrometer. The observed absorption bands correspond to the excitation of electrons from inner shells to the conduction band and have edge profiles. The data is closely related to that from photoelectron spectroscopy and, until recently, could be obtained more readily and with greater accuracy. X-ray emission spectra are obtained by a primary X-ray beam exciting secondary X-ray emission from the sample since direct emission by electron bombardment leads to decomposition of most chemical compounds. Line spectra are obtained (superimposed on a continuous bremsstrahlung spectrum) from which the energy differences within the atom are obtained with considerable accuracy. BE's are not obtained, however. The combined X-ray spectroscopy was much more successful than contemporary photoelectron spectroscopy, consequently the latter went into recession apart from a few isolated attempts to extend the early work of Robinson and de Broglie.⁸⁻¹²

In connection with studies in nuclear physics in the early 1950's an iron-free magnetic double-focussing electron spectrometer with high resolution properties was developed by Siegbahn and co-workers at Uppsala.¹³ The precision for momentum resolution measured for β -particles

emitted from a radioactive source was within $1:10^{-5}$ (equivalent to a precision of 0.1 eV in the measurement of a peak position in the 10,000 eV region). In 1954 attempts were made, using this instrument, to record, at high resolution, photoelectron spectra produced by X-rays. A new observation then changed the course of future development of the technique. This was the appearance, under high resolution, of a very sharp line which could be resolved from the edge of each electron veil (Fig. 1.1). It was realised that the photoelectrons to which this line corresponded had the important property that they did not suffer energy absorption and, therefore, possessed the BE of the core level from which they arose. The peak position could be measured with considerable precision, to a few tenths of an eV.

It was already known at this time that the positions of emission lines and absorption edges in X-ray spectroscopy were not solely an atomic property but were to a small extent dependent on the chemical state of the atom.^{14,15} However, the chemical effects were difficult to measure accurately and very often difficult to interpret theoretically. Siegbahn and co-workers first studied these chemical effects for copper and its oxides; the value of electron spectroscopy for measurement of chemical 'shifts' was apparent from this work,¹⁶ but its general utility was appreciated only as recently as 1964.^{17,18} The effect is illustrated by the much reproduced, but nevertheless elegant, example in Fig.1.2.

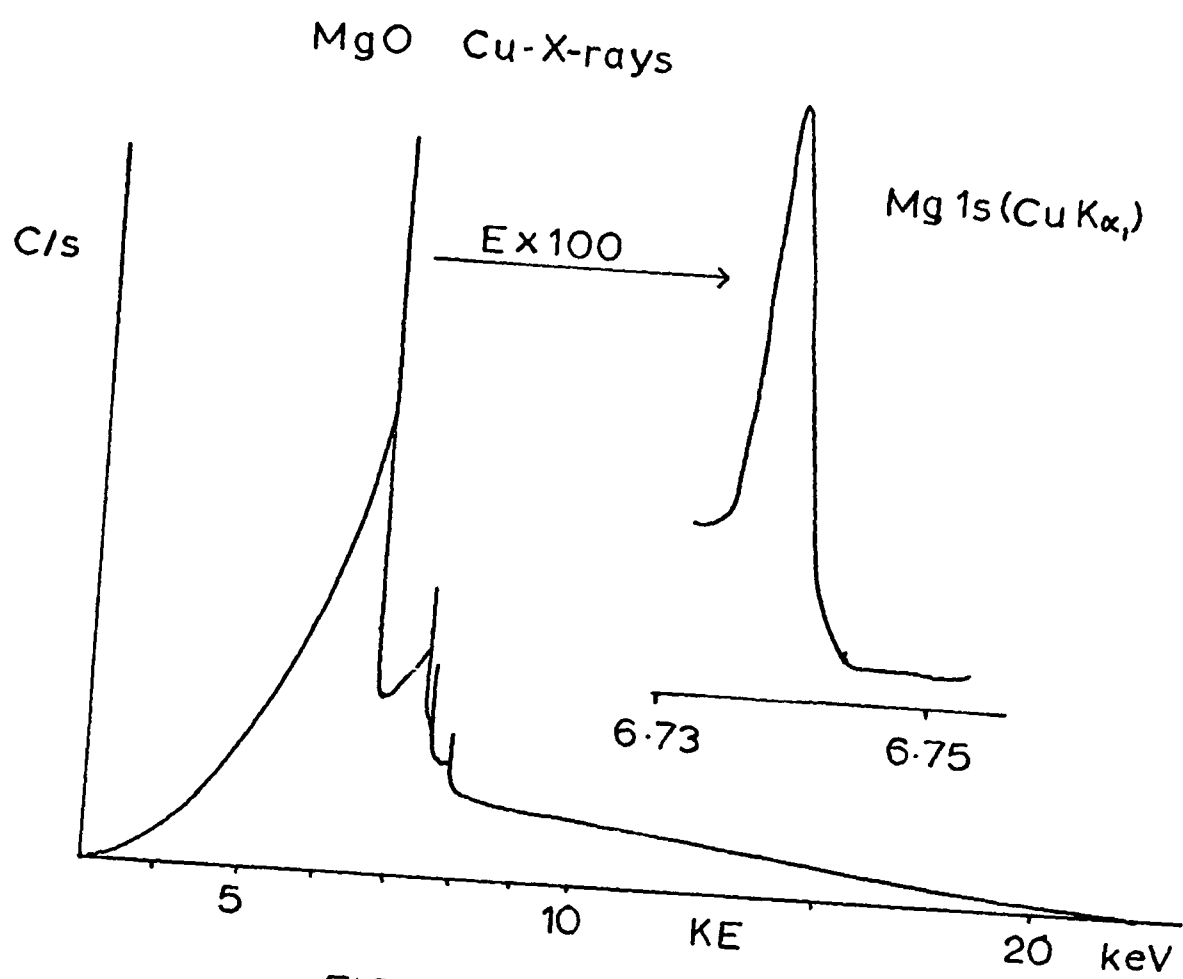


FIGURE 1.1 (after Siegbahn)

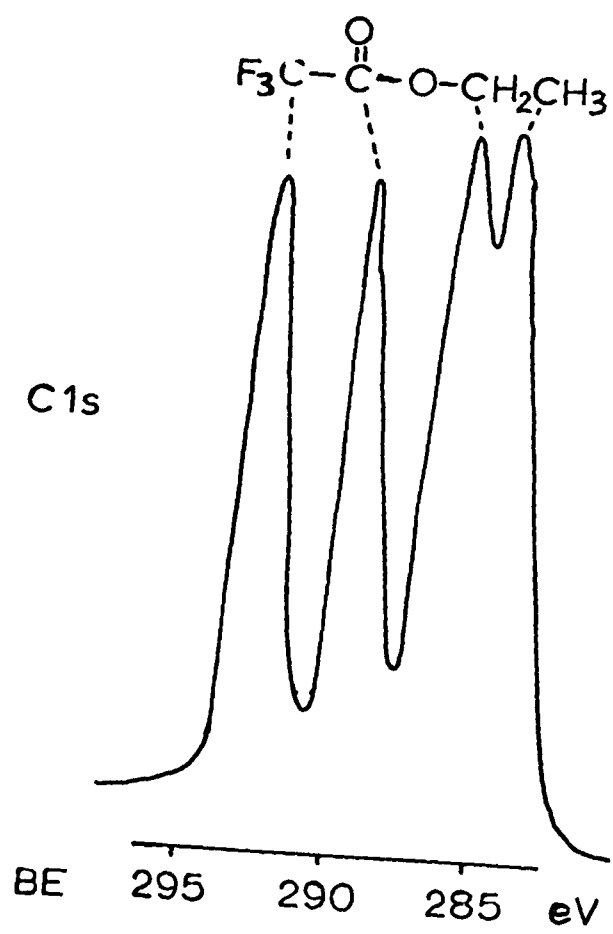


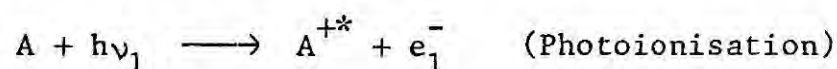
FIGURE 1.2

(iii) Theory of Electron Spectroscopy

This section outlines the theory of electron spectroscopy as it relates to the chemical applications described in the following chapters.

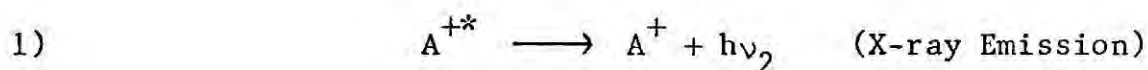
The fundamental processes involved in ESCA are:

Electron Ejection



where ν_1 is the frequency of the exciting X-radiation.

Electronic Relaxation

(a) Photoionisation Processes

The energy level diagram for an electrical insulator is shown in Fig.1.3; this differs from the equivalent diagram for a conducting solid in the position of the Fermi level* which for the latter interfaces the merging valence and conduction bands. The vacuum level

* The Fermi level E_f may be defined by

$$\int_0^{E_f} N(E) dE = N$$

where $N(E) = Z(E)F(E)$ (functions of energy, E), $Z(E)$ is the density of states for fermi particles (electrons in this case) i.e. the number of states (energy levels) between E and $E + \Delta E$, $F(E)$ is the fermi probability distribution; the probability that a fermi particle in a system at thermal equilibrium at temperature T will be in a state with energy E .

$F(E) = 1/e^{(E-E_f)/kT} + 1$ ($kT \ll E_f$). N is the total number of particles in the system. Hence the electrons fill the available states up to the Fermi level.

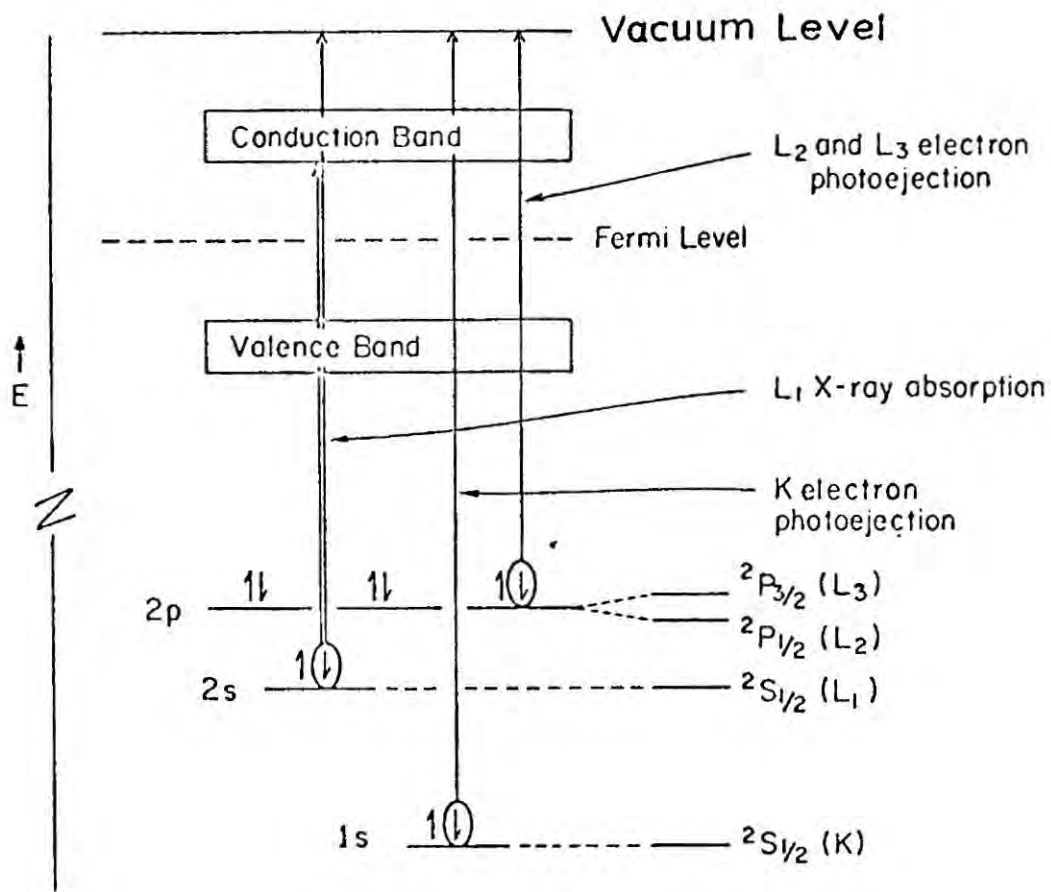


FIGURE 1-3

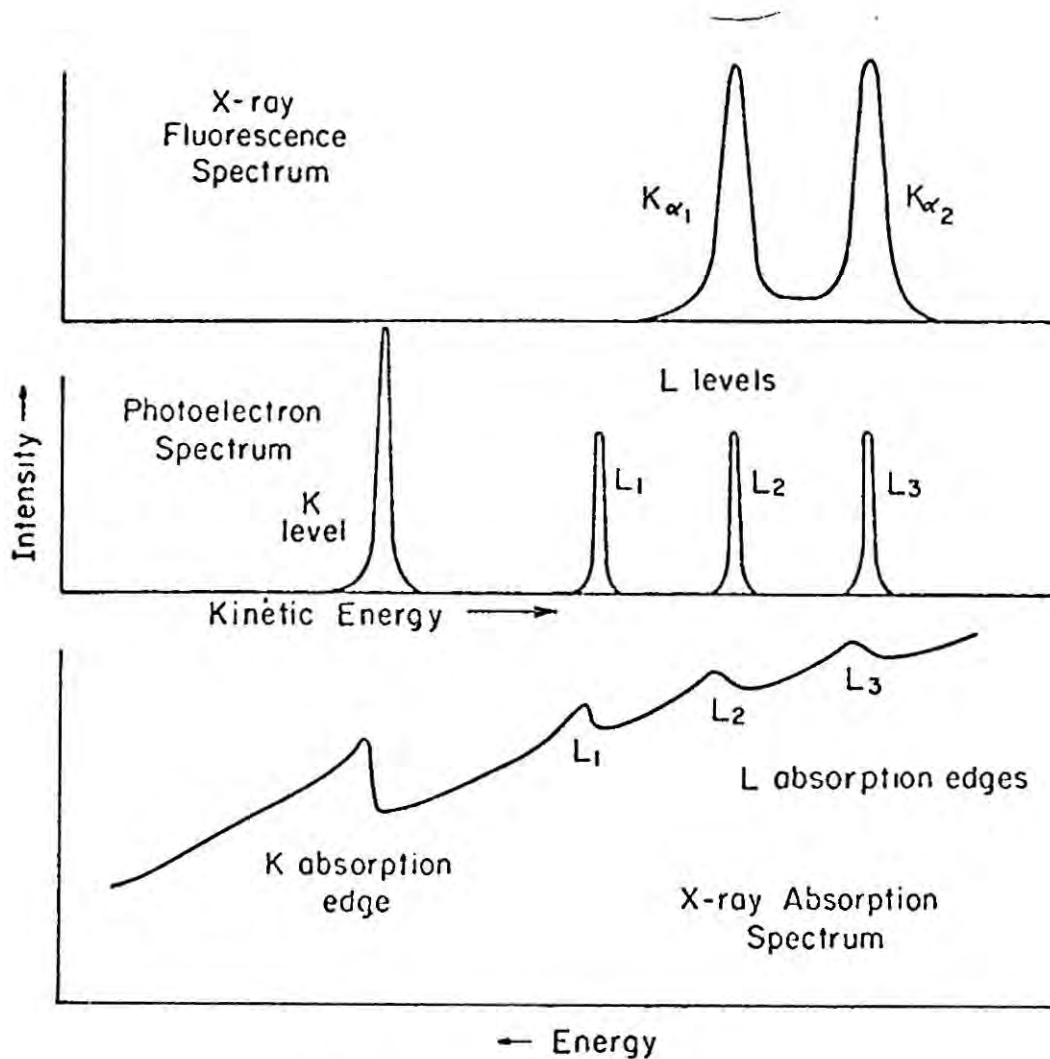


FIGURE 1-4

represents the energy of an electron which has been removed to infinity. In this diagram photoejection is shown for 1s and 2p electrons while X-ray absorption is demonstrated for the 2s electron, showing the low and high energy limits of the transition. The upper energy limit for this transition (the vacuum level) is the same energy as required for photoionisation. Hence, as indicated above, the information contained in binding energy studies from photoelectrons is intrinsically contained in X-ray absorption data although it is much more difficult to extract in the latter case. The relationship between the two types of spectra illustrates these points (Fig.1.4). The photoelectron peaks are designated by the term symbols of the positive hole state left behind. Thus photoejection of the 1s electron leaves a K hole - a $2S_{1/2}$ state.

Photoionisation is not equally probable for all electrons within a given atom or of the same energy level among different atoms. Generally, photoionisation is inversely proportional to r^2 where r is the orbital radius. Hence for light atoms photoionisation of a 2s electron is about 20 times less probable than for the 1s electron. However, orbital radius contraction with increasing nuclear charge (Z) renders this less important as atomic number increases whilst the cross-section for photoionisation from a given core level is approximately proportional Z^3 .

Although for soft X-ray sources core electrons have the highest photoionisation cross-sections, ionisation of outer (valence) electrons can still occur with reasonable probability. Indeed observation of these peaks is important because the cross-section for photoionisation of valence electrons varies in markedly different ways, depending on

the symmetry of the orbital involved, with the energy of the exciting radiation. Hence comparison of ESCA valence peaks with corresponding peaks from PES experiments can give valuable information with regard to orbital symmetry (Fig.1.5).

(b) Electronic Relaxation Processes

Fig.1.6 summarises the electronic relaxation processes for an excited ion with a primary vacancy in the K shell ($2s_{1/2}$ hole state). If an electronic transition from a higher orbital to fill the 1s vacancy occurs new hole states will result (shown on the right of the diagram) together with the emission of excess energy as a photon. The normal $K\alpha$ and $K\beta$ X-ray emission lines are shown as transitions from the 2p and 3d orbitals to the 1s orbital respectively. These represent normal X-ray fluorescence (photoionisation by X-rays) or X-ray emission (electron excitation).

Alternatively the excited ion can relax by Auger electron emission, also shown in Fig.1.6. Auger emission is a radiationless process in which an electron from a higher orbital undergoes a transition to the primary vacancy, the energy being transferred to another electron in one of the outer shells which is ejected from the atom. Two such events are shown in Fig.1.6. In the KLL Auger emission a 2p (L) electron drops to the 1s(K) vacancy while another 2p (L) electron is ejected. In the second case a 3p (M) electron is ejected instead giving a KLM Auger electron emission. When the primary vacancy is created in one of the inner subshells of the L,M ... shells, the excitation energy is often sufficient to bring about a process in which one of the two final vacancies lies in an outer subshell of the

CO

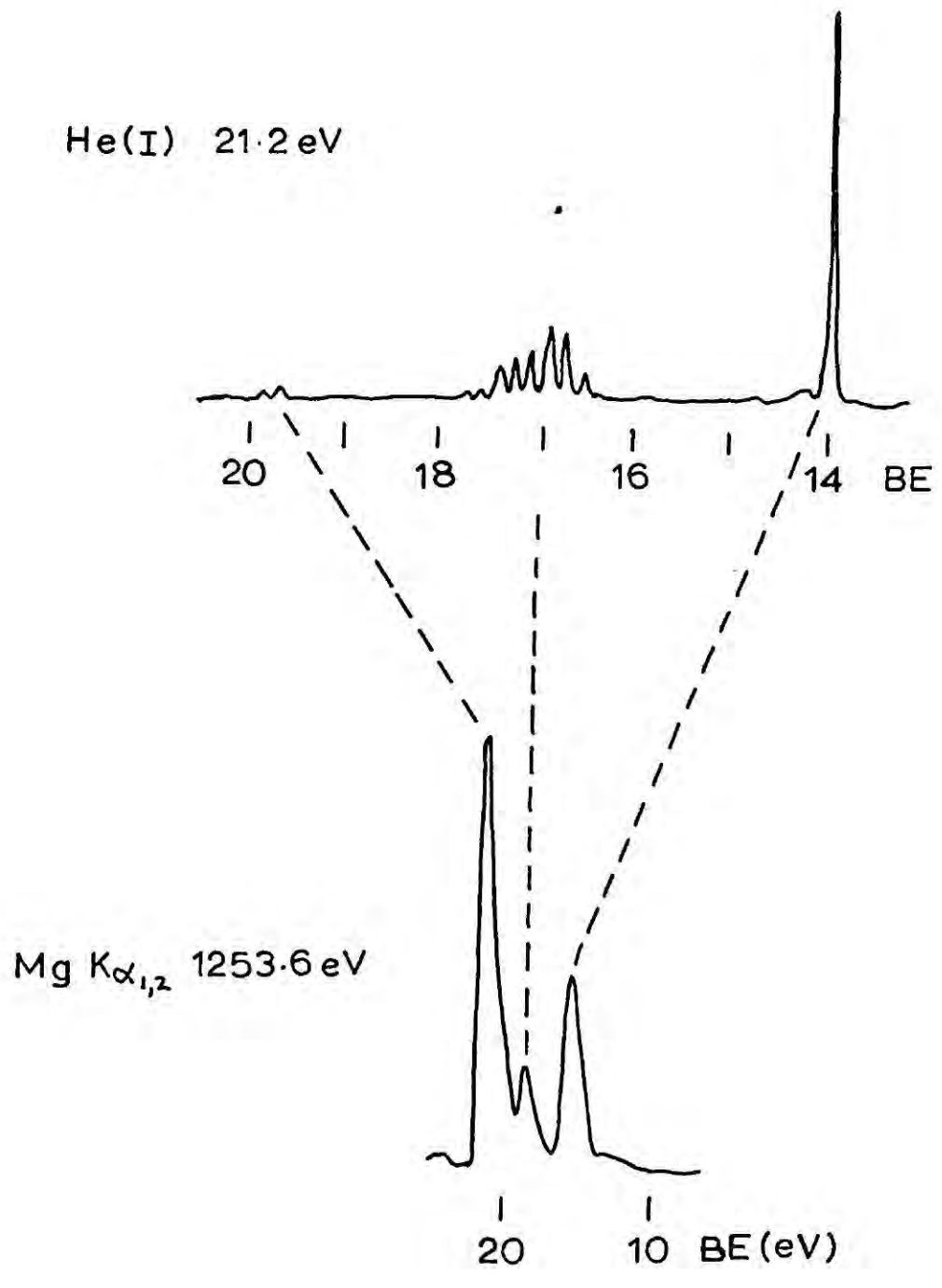


FIGURE 1.5

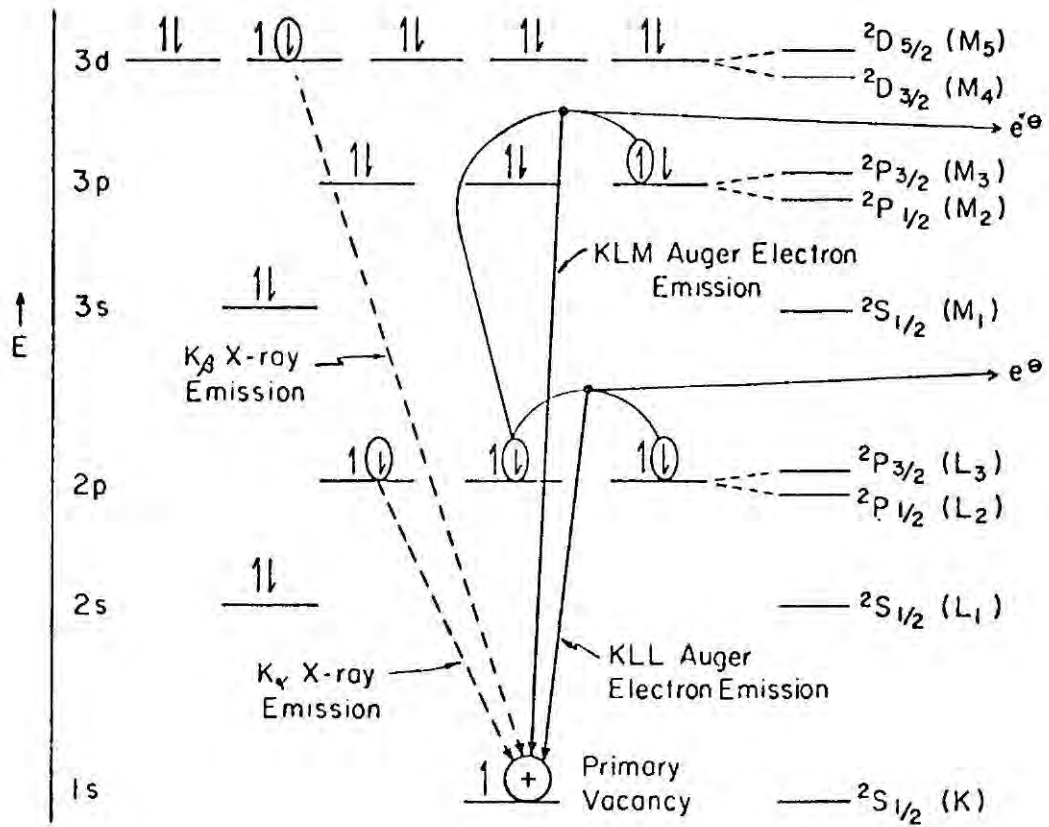


FIGURE 1-6

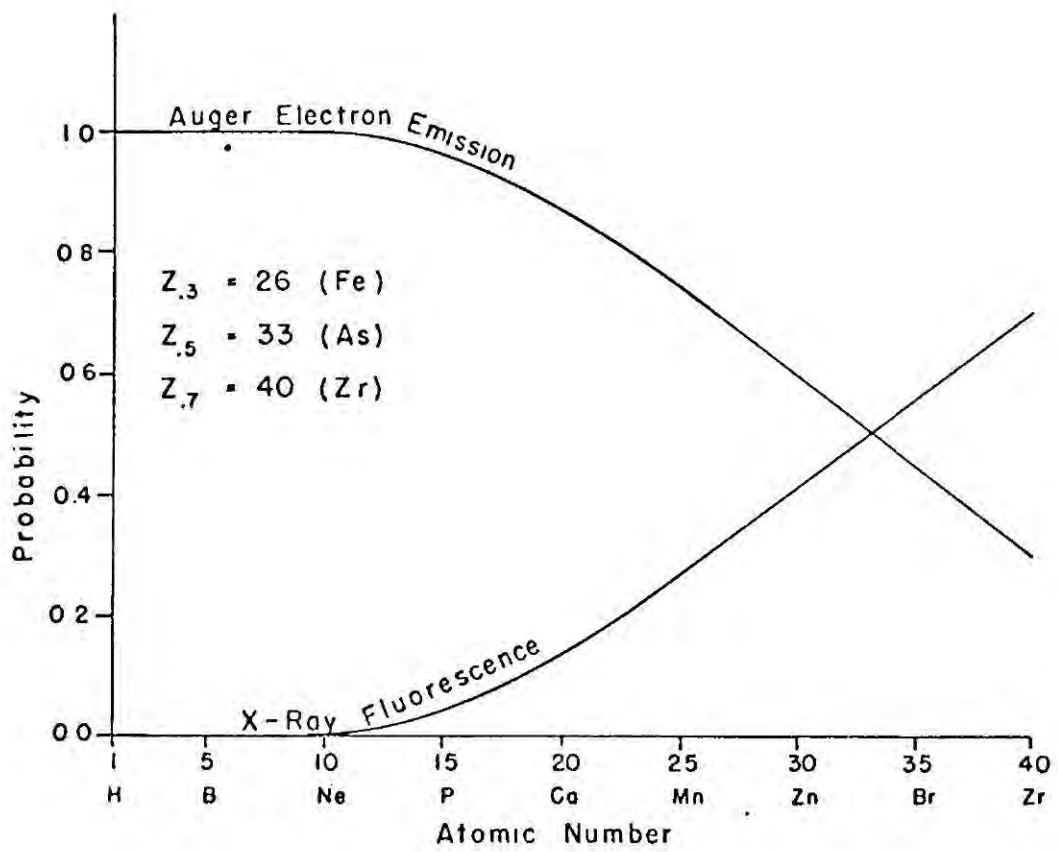


FIGURE 1-7

primary vacancy's shell, e.g. $L_1L_3M_5$. These are called Coster-Kronig transitions.

As shown in Fig.1.7 the radiationless de-excitation of an atom by emission of electrons is often more probable than the radiative de-excitation by X-ray emission. At low atomic numbers the Auger yield is virtually 100% which explains why X-ray fluorescence is not a useful technique for studying light elements. Auger peaks occur in ESCA spectra along with photoelectron peaks but their KE's are independent of the energy of the exciting radiation; this property allows them to be readily identified when there is possible confusion.

(c) Comparison of ESCA and X-ray Spectroscopy

The above discussion of photoionisation and electronic relaxation indicates the relationship between ESCA and X-ray absorption and emission spectroscopy. Referring again to Fig.1.4 and remembering that photoionisation occurs at the upper energy limit of the absorption band the spacing of L and K ESCA peaks should correspond to the spacing of absorption edges in the X-ray spectrum. Similarly, because X-ray fluorescence involves transitions from higher orbitals to the core-hole, spacing of X-ray fluorescence (or emission) lines should also correspond to those in the ESCA spectrum. From Fig.1.4 the $K\alpha_1 - K\alpha_2$ separation should equal the L_2-L_3 ($2p_{1/2}-2p_{3/2}$) separation. In the measurement of BE's and chemical shifts ESCA scores highly over either of these techniques. The advantage of measuring narrow lines rather than ill-defined edges (as in X-ray adsorption) has already been noted, hence ESCA is much more readily applied to the measurement of chemical shifts. Line widths in ESCA are generally narrower than in X-ray fluorescence spectra, hence spacings can be measured with greater

precision. Fig.1.8 compares the $K\alpha_1$ and $K\alpha_2$ emission lines from Cu and the corresponding $2p_{1/2}$, $2p_{3/2}$ lines in an ESCA spectrum using $MgK\alpha$ excitation. The attainable resolution is much higher in the emission experiment than in ESCA but the linewidths are much narrower in the latter spectrum. This is because the emission lines involve two levels, Cu2p and Culs (broad), while the ESCA lines involve only the 2p level.

(d) Calculation of Binding Energies from ESCA spectra

Fig.1.9 is a representation of the relevant energy levels of sample and spectrometer material for calculation of the BE of a core level in the sample. Again the sample is taken to be an electrical insulator and is further assumed to be in electrical contact with the spectrometer so that both have a common Fermi level.

The energy of the incident photon which brings about photo-ionisation of a core electron in the sample is distributed amongst four processes:

- 1) E_b - the binding energy of the core electron relative to the Fermi level of the sample.
- 2) ϕ_s - the work function of the sample; the energy required to promote the electron from the Fermi level to the vacuum level.
- 3) E_r - the recoil energy resulting from conservation of momentum in the photon collision leading to photoionisation.
- 4) E_{kin} - the kinetic energy of the free electron.

Upper limits for recoil energies have been calculated¹ for photo-ejection of a valence electron for Ag, Cu and AlK α excitation (in eV):

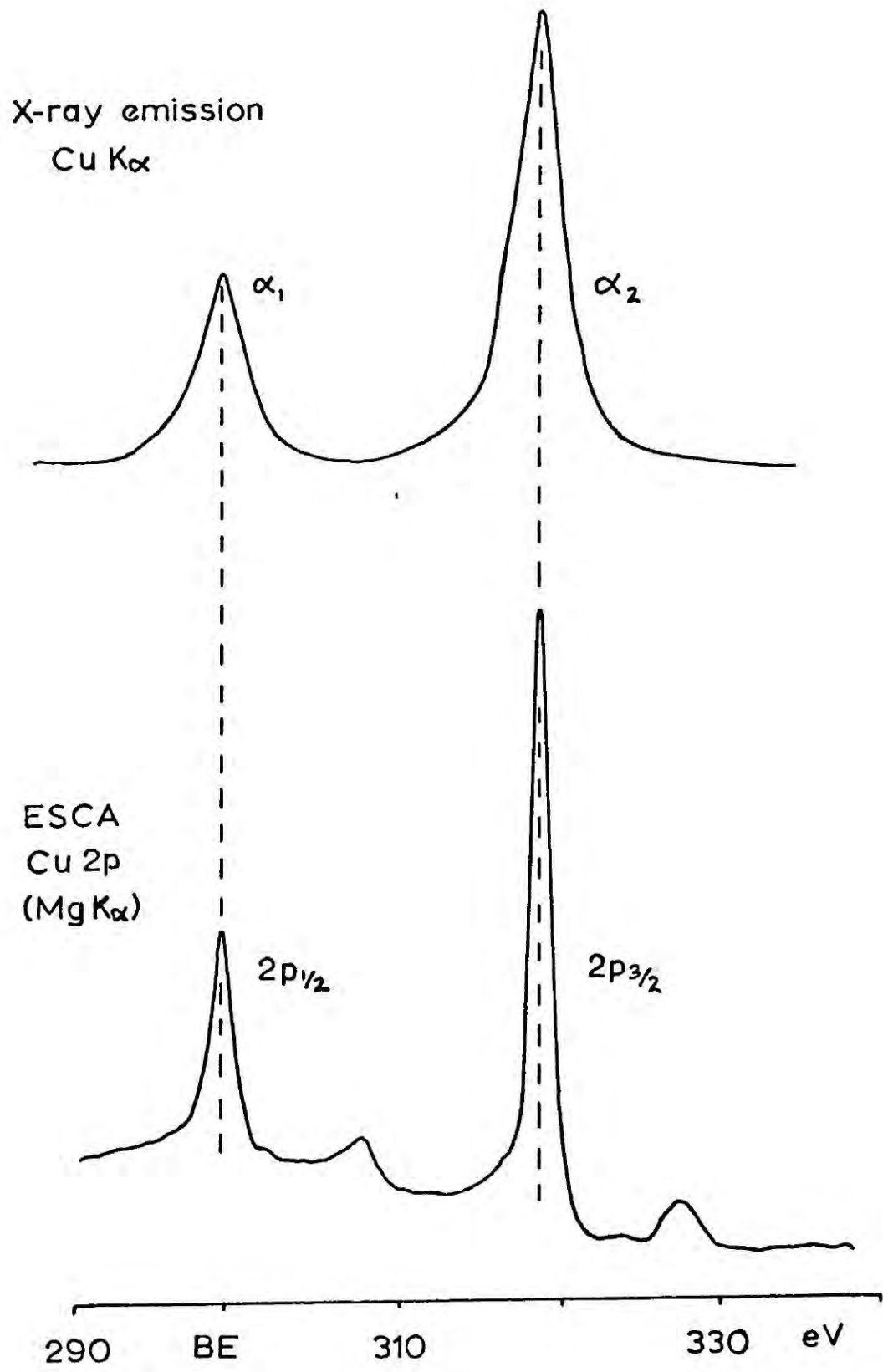


FIGURE 1.8

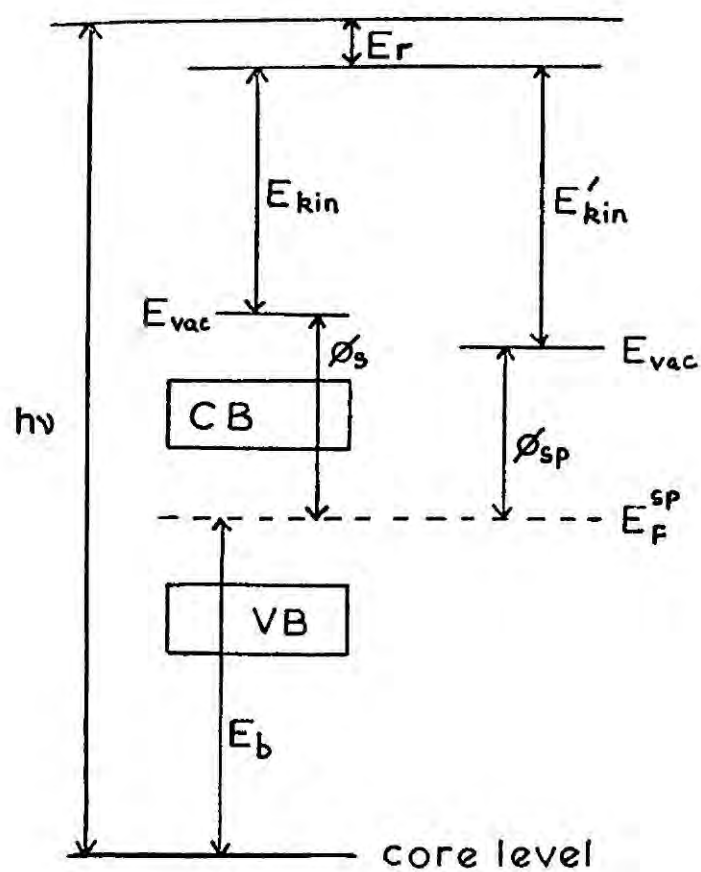


FIGURE 1.9

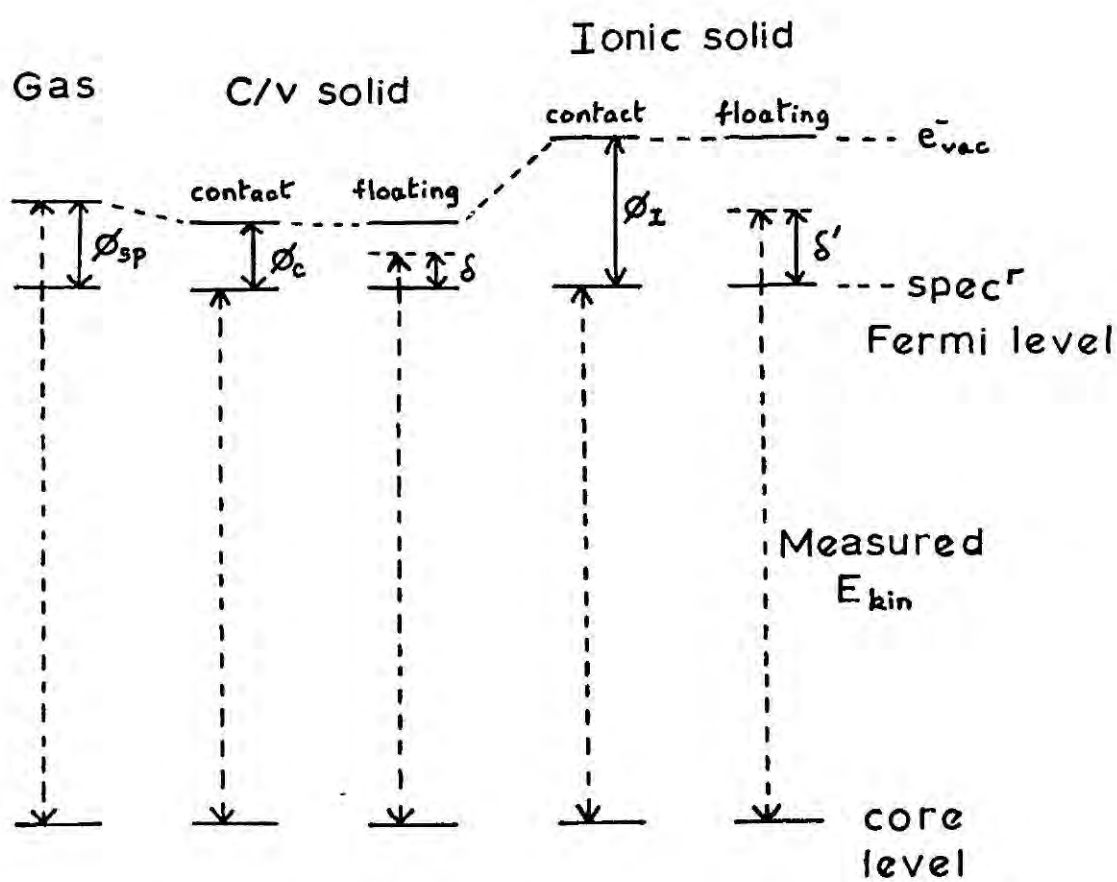


FIGURE 1.10

	AgK α	CuK α	AlK α
H	16	5	0.9
Li	2	0.8	0.1
Na	0.7	0.2	0.04
K	0.4	0.1	0.02
Rb	0.2	0.06	0.01

Hence for the targets used in this work (Al, Mg) recoil energies are sufficiently small for E_r to be negligible for elements after Li in the periodic table.

In general, there exists a small electric field in the space between the sample and the entrance slit to the spectrometer (i.e. the analyser) even if both are in electrical contact. Since their Fermi levels are the same, any difference in work function of sample material and spectrometer material gives rise to a potential difference and hence an electric field gradient in the space between the two. E'_{kin} of the electron when it enters the analyser is thus slightly different, due to acceleration or deceleration, from the kinetic energy, E_{kin} , possessed when leaving the sample. If ϕ_{sp} is the work function of the spectrometer material, then:

$$E_{kin} + \phi_s = E'_{kin} + \phi_{sp}$$

From Fig.1.9 it can be seen that conservation of energy for the photo-ionisation event gives:

$$h\nu = E_b + \phi_{sp} + E'_{kin} + E_r \quad (E_r \approx 0)$$

$$E_b = h\nu - \phi_{sp} - E'_{kin}$$

Since ϕ_{sp} does not depend on the sample material, the same work function correction can be applied to all measurements, providing it does not vary with time. A sufficient number of free charge carriers

must be present in the specimen so that a thermodynamic equilibrium is maintained. This situation obtains for conductors in contact with the spectrometer but for insulating materials the equilibrium position depends on the composition of the material and the X-ray flux (giving rise to 'charging effects', see Fig.1.10). By calibrating the KE scale of the instrument to $\text{Au}4f_{7/2}$ BE = 84.0 eV, ϕ_{sp} is included in all measurements (BE's then being relative to the spectrometer Fermi level). Relative BE's are thus calculated from:

$$E_{\text{b}} = h\nu - E'_{\text{kin}}$$

where E'_{kin} is the measured KE of the photoelectrons.

(e) Relationship between energy levels of gaseous and solid samples

In discussing charge distributions in molecules, as inferred from BE data from ESCA measurements and especially when comparisons of observed shifts are made with those calculated theoretically, it is important to understand the relationship between the measured BE's in the solid phase and those of the free molecule.

Fig.1.11 illustrates the relationship between energy levels for the case of a covalent solid having no strong intermolecular interactions (e.g. hydrogen bonding). For the two photoionisations indicated (from A and B) the BE separation is:

$$\Delta = (I_{\text{A}} - I_{\text{B}})_{\text{vac}} = (I_{\text{A}} - I_{\text{B}})_{\text{F}} + [(\Delta H'_{\text{sub}} - \Delta H''_{\text{sub}}) = 0]$$

and for photoionisations from different samples the BE shift in the general case is:

$$\begin{aligned} \Delta &= (I_{\text{A}} - I_{\text{X}})_{\text{vac}} \\ &= (I_{\text{A}} - I_{\text{X}})_{\text{F}} + (\phi_{\text{A}} - \phi_{\text{X}}) + (\delta_{\text{A}} - \delta_{\text{X}}) + (\Delta H'_{\text{X}} - \Delta H'_{\text{A}})_{\text{sub}} + \\ &\quad (\Delta H'_{\text{A}} - \Delta H'_{\text{X}})_{\text{sub}} \end{aligned}$$

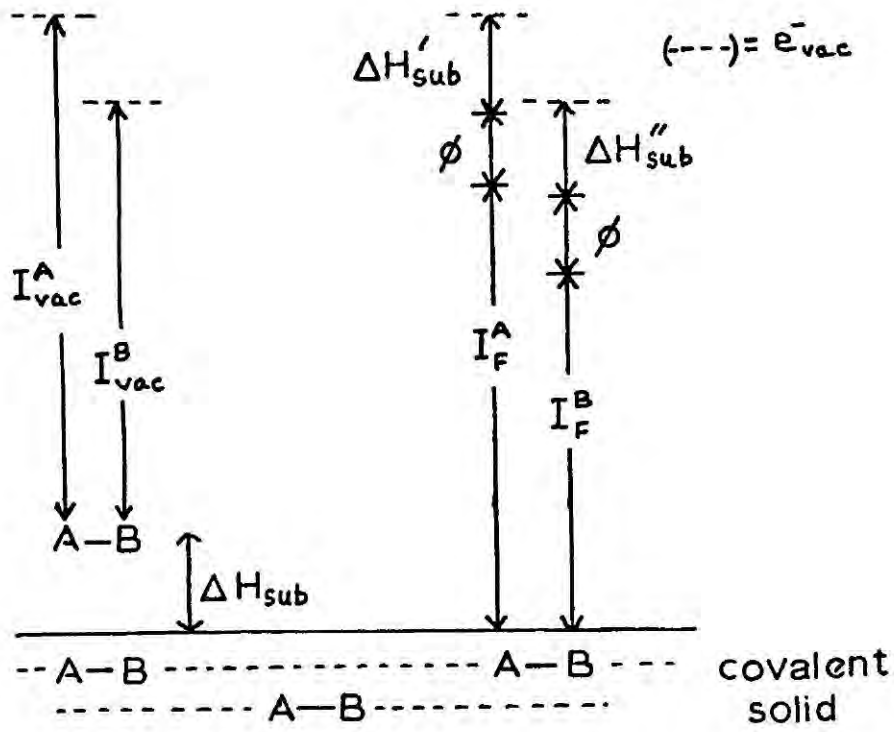


FIGURE 1-11

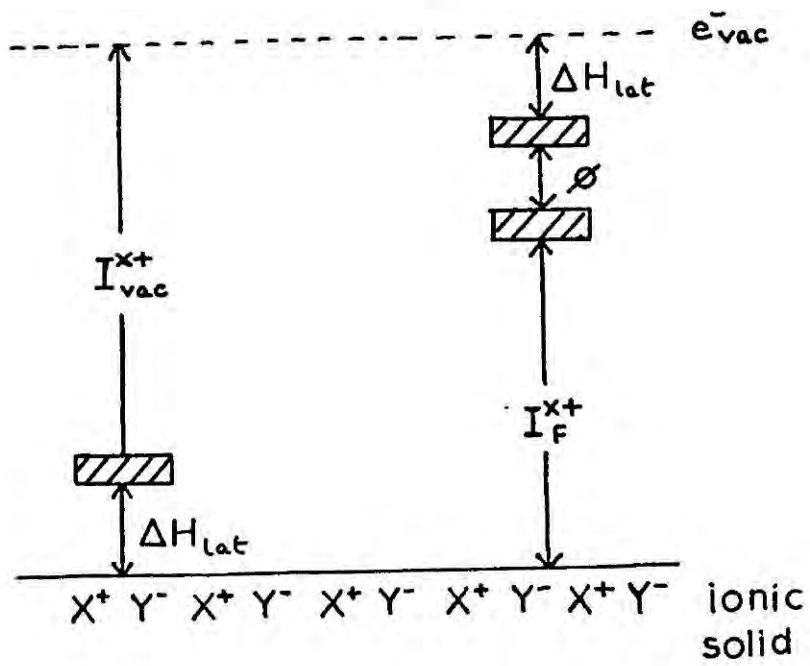


FIGURE 1-12

where I = ionisation energy (100-1000 eV)

ϕ = work function (~ 5 eV)

δ = charging effect (< 2 eV)

ΔH_{sub} = sublimation energy for the molecule considered (M) (~ 0.5 eV)

$\Delta H'_{\text{sub}}$ = sublimation energy for the photoionised state M^{*+}

typical values for these energies being shown in parentheses.

For closely related materials in contact with the spectrometer:

$$(\phi_A - \phi_X) \approx 0, \quad (\delta_A - \delta_X) = 0 \text{ and } \Delta(\Delta H)_{\text{sub}} \text{ terms} \approx 0$$

Hence $(I_A - I_X)_{\text{vac}} \equiv (I_A - I_X)_F$ and shifts can be understood in terms of isolated molecules.

Fig.1.12 shows a similar relationship for the energy levels of a gaseous ion and the ionic lattice; the terms are equivalent to those used above. Typical values are:

$$I_{\text{vac}}^{x+} \text{ (} I_F^{x+} \text{)} \text{ 100-1000 eV, } I_F^{x+} \text{ depending on lattice environment}$$

$$\phi < 10 \text{ eV}$$

$$\Delta H_{\text{lat}} \sim 10 \text{ eV}$$

For atoms in the same lattice the BE shift is:

$$\Delta = \Delta I_{\text{vac}} = \Delta I_F + \text{lattice contribution}$$

and for different samples (assuming no charging effects)

$$\Delta = \Delta I_F + \Delta\phi + \Delta(\Delta H_{\text{lat}} - \Delta H'_{\text{lat}}) + \text{lattice contributions}$$

In this case the last three terms may not approximate to zero as in the covalent solid case, mainly because of the magnitude of the lattice contribution and $\Delta(\Delta H_{\text{lat}})$ terms, so shifts are only approximately related to free ion shifts and care in interpretation is required.

When materials are not in contact with the spectrometer charging effects vary from sample to sample and terms like $(\delta_A - \delta_X) \neq 0$. Corrections for this effect can be made and are discussed in later chapters.

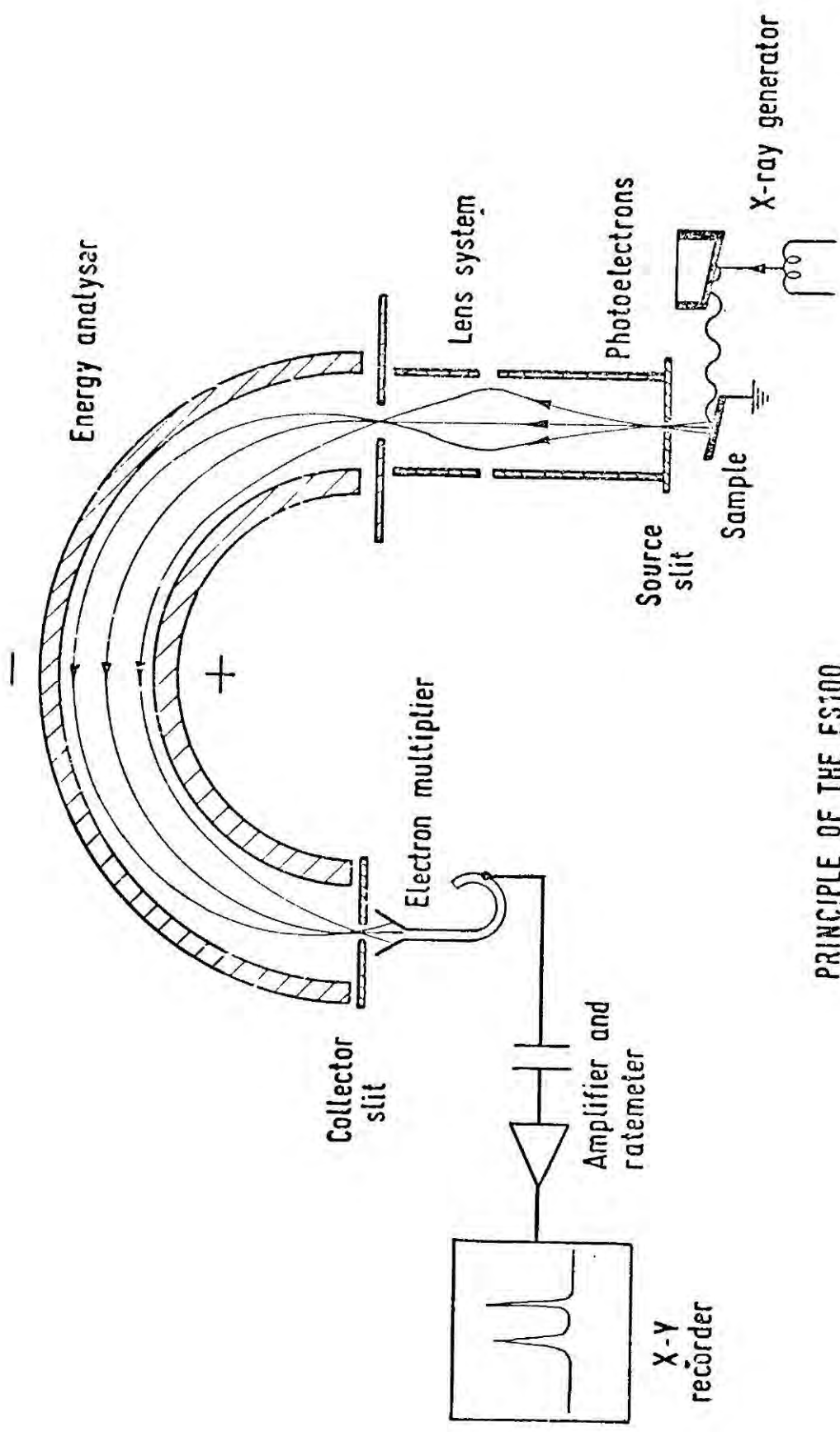
(iv) Instrumentation

Fig.1.13 indicates the major components which make up a photo-electron spectrometer used for X-ray excitation (ESCA) work. Fig.1.14 is a detailed cross-section of the source region of the ES100 instrument manufactured by AEI Ltd. and used in this work.

(a) The Source

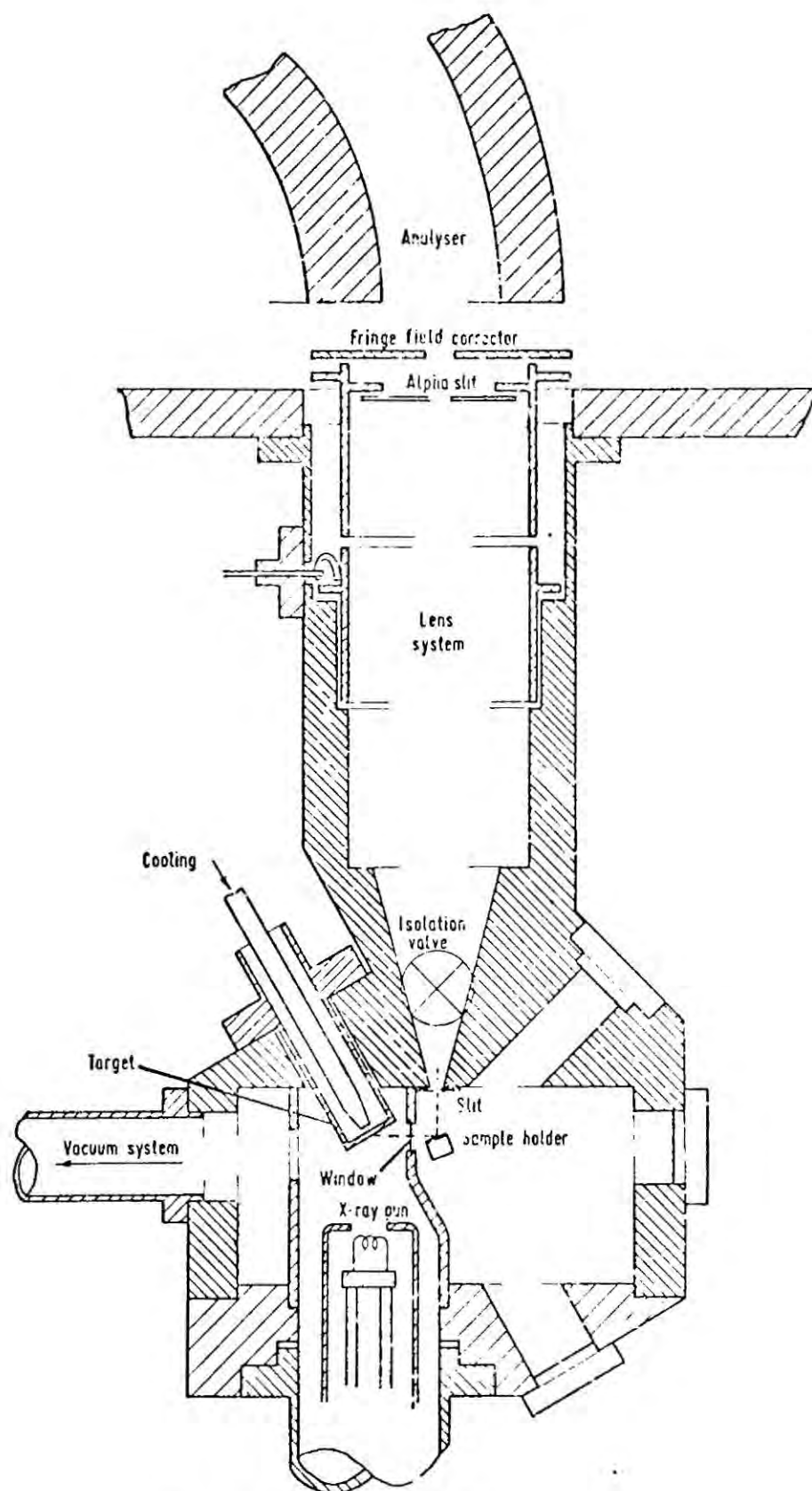
X-ray tubes used in ESCA are of conventional design and consist of a heated cathode at high negative (or earth) potential and a water-cooled anode at ground (or high positive) potential. The anode is usually a hollow copper tube faced with the required anode material (aluminium or magnesium here). Cooling is by means of a water jet directed onto the back of the anode face and is essential because of the high power dissipated. Operating conditions of 10-15 kV at 20-50 mA are common. Rotating anodes can be used to minimise localised heating effects. Fig.1.13 shows the anode to be in direct line with the cathode filament. In more recent designs the electron beam is focussed by electrostatic deflection onto the anode so avoiding the possibility of deposition of tungsten from the filament onto the anode, a problem which can be significant when light elements are used for the anode.

As shown, the X-ray tube and sample compartments are separated by a thin window (usually Al foil), through which the X-ray beam passes, which prevents scattered electrons from the X-ray source getting to the sample. Tungsten deposition on this window (causing loss of transmission) can also be a problem.



PRINCIPLE OF THE ES100 PHOTOELECTRON SPECTROMETER

FIGURE 1-13



LENS AND SOURCE ARRANGEMENT ES100

FIGURE 1:14

It is possible to monochromatise the X-ray beam but this is considered separately in Part (e).

(b) Electron Energy Analysers

The types of analyser which have been used in photoelectron spectroscopy (high and low energy) have been briefly reviewed recently.¹⁹ In much of the early, low energy (PES) work the cylindrical retarding grid analyser was used²⁰ but this has several disadvantages compared with the magnetic and electrostatic deflection analysers which have superseded it, the simplest being the 127° cylindrical sector analyser²¹ (the angle $127^{\circ} 17'$ is chosen because there is an electron trajectory refocussing property at that angle²²). This arrangement is shown in Fig.1.15(a). The method of varying the potential on the analyser plates so that electrons of different energies are focussed in turn on the exit slit finds another variation in the parallel plate analyser²³ shown in Fig.1.15(b). Both these devices are of the single-focussing type.

Double-focussing analysers provide a higher intensity signal for a given resolution; the focussing action in the plane of the analyser (as in the single-focussing types) is supplemented by directional focussing along great circles of a spherical sector. This latter idea was first suggested by Aston in 1919.²⁴ This is clearly seen in comparing the cylindrical mirror analyser²⁵ (double-focussing) shown in Fig.1.15(c) with the parallel plate analyser (Fig.1.15(b)).

ESCA instruments use double-focussing analysers with either magnetic or electrostatic deflection. Magnetic systems were, as mentioned earlier, the first to be used and designs are still based on the original of Siegbahn et al.²⁶ These are iron-free instruments

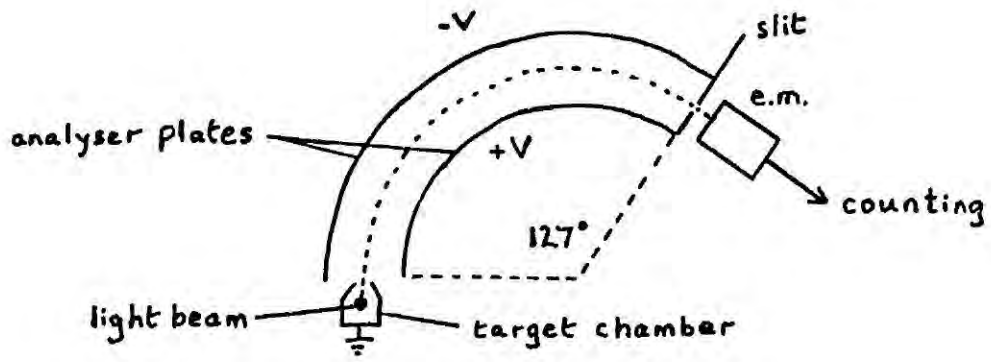
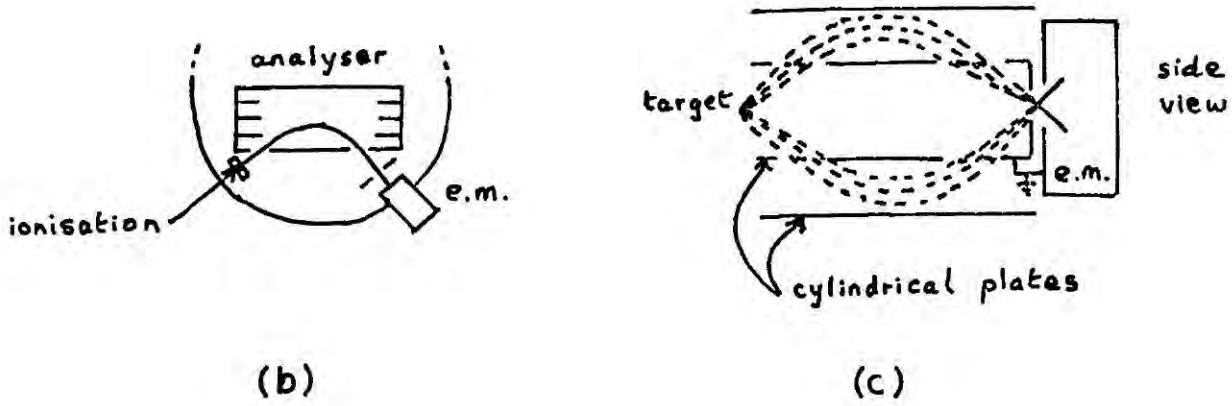


FIGURE 1.15(a)



(b)

(c)

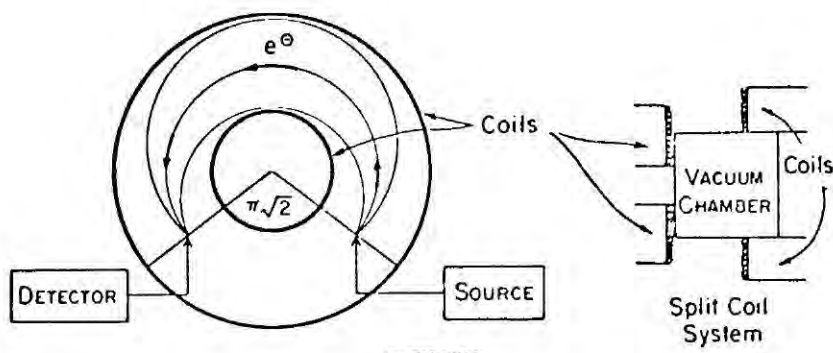


FIGURE 1.16

generally made from brass or aluminium with a radius of about 30 cm. Double-focussing is provided by an inhomogenous magnetic field produced by a set of four cylindrical coils placed about the electron trajectory, as shown in Fig.1.16, the critical angle being $\pi/\sqrt{2}$. The double-focussing spherical electrostatic analyser was first described by Purcell in 1938²⁷ and has now been developed and widely applied. Various sections of the two spherical analyser plates are used, the most popular being the hemispherical (180°) system,²⁸ shown in Fig. 1.13.

Because electron paths are influenced by magnetic fields, it is necessary to have the electron trajectory determined only by the field of the analyser. This means that the earth's magnetic field must be reduced to effectively zero in the spectrometer vicinity. The earth's field can be compensated for in two ways. A series of vertical and horizontal Helmholtz coils²⁹ can be used with the magnetic spectrometer but elaborate coil and monitoring systems are often needed.³⁰ Shields made of paramagnetic materials such as μ -metal function by concentrating the lines of force of the earth's field and can be used with electrostatic instruments. They cannot be used with magnetic instruments since they would also perturb the spectrometer field. It is probably for this reason that all the commercial ESCA instruments use the more compact electrostatic analyser systems, despite the problems involved in engineering spherical sector plates to high tolerances.

An instrument resolving power of $E/\Delta E = 300$ or better is obtained readily with the deflection instruments described above, which corresponds to a peak half-width (full width at half maximum peak height) of 3.3 eV (ΔE) for a 1 keV electron (E). Since the inherent

width of the exciting X-ray line is less than 1 eV (0.7 eV for $\text{MgK}\alpha_{1,2}$; 0.9 eV for $\text{AlK}\alpha_{1,2}$) with this sort of energy (1253.6 eV for $\text{MgK}\alpha$, 1486.6 eV for $\text{AlK}\alpha$) there is room for improvement. Since the fractional resolution $\Delta E/E \propto R/W$ where R is the mean radius of the instrument and W is the combined width of the entrance and exit slits, the resolution can be increased by:

- (i) making W smaller by reducing the slit dimensions. This also reduces the signal intensity.
- (ii) increasing R by choosing a larger radius analyser. This increases the engineering difficulties.
- (iii) reducing E by retarding the electrons before they enter the analyser.

Compromise solutions for (i) and (ii) are necessary but (iii) is an ingenious idea because it can simultaneously enhance the signal intensity. This system is incorporated in the AEI ES100 design used in the present work and worthy of fuller description.

The theory of electron retardation was described by Helmer and Weichert, the following summary being based on their original paper.³¹ The transmitted electron current, I , of an ESCA spectrometer is given by:

$$I = BA\Omega \quad (1)$$

where B is the brightness of electron illumination of the entrance slit (in units of current/unit area/unit solid angle) and $A\Omega$ is the luminosity of the spectrometer where A is the area of the entrance slit and Ω is the solid-angle aperture of the spectrometer as viewed from the entrance slit.

The brightness, B , is determined by the intensity of the X-ray beam which irradiates the sample and is relatively low, hence the double-focussing designs to achieve high luminosity. It turns out that the luminosity can be expressed by:

$$A_{\Omega} = CR^2(\Delta E/E)^2 \quad (2)$$

where R is the radius of curvature of the beam centre line and C is a constant. The brightness law indicates that the brightness of the electron beam is proportional to its kinetic energy:

$$B = (B_0/E_0)E \quad (3)$$

combining (1), (2) and (3) gives:

$$I = B_0 CR^2 [(\Delta E)^2/E_0 E] \quad (4)$$

Retarding the source electrons by a factor of ten (e.g. $E/E_0 = 100/1000$) correspondingly reduces the brightness (3) but from (2) the luminosity can be increased by a factor of 100, by increasing the slit dimensions and acceptance angles, without affecting ΔE (the peak width). So from (4) the overall gain in intensity (I) is a factor of 10.

The energy spread of the source electrons is unaltered when all the electrons are retarded by the same potential difference, which gives rise to the decrease in peak width (ΔE) noted above. The only limit to the increase in transmission achievable from (4) is the practical difficulty of focussing very slow electrons coupled with the difficulty in designing very large aperture spectrometers.

(c) Detection systems

The detector is an electron counter. Three methods have been used in ESCA instruments: G-M counters, electron multipliers and photo-

graphic plates. The G-M type detector originally used by Siegbahn et al¹ was a proportional flow counter using a Formovar window and a post-acceleration system for detection of electrons with energies less than 2 keV.

Electron multipliers are more convenient, especially the continuous channel ('channeltron') type which counts electrons with high efficiency to very low energies and, being small, can be placed readily in the focal plane of the analyser. Sensitivity can be improved by using several tiny multipliers arranged over the length of the exit slit. Dynode-type electron multipliers in conjunction with charge sensitive amplifiers have also been used.

Photographic detection offers the advantage of integrating over fluctuations in the exciting radiation (dependent upon the stability of the X-ray generator) and is capable of detecting very low electron signals. In most cases it is much less convenient than the multiplier system but comes to prominence when X-ray monochromation is used (see later).

(d) Data Acquisition

There are basically two ways of obtaining the required information from the detection system: continuous scanning and incremental (step) scanning, multichannel analysis being a variation on both themes.

In the continuous scan system the potential difference across the plates (in the electrostatic instruments) or the field (in magnetic instruments) is continuously increased with time while the detector signal is monitored by a ratemeter. Synchronisation of the spectrometer current and the rate meter output allows the continuous recording of a

spectrum (electron counts against kinetic energy) on an X-Y plotter if the signal-to-noise ratio is high enough.

The step scan mode increases the current through the spectrometer in a series of small steps (e.g. corresponding to a 0.1 eV step in kinetic energy of the electrons) and uses a scalar to count the detector signal during the time interval giving a point spectrum. This system is easily automated and computerised.

The multichannel analyser approach essentially combines the two by scanning a large number of increments continuously between two set limits of the field. The counts detected at each stopping points are accumulated in separate channels, the contents of which can be outputted in a variety of ways. This system is particularly amenable to computerisation.

(e) Recent Developments

In the instrument designs described above the X-rays are not filtered before striking the sample. As a result the presence of the bremsstrahlung background and other (less intense) X-ray emission complicates the ESCA spectrum which is primarily due to $K\alpha_{1,2}$ excitation. The attainable resolution is limited by the inherent width of this line (0.7 eV for Mg, 0.9 eV for Al) which is not negligible compared with the range of chemical shifts for a given element (~ 10 eV) and greater than most conveniently studied core level line widths (~ 0.3 eV).

Monochromation of the X-ray beam was described by Siegbahn's group¹ as a way of dealing with these problems. They now report³² progress in this direction using a spherically bent quartz crystal monochromator and a 'dispersion compensation' system to increase sensitivity without losing resolution. In this the various geometrical and electrical parameters

of the system are chosen so that the dispersion of the lens-analyser combination for the electrons is equal in magnitude and opposite in sign to the dispersion of the monochromator for the X-ray beam, so that they effectively cancel. This means that, in principle, the X-ray line width does not contribute to the width of the electron lines at the exit plane of the analyser, no slits being used.

Alternatively, or when dispersion compensation is difficult to achieve, as with solids with very uneven surfaces or with gas samples, a narrow slit placed between the monochromator and the target can be used to produce, in principle, a line width, less than that of the $K\alpha_{1,2}$ doublet, which will not greatly contribute to the measured photoelectron line-width (slit filtering). In practice the severe loss in intensity in this case necessitates a compromise and the use of very high power rotating anodes (e.g. 5-10 kW) plus improved detection systems.³² However, the situation is not as bad as it seems at first sight because the signal-to-background ratio is greatly improved by the absence of the bremsstrahlung radiation. Using this system with an effective X-ray line width of 0.2 eV (Al) the Cls line-width from gaseous CF_4 is only 0.52 eV,³³ compared with about 1.2 eV obtainable from the best present generation instruments for similar intensities, (as a condensed film).³⁴

(v) Review of ESCA applications in Inorganic Chemistry

The growth of the field of X-ray photoelectron spectroscopy has been quite dramatic. Research papers dealing with ESCA as a technique or using ESCA as a technique to investigate chemical phenomenon have been appearing for less than four years - recognition of the utility of

chemical shift data occurred only in 1964 - yet the number of commercial instruments in existence or under development fast approaches double figures. The ESCA literature is expanding very rapidly: of the two purposeful reviews to date the first³⁵ covered the literature to the end of 1970 and included about 20 references to applications in inorganic chemistry whilst the second³⁶ covered 1968-1971 with some 60 references in the same area. The 1972 literature indicates further rapid growth of the field. In this section, therefore, attention is concentrated on defining the major directions of work and discussing those reports which best illustrate the contributions ESCA can make in inorganic studies in general.

Since ESCA is a new spectroscopic technique one of the trends has been the correlation of new data with those obtainable by other techniques. The origin of core electron shifts being primarily due to valence shell changes a correlation between nmr and ESCA shifts has been predicted³⁷ and claims made for its observation for P2p BE's and ³¹P chemical shifts in quaternary phosphonium complexes.³⁸ However, in the organic field ¹³C nmr data and Cls BE's for the halogenated methanes have now shown such correlations to be invalid^{39a} though early data on restricted series gave inconclusive results.^{39b} Providing similar series of complexes are chosen there is a correlation between ³⁵Cl nqr frequencies and Cl 2p BE's in square-planar Pt complexes (this work).⁴⁰ A correlation between core level BE's and Mossbauer chemical shifts might also be anticipated and this has been observed for both tin⁴¹ and iron^{42,43} compounds.

A large part of the work to date has been the general investigation of series of compounds of a given element in order to gather data on

chemical shifts, particularly with a view to establishing BE regions corresponding to certain oxidation states. Chemical shift data of some kind has now been accumulated for well over half the elements in the periodic table. Chemical shifts for sulphur compounds^{17,18} constituted the first detailed investigation of these effects and included data for various sulphur oxyanions. Binding energies for chlorine in oxidation states -1 to +7 range cover some 10 eV⁴⁴ while for a given change in oxidation number the shifts for Br⁴⁵ seem to fall between those reported for Cl⁴⁴ and I.⁴⁶ With compounds of low atomic number elements attempts have been made to correlate these BE's with calculated charges from MO calculations of various levels of sophistication, e.g. compounds of B,⁴⁷ N,⁴⁸ Si,⁴⁹ P,⁵⁰ and As.⁵¹ These have met with limited success, the only definite result being the increase in BE as the electronegativity of attached groups increases. BE data have been reported for compounds of various transition metals. A linear correlation between BE and oxidation state emerged from a study of Mo compounds.⁵² First row transition metal compounds studied have been those of Cr,^{47,53,54} Fe,^{53,55} Mn,⁵³ Co,⁵³ Cu,⁵⁶ and Ni.⁵⁷ It has often been the case that general studies of this kind have led to the observation of unexpected phenomena; the discovery of 'shake-up' satellites in transition metal spectra is a case in point (see Chapter II, Section (i)e for a brief review). Platinum and palladium compounds have now been extensively studied,^{40,58-62} These results impinge directly on this work and are discussed as appropriate. Not surprisingly, there have been attempts to unravel the vexed question of the nature of the iron sites in Prussian blue, with marked success.^{63,64}

The ability of ESCA to give information, in principle, on all atoms in a molecule (except hydrogen) has been especially put to good use in

the study of metal complexes. An early application of this kind was the demonstration that the ligand $\text{NH}_2\text{COCH}_2=\text{CH}_2$ binds to SnCl_4 through nitrogen rather than oxygen by measuring the N1s and O1s BE's for the free and complexed ligand.⁶⁵ Complexation was accompanied by an increase in N1s BE (loss of electron density through lone-pair donation) without significant change in O1s BE. The co-ordination of substituted phosphines has been studied in an attempt to assess π -bonding effects.^{66,67} Thus the P2p BE for the free phosphine is lower than in R_3PX ($\text{X} = \text{O}, \text{S}, \text{Se}$) but similar to that found for R_3P bonded to metals; effective balance of σ -donation and π -back bonding are invoked to explain the latter result. Qualitative charge distributions have been inferred from studies of transition metal carbonyls^{68,69} and cyclopentadienyls.⁶⁸ The attached nitrogen atom in $\text{Re}(\text{N}_2)\text{Cl}(\text{diphos})_2$ is distinguishable from the unattached nitrogen by its higher BE,⁷⁰ but complexed azide (N_3) shows⁷¹ a similar 2:1 doublet (of ~ 4 eV separation) to ionic azide.¹ BE data for salts of the kind $[(\text{Ph}_3\text{P})_2\text{N}(\text{Ph}_3\text{P})_2]^+\text{X}^-$ indicate that $\text{R}_3\text{P}^+-\bar{\text{N}}^+-\text{PR}_3$ is probably a better representation of the cation structure than $\text{R}_3\text{P}^+=\text{N}=\text{PR}_3$.⁷² However, the negligible effect of changing X^- suggests that varying crystal (Madelung) potentials are exerting a marked influence and illustrates the care required in interpretation of BE data from ionic complexes (See Chapter III, Section (ii)).

Additional information on chemical bonding can be obtained from an examination of the multiplet splittings which arise through the interaction of electrons in a partially filled inner orbital, produced in photoionisation, with electrons in a partially filled valence shell. First demonstrated for gaseous O_2 and NO^2 , the phenomenon has been

discussed for transition metal complexes in a series of papers by Fadley et al (see e.g. ref.73 and references included therein) and for some rare earth compounds.⁷⁴ The fairly large splitting of the 3s core level (up to 9 eV) by 3d valence electrons make paramagnetic first row transition metal compounds ideal for studies of this kind. The effects of covalency and ligand field strength on multiplet splittings in ionic compounds of this type have been well illustrated⁵⁴ and multiplet splitting measurements on MnO and MnS have been shown to substantiate the fact that the individual molecules are paramagnetic even though the bulk material is antiferromagnetic.⁵⁴ A further neat illustration of the usefulness of multiplet splittings comes from a study of $\text{Cr}(\text{CO})_6$, $\text{Cr}(\pi\text{-C}_5\text{H}_5)_2$ and $\text{Cr}(\text{hfa})_3$ ^{*75} which have 0, 2 and 3 unpaired valence (3d) electrons and oxidation states, 0 +2 and +3 respectively. Splittings of the 3s level agreed well with theoretical predictions. Shifts due to oxidation state changes were followed through measurements of the $2p_{3/2}$ BE - this level being only slightly broadened by multiplet splitting effects. In connection with this it is interesting to note that changes in the position of peak maxima for the $2p_{1/2}$ and $2p_{3/2}$ peaks of Co due to multiplet splitting effects in paramagnetic compounds can result in the apparent increase in separation of these two peaks.⁷⁶

As mentioned earlier, valence orbitals can also be studied by ESCA although count rates are often inconveniently low. Valence bands for the cuprous halides have been reported⁷⁷ and for the isoelectronic series LiF, BeO, BN and graphite.⁷⁸ From similar observations, information on the bonding in salts of oxyanions, interpreted with the help of MO calculations is beginning to appear.⁷⁹⁻⁸¹

* hfa = hexafluoroacetylacetonate

The basic use of ESCA as an analytical tool has been demonstrated in a study of 'polywater'.⁸² The spectra indicated the presence, in high concentration, of Na, K, SO_4^{2-} , Cl^- , NO_3^- , borates, silicates, C-O compounds and other impurities, but very little water. On the basis of this evidence the existence of 'polywater' has been doubted.

CHAPTER II

ESCA STUDIES OF SOME SQUARE-PLANAR PLATINUM COMPLEXES (I)

(i) Platinum-olefin complexes.(a) Introduction

Complexes of the type $(R_3P)_2PtL$ ($L = C_2X_2, C_2X_4$) in which the metal is formally considered to be in the zero oxidation state offer the closest model system to the interaction of platinum and unsaturated hydrocarbons. The description of bonding between metal and ligand in complexes of this kind is still the subject of much discussion. Essentially the problem is whether the olefin complex, say, should be represented as a metallocyclopropane derivative involving two Pt-C σ bonds in a formally Pt^{II} complex or as a π -adduct of Pt^0 (Fig. 2.1), and what effect substituent groups in the olefin have on the bonding situation.



Fig. 2.1

As Collman has pointed out⁸³ the question is also whether these two bonding types represent energy minima or whether they are extreme descriptions of a gradual transformation. There appears to be no a priori reason for a sharp boundary between these extremes and, indeed, the fact that the reported infrared stretching frequencies ($\nu_{C=C}$) for the closely related, more stable, acetylene complexes, are scattered over

the range 2100-1600 cm^{-1} suggests a gradual change rather than two distinct bonding types. The Dewar-Chatt-Duncanson⁸⁴ description of the bonding in such complexes, and a more recent embellishment⁸⁵ of it can accommodate any reasonable oxidation state of platinum (fractional or integral) in the range 0 to 2. In this description the π orbital of the olefin overlaps with an empty platinum orbital of appropriate symmetry forming a bonding molecular orbital of σ -type. The accumulation of negative charge on the metal can be relieved by back donation from filled metal d orbitals into the relatively low-lying π^* antibonding orbital of the olefin, forming a bonding molecular orbital of π symmetry. Thus the net electron transfer depends on the relative magnitudes of the σ and π contributions.

In the last few years X-ray crystal structure determinations have been reported with sufficient accuracy to allow well-grounded conclusions about the structure of these complexes to be reached. Subsequently attempts have been made⁸⁶ to account for the observed perturbation of the free-ligand geometry upon co-ordination by calculating the changes in ligand geometry which would accompany electron transfer processes implicit in the Dewar-Chatt-Duncanson model and by performing calculations⁸⁵ on the total complex, of known geometry, in order to estimate overall charge distributions.

ESCA has the potential to increase our understanding here since molecular core binding energies reflect the charges associated with the atom in question and hence provide the means to study directly the types of electron redistribution which are thought to occur.

(b) Experimental.

Spectra were recorded on an AEI ES100 electron spectrometer using $\text{MgK}\alpha_{1,2}$ (1253.6 eV) or, occasionally, $\text{AlK}\alpha_{1,2}$ (1486.6 eV) radiation. Samples were studied either as powders pressed onto a scotch tape backing or, whenever possible, as thin films deposited from solution (CH_2Cl_2 or CHCl_3) on gold, care being taken to prevent contamination of the surface. Electrons expelled from the sample enter the analyser region consisting of a two element retarding lens and a 10 in. mean diameter hemispherical analyser. A Mullard channeltron electron multiplier is used as a detector, the output being fed to Nuclear Enterprises counting electronics and the spectra being plotted on an X-Y recorder.

Overlapping peaks were deconvoluted by using a Du Pont 310 curve resolver and line shapes of Gaussian form. This line shape was found to be quite satisfactory in fitting peaks known to arise from atoms in a single environment (ie of one 'type'). Under the conditions used in this work the gold $4f_{7/2}$ level at 84 eV binding energy (used as a reference) had a half width of 1.15 eV. Sample charging effects are particularly serious in studies of insulators; methods used to overcome them are described as appropriate.

(c) Results.

Binding energies for the core levels studied are collected in Table 2.1. As noted above charging effects are a serious problem with insulating solids. They can be minimised if a sufficiently thin layer of sample on gold is studied. The uniform shifting of the energies of the emitted photoelectrons due to the formation of a surface potential seems to be a rapid and fairly random process. Within experimental

error, estimated on the basis of the expected confidence of peak position and its accuracy of measurement to be ± 0.3 eV, the BE of the Cls electrons from the phenyl groups in the Ph_3P ligands which these complexes contain is expected to be constant since any charge transfer to or from the ligand is spread over so many centres. This BE is taken to be 285.0 eV and data from all complexes are referenced to this value, so eliminating random charging effects.

For comparison equivalent data for two acetylene complexes are included together with $(\text{Ph}_3\text{P})_4\text{Pt}$ and Pt metal. This last comparison is not strictly valid since this is a conductor and is in electrical contact with the spectrometer in contrast to the remaining samples (as discussed in Chapter I, Section (iii)e). However, the error involved in this comparison is not thought to be so great as to preclude meaningful comment.

(d) Discussion.

The main points which emerge from Table 2.1 are as follows:

- (i) Within experimental error the phosphorus BE's are constant throughout the series.
- (ii) The platinum B.E's for the olefin and acetylene complexes are the same, again within experimental error, with the exception of $(\text{Ph}_2\text{MeP})_2\text{Pt}[\text{C}_2\text{F}_4]$ with the metal slightly less tightly bound. The 71.2 eV B.E. quoted for $(\text{Ph}_3\text{P})_2\text{Pt}[\text{C}_2\text{Cl}_4]$ has previously been interpreted⁸⁷ as a value for this complex, which undergoes isomerisation to $(\text{Ph}_3\text{P})_2\text{PtCl}(\text{CCl} = \text{CCl}_2)$ as will be described

TABLE 2.1

Complex	Core Binding Energies (eV)			
	Pt4f _{7/2}	P2p _{3/2}	F1s	N1s
Pt Metal	71.4			
(Ph ₃ P) ₄ Pt	72.0	130.9		
(Ph ₃ P) ₂ Pt[H ₂ C=CH ₂]	72.6	130.7		
(Ph ₂ MeP) ₂ Pt[F ₂ C=CF ₂]	72.2	130.7	688.4	
(Ph ₃ P) ₂ Pt[(NC) ₂ C=C(CN) ₂]	72.5	130.9		399.6
(Ph ₃ P) ₂ Pt[Cl ₂ C=CCl ₂]*	72.4 (71.2)	131.0		
(Ph ₃ P) ₂ Pt[HC≡CH]	72.6	130.7		
(Ph ₃ P) ₂ Pt[HC≡CPh]	72.5	130.8		

* Thought to undergo isomerisation and possibly decomposition (See text).

fully in Chapter IV. Comparison with these other results now leads us to believe that this may be a contribution from metallic platinum. A similar situation pertains to the ethylene complex. Figure 2.2 shows the Pt4f_{5/2,7/2} spectrum from the ethylene complex which can be resolved into two doublets of expected half width and separation. The doublet with Pt4f_{7/2} BE of 71.1 eV is again close enough to the value for metallic platinum to suggest that decomposition under X-irradiation to produce free metal occurs. This situation is consistent with the known susceptibility of this complex to loss of olefin compared with the more stable substituted olefin and acetylene complexes.

- (iii) The platinum B.E. in $(\text{Ph}_3\text{P})_4\text{Pt}$ is roughly intermediate between the metal and the olefin/acetylene complexes.

It is important to note at this point that observed B.E. for Pt4f_{7/2} electrons in complexes of the general type $\text{cis}-(\text{R}_3\text{P})_2\text{PtCl}_2$ are, within experimental error, the same as those for the olefin/acetylene complexes, e.g. $\text{cis}(\text{Ph}_3\text{P})_2\text{PtCl}_2$: Pt4f_{7/2} = 72.5 eV. These complexes are discussed in later sections but this result has notable significance in the interpretation of the above results.

During the course of this work B.E. data for some of these complexes have been reported. Cook et al⁸⁸ have given data for $(\text{Ph}_3\text{P})_4\text{Pt}$, $(\text{Ph}_3\text{P})_2\text{Pt}(\text{C}_2\text{H}_4)$, $(\text{Ph}_3\text{P})_2\text{Pt}(\text{C}_2\text{Ph}_2)$ and $(\text{Ph}_3\text{P})_2\text{PtCl}_2$ while Mason et al⁸⁹ discuss $(\text{Ph}_3\text{P})_2\text{Pt}(\text{C}_2\text{X}_4)$ (X = H, Cl, F, CN) and $(\text{Ph}_3\text{P})_2\text{PtCl}_2$. At the present time it seems unwise to concentrate on

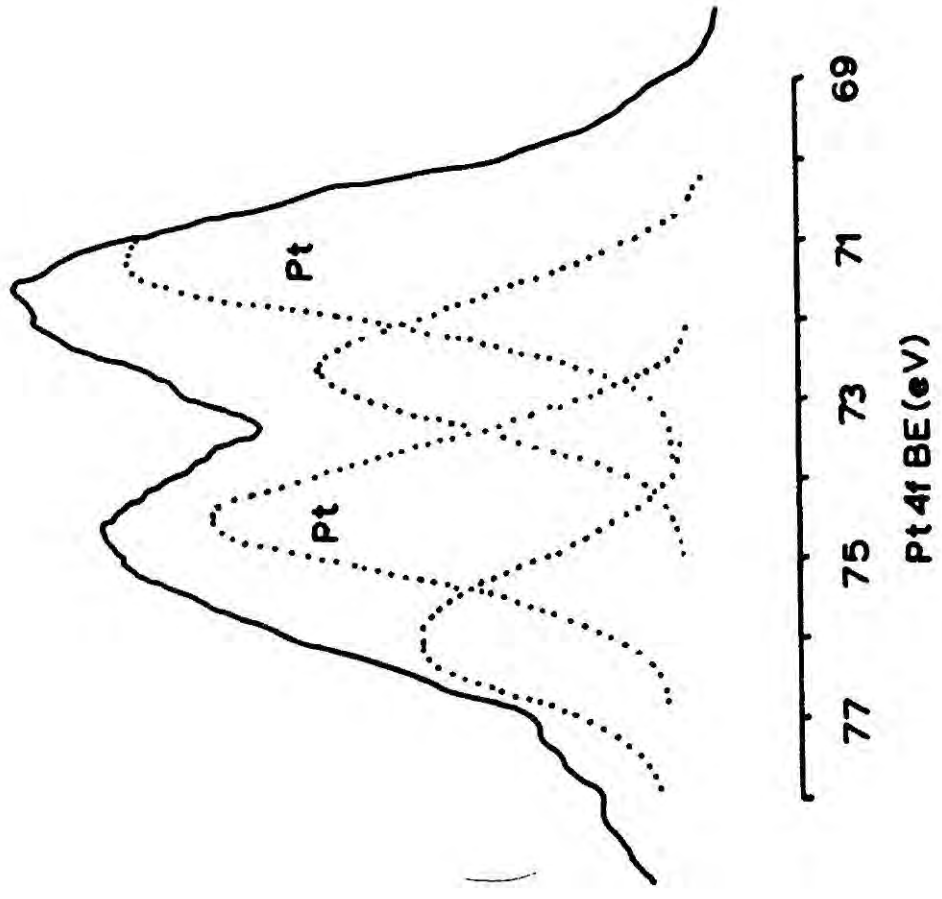
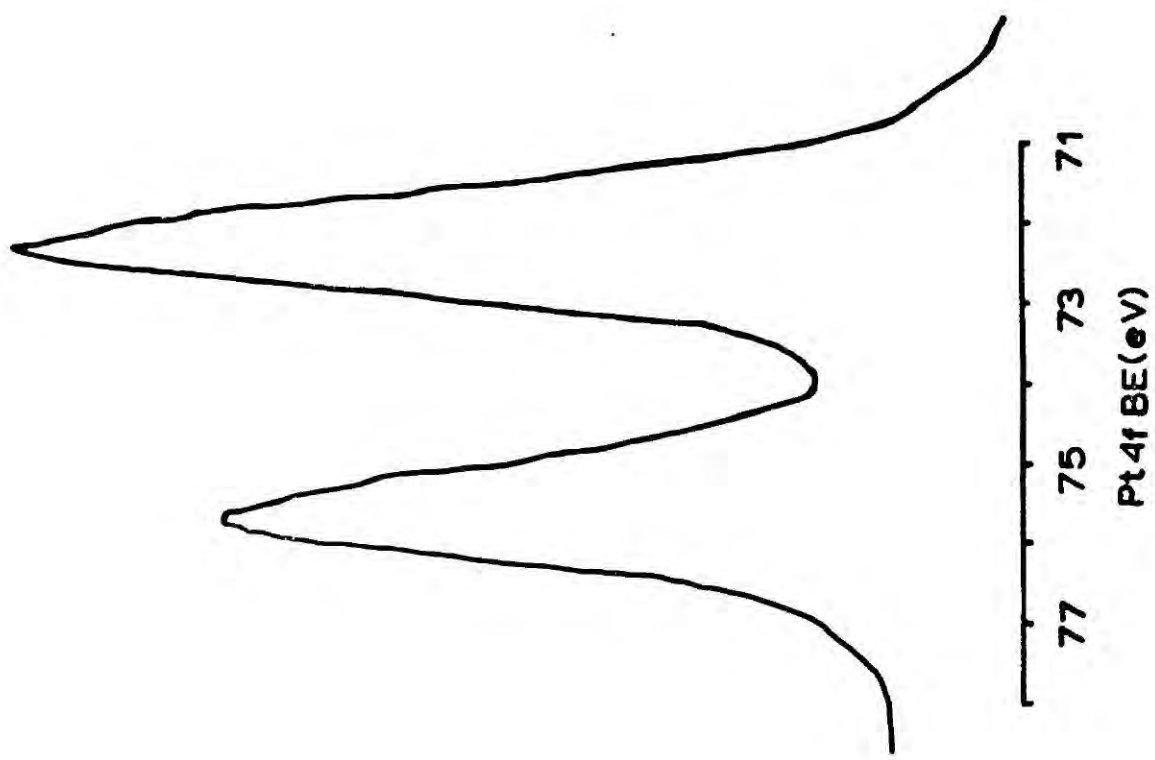


FIGURE 2.2

'absolute' values of B.E.'s since these are heavily dependent on instrumental calibration and correction factors; for interpretational purposes the relative B.E.'s of a given core level within a series are of prime importance. Broadly speaking the results are in satisfactory agreement with one important exception. The Pt $4f_{7/2}$ B.E. for $(\text{Ph}_3\text{P})_2\text{PtCl}_2$ reported by Cook et al⁸⁸ is ~ 1 eV higher than for the ethylene complex whereas the present results and those of Mason et al⁸⁹ indicate similar B.E.'s in the two complexes. This point will be returned to later. Mason's results⁸⁹ indicate no significant difference in the platinum B.E.'s of the $(\text{Ph}_3\text{P})_2\text{Pt}(\text{C}_2\text{X}_4)$ series while a slightly lower B.E. for the C_2F_4 complex was found in this work as mentioned above. It is possible that the difference in phosphine ligand (Ph_2MeP in this case) may partly account for this: Ph_2MeP is thought to be a better σ -donor & weaker π -acceptor than Ph_3P . Complexes differing only in these ligands would have slightly higher electron density of the metal, and hence, lower B.E., in the case of the former ligand. However, this effect is expected to be small (see Section (iii)). Also it has been shown that at ambient temperatures $(\text{Ph}_3\text{P})_2\text{Pt}(\text{C}_2\text{Cl}_4)$ gives spectra due to $(\text{Ph}_3\text{P})_2\text{PtCl}(\text{CCl} = \text{CCl}_2)$ (see Chapter IV) while Mason et al⁸⁹ note only that their Cl 2p peak was 'very broad'.

It is difficult to say anything about the carbon atoms of the complexed olefin since the 36 carbon atoms of the Ph_3P ligands dominate the Cls spectrum. From some spectra of the ethylene complex it seemed that the low B.E. side of the Cls peak exhibited distinct asymmetry. Deconvolution on the assumption that a peak due to the ethylenic carbons was giving rise to this feature indicated a B.E. for the latter of ~ 283.4 eV, a shift to lower B.E. of ~ 1.6 eV compared with the

free ligand. This indicates charge transfer to the olefinic carbons but in view of the deconvolution uncertainty it is unprofitable to quantify this further.

X-ray crystal structure determinations have been reported for a number of these complexes: $(\text{Ph}_3\text{P})_2\text{Pt}(\text{C}_2\text{H}_4)$,⁹⁰ $(\text{Ph}_3\text{P})_2\text{Pt}(\text{C}_2(\text{CN})_4)$,⁹¹ $(\text{Ph}_3\text{P})_2\text{Pt}(\text{C}_2\text{Cl}_4)$ ⁹² and also for $(\text{Ph}_3\text{P})_3\text{Pt}$ ⁹³ and $(\text{Ph}_3\text{P})_2\text{Pt}(\text{C}_2\text{Ph}_2)$.⁹⁴ The Pt-P bond lengths are constant at $2.27 \pm 0.03 \text{ \AA}$ which result is reflected in the constancy of the $\text{P}2\text{p}_{3/2}$ B.E. found in this work. For the substituted olefin complexes $(\text{Ph}_3\text{P})_2\text{Pt}(\text{C}_2\text{X}_4)$ the Pt-C distances are 2.11 \AA ($\text{X} = \text{H}, \text{CN}$) and 2.03 \AA ($\text{X} = \text{Cl}$) while the C-C distances are 1.43 \AA ($\text{X} = \text{H}$), 1.49 \AA ($\text{X} = \text{CN}$) and 1.62 \AA ($\text{X} = \text{Cl}$) with some uncertainty attached to the last result. It can also be inferred from studies on $(\text{Ph}_3\text{P})_2\text{Pt}(\text{F}_2\text{C} = \text{CCl}_2)$ ⁹² that the Pt-C bond length in $(\text{Ph}_3\text{P})_2\text{Pt}(\text{C}_2\text{F}_4)$ might be close to those for the cases $\text{X} = \text{H}$ and CN . The interesting feature is the similarity of the data for $\text{X} = \text{H}, \text{CN}$ and F while the $\text{X} = \text{Cl}$ case is slightly anomalous, probably due to inaccuracies.

The ESCA data is in good agreement with this crystallographic data in that (a) it reproduces the similarities of geometry in terms of similar charge distributions (as reflected in the B.E. data) and (b) the charge transfer from metal to olefin/acetylene ligand, inferred from the increase in $\text{Pt}4\text{f}_{7/2}$ B.E. compared with $(\text{Ph}_3\text{P})_4\text{Pt}$ and tentatively observed directly for C_2H_4 on co-ordination, is in accord with the observed increase in C-C bond length on co-ordination, as predicted by the Dewar-Chatt-Duncanson model.⁸⁴

Cook et al⁸⁸ assumed a simple model whereby platinum has a charge of zero in $(\text{Ph}_3\text{P})_4\text{Pt}$ and +2 in $(\text{Ph}_3\text{P})_2\text{PtCl}_2$ and then used a linear correlation between B.E. and charge to estimate charge transfer to the ligand in $(\text{Ph}_3\text{P})_2\text{Pt}(\text{C}_2\text{H}_4)$ and $(\text{Ph}_3\text{P})_2\text{Pt}(\text{C}_2\text{Ph}_2)$. These estimates were then matched to perturbations in ligand geometry using theoretical arguments developed by Walsh⁹⁵ and Blizzard and Santry⁸⁶ which relate the ligand geometry when co-ordinated to that of its first excited state. As pointed out above, it now appears that the difference in metal B.E. between the supposed Pt^{II} representative and the olefin/acetylene complexes is not significant thus casting doubt on the meaningfulness of these results.

Recent measurements of ^{13}C -H coupling constants for these complexes (i.e. of the type $(\text{Pd}_3\text{P})_2\text{Pt}(\text{}^{12}\text{CH}_2 = \text{}^{13}\text{CH}_2)$ where $\text{Pd} = \text{d}^5 - \text{Ph}$)⁹⁶ have been interpreted as giving information on the s-character of the Pt-C σ -bonds and suggesting that π -bonding is insignificant. The results are difficult to interpret, largely as a result of the inadequacy of the valence bond approach to bonding in these complexes and associated calculations of the carbon bond angles are in reasonable agreement with the measured values only in one of the two cases studied.

The semi-empirical MO calculations⁸⁵ mentioned earlier also give an indication of the ratio of σ -donation to π -back bonding. Electron densities on the platinum were estimated by both Lowdin and

Mulliken population analyses.* The former results, favoured by the authors, indicate a Pt^0 situation while the latter are closer to Pt^{II} and also reflect experimental trends. These results are based on a planar trigonal dp^2 hybridisation for Pt which neglects participation of the 6s orbital involved in the Dewar-Chatt-Duncanson scheme. The dp^2 scheme does, however, give a good theoretical reproduction of ligand rotational processes.⁹⁷

Clearly there are inconsistencies in both these sets of results which further illustrates the confusion which still exists. The conclusion to be drawn from the ESCA results presented here is that the $\text{Pt} \rightarrow \pi^*$ back donation process is very significant in these complexes and that the enhancement of this processes (with simultaneous repression of $\text{M} \leftarrow \pi$ σ -donation) brought about by substituting electron withdrawing groups into the complexing olefin (by lowering the π and π^* orbital energies) has but a minor effect. The similarity between platinum B.E.s in the olefin and acetylene

* Lowdin orbitals are symmetrically orthogonalised, thus each electron occupying MO X_m contributes charge L_{mi}^2 to AO ϕ_i where L_{mi} are the Lowdin orbital coefficients in the MOs. Summing the L_{mi}^2 terms over the occupied MO's gives the Lowdin population analysis. Mulliken orbitals are nonorthogonal; each electron contributes charge C_{mi}^2 to ϕ_i and also charge $2C_{mi}C_{mj}S_{ij}$ to the distribution described by $\phi_i\phi_j$ whose overlap integral is S_{ij} . The gross Mulliken population is defined as the sum of C_{mi}^2 terms and half of all overlap involving the orbital in question. See ref. 97 for a more detailed discussion.

complexes, indicating similar electron distributions, confirms the conclusions advanced by Greaves et al⁹⁸ from their work on orbital energy matching schemes for acetylene complexes.

(e) Satellite peaks.

An interesting feature of the spectra obtained from these complexes is the appearance of satellite peaks on the low K.E. side of the Cls peak. The intensities are relatively low ($\sim 5\%$) and the shift with respect to the main peak usually ~ 6.5 eV (Fig. 2.3).

The existence of satellite structures, as such, in the ESCA spectra of solid samples has been recognised only relatively recently although similar structures ascribed to electron 'shake-up' processes have already received detailed attention for the noble gases and some simple gaseous molecules.^{2,99,100} The process is simply illustrated in Fig. 2.4. In solids, satellites of this type have been observed on the 3s levels of alkali metal and halogen ions,^{101,102} on the 2p levels of NiO and various copper salts,^{103,104,56} and of oxide layers formed on copper and nickel,¹⁰⁵ and on the 3p and 3d levels of transition metal ions.¹⁰⁶⁻¹⁰⁸ Strong satellites on the Cls and Ols peaks, and possibly on the metal peaks, have been observed for metal carbonyls and their origins discussed¹⁰⁹⁻¹¹¹ as have Cls and Nls satellites from complexes of tetracyano-p-quinodimethane (TCNQ).¹¹²

In these two latter cases the most reasonable explanation for the origin of the satellite peaks is again an intramolecular

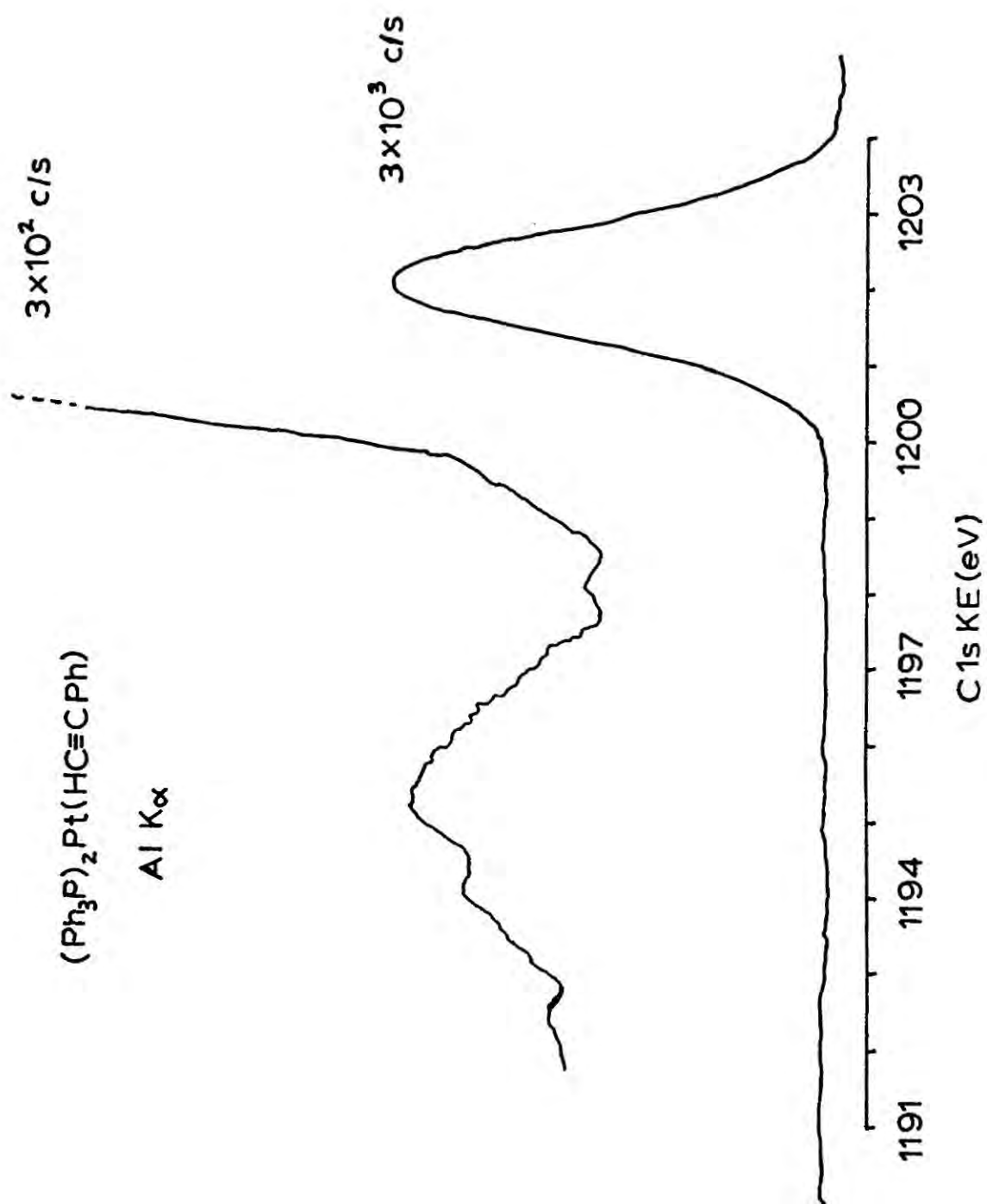


FIGURE 2.3

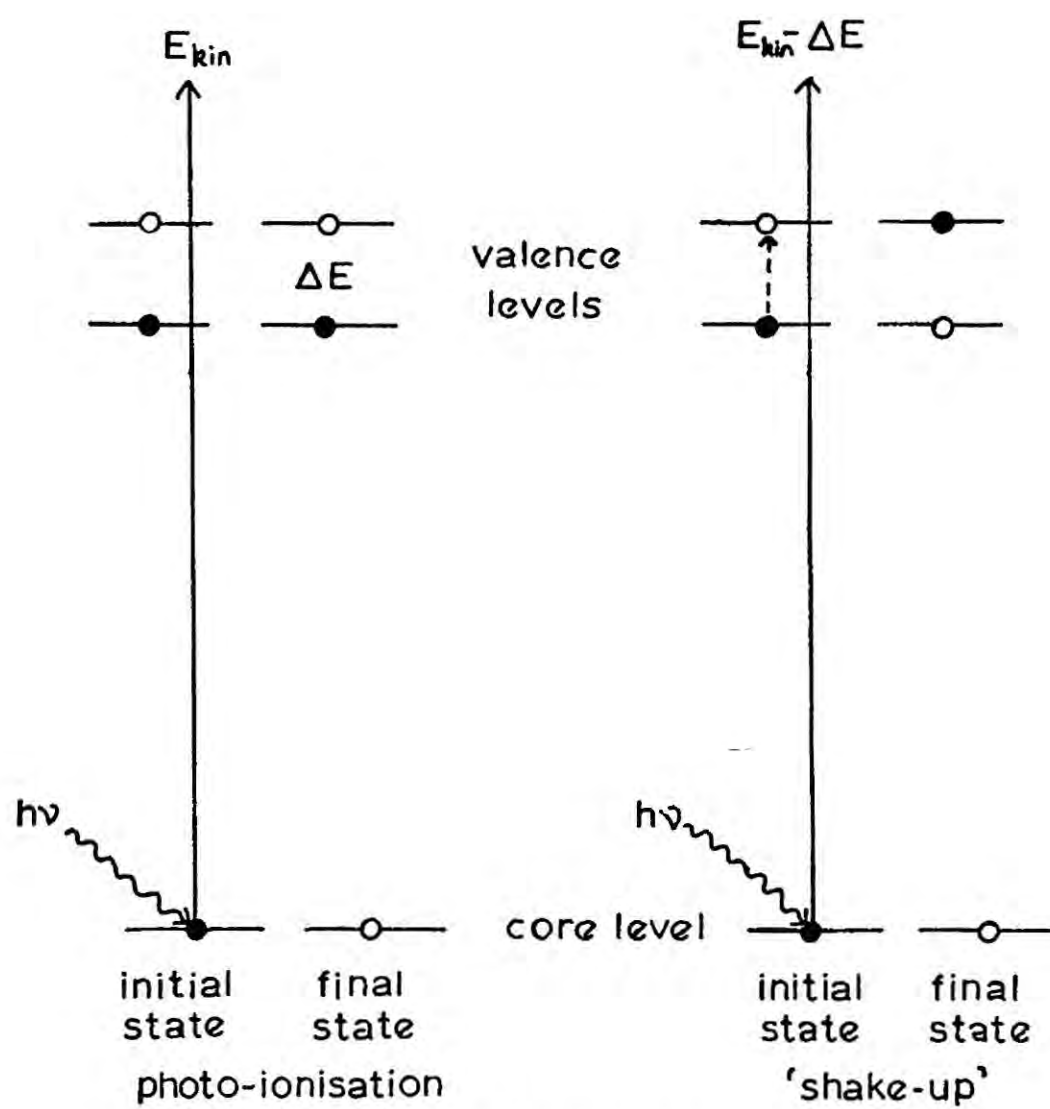


FIGURE 2.4

excitation process equivalent to 'shake-up'. For the carbonyls it is suggested¹¹¹ that, since satellite peaks observed for complexed CO are absent in the spectra of free CO, additional valence electron relaxation is possible for CO on complexation thus allowing transitions to 'shake-up' states normally forbidden in the frozen valence shell approximation (Koopmans theorem). It is interesting to find, therefore, a satellite peak of the same order of relative intensity for the Cls peak from triphenylphosphine itself. This satellite also represents an energy loss of ~ 6 eV (Fig. 2.5).

The existence of satellites in the spectra of these compounds and the free Ph_3P ligand has also been noted by Mason et al⁸⁹ but not discussed in detail. In particular no details of the P2p peak shape for free Ph_3P were given. In this work a marked broadening of this peak compared with complexed Ph_3P and also a colouration effect on irradiation (white \rightarrow pink) was observed. Because of this latter complication it would be unwise at this stage to speculate further on the origin of these satellites. These results indicate, however, that more detailed investigations in this area are necessary before we can utilise fully this additional information contained in the photoelectron spectra.

A final point concerns the search for Cls satellites from $(\text{Ph}_2\text{MeP})_2\text{Pt}[\text{C}_2\text{F}_4]$. As Figure 2.6 shows there is no evidence for even a very low intensity peak shifted ~ 6 eV from the main peak as found in the other complexes and as reported for $(\text{Ph}_3\text{P})_2\text{Pt}[\text{C}_2\text{F}_4]$.⁸⁹ This would seem to be additional evidence for a suggestion that the satellites are due to a 'shake-up' process involving valence bands

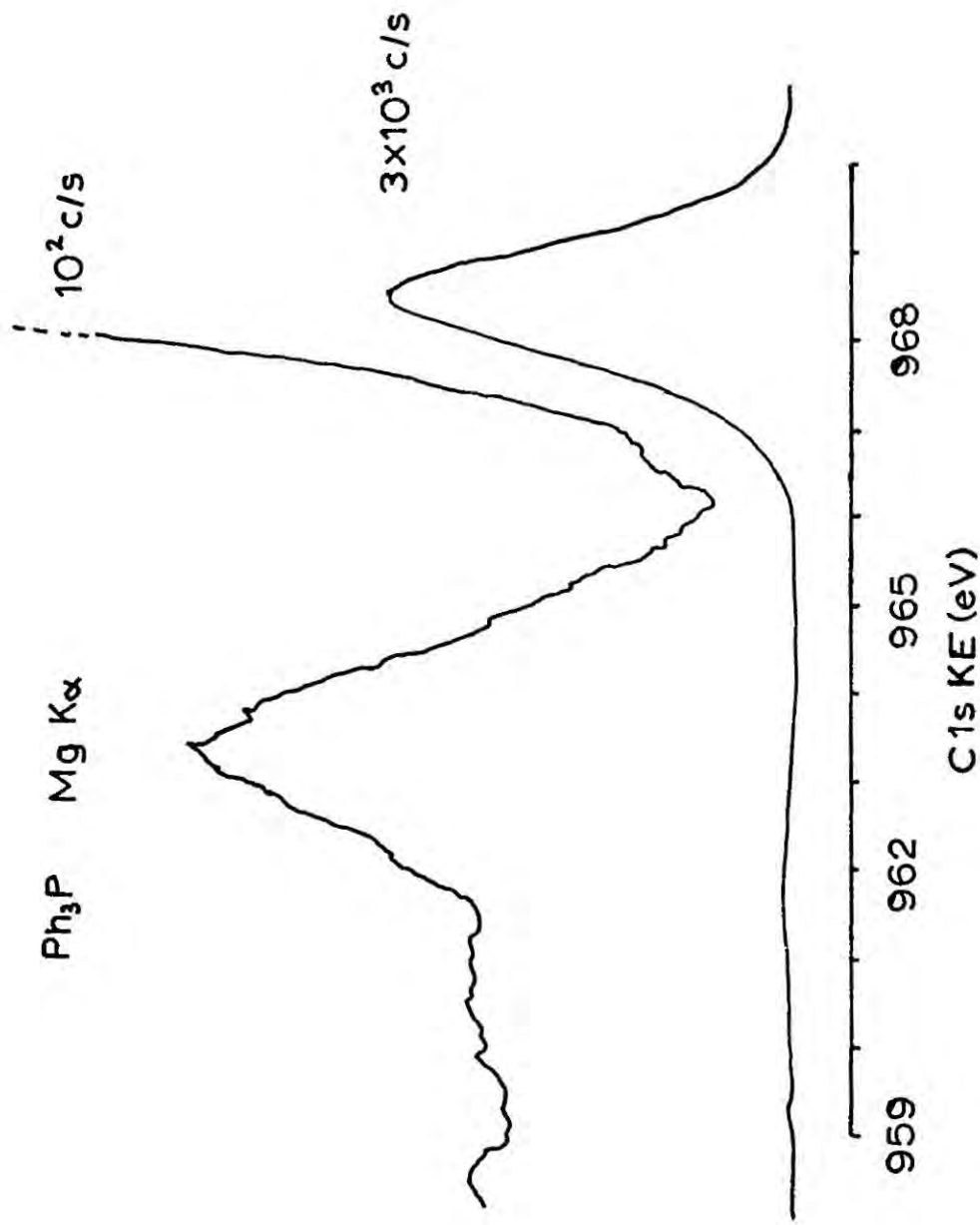
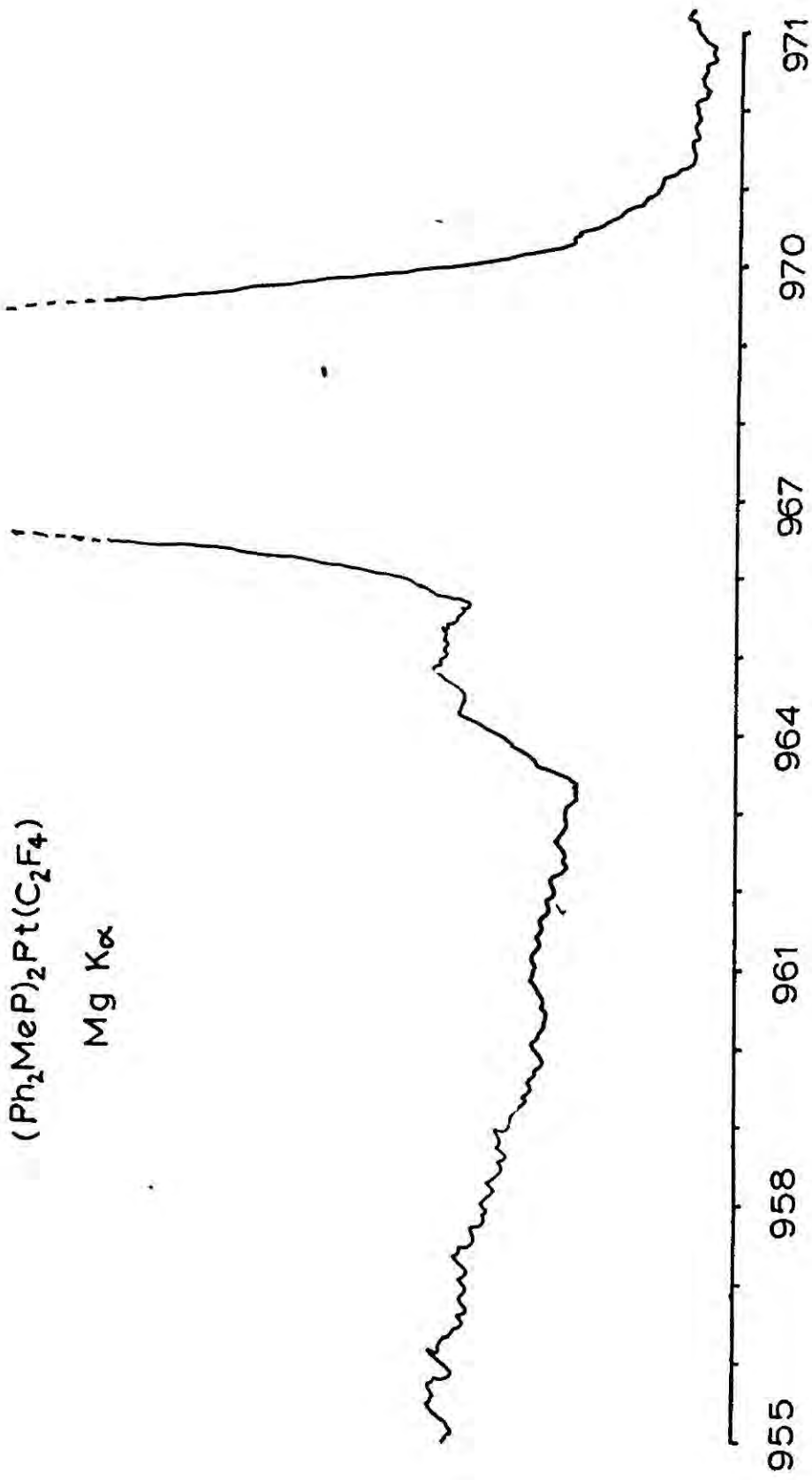


FIGURE 2.5



C1s KE (eV)

FIGURE 2.6

of Ph_3P . However, there is a distinct peak discernable at ~ 3.5 eV lower K.E. The expected region for the carbon atoms of the C_2F_4 ligand would be about 6 eV lower K.E. than the phosphine carbon atoms. It is possible that this peak represents the olefinic carbons since the transfer of charge to them from the metal would offset this shift. Even so, it is necessary to invoke a 2.5 eV decrease in the carbon B.E's relative to free C_2F_4 which is substantially greater than the corresponding decrease for C_2H_4 (~ 1.6 eV). While this may seem intuitively reasonable it is somewhat incompatible with the fact noted above, namely that the $\text{Pt}4f_{7/2}$ binding energy in this complex appears slightly lower than the other olefin complexes.

(ii) $(\text{R}_3\text{P})_2\text{PtXY}$ complexes.

(a) Introduction.

Having found the B.E. difference between formally Pt^0 and Pt^{II} complexes to be small - indeed, within the oxidation state formalism, complexes $(\text{R}_3\text{P})_2\text{PtL}$ (L = olefin, acetylene) are better described as Pt^{II} complexes - it seemed interesting to explore the range of binding energies in ' Pt^{II} ' complexes. In order to best judge the effect of various ligands, complexes of fixed stereochemistry were chosen: $\text{trans}-(\text{R}_3\text{P})_2\text{PtXY}$. Differences in B.E. data may be observed between cis- and trans-isomers of a given complex but this is discussed more fully in the following chapter.

(b) Results and Discussion.

The results are summarised in Table 2.2.

In order to correct for charging effects the B.E. data is

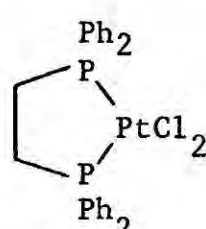
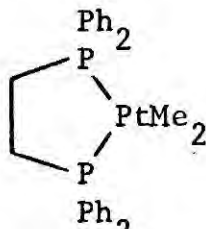
referred to the carbon atoms of the phosphine ligands at 285.0 eV. In considering the data in Table 2.2 it is important to establish that the effect of changing the group R in $(R_3P)_2PtXY$ does not have a significant effect on the B.E.s of the metal and other ligands. The first three complexes in Table 2.3 illustrate that within experimental error (± 0.2 eV) there is no effect on changing the R group from alkyl to aryl or in substituting a chelating diphosphine ligand for two monodentate phosphines. It is especially noticeable that throughout the whole range of cis- and trans-complexes the phosphorus B.E. does not vary significantly and is the same as observed for the olefin and acetylene complexes at 130.8 ± 0.3 eV.

From Table 2.2 it can be seen that the platinum B.E. in trans- $(R_3P)_2PtXY$ increases in the order $XY = Me_2 < I_2 \approx H,Cl < Cl_2 < (CN)_2$. In a preliminary report⁵⁸ of some of these results it was indicated that the $Pt4f_{7/2}$ B.E. for trans- $(Me_3P)_2PtI_2$ was greater than for $(nBu_3P)_2PtCl_2$ and this was interpreted as a confirmation of Parshall's order of σ -donation ($Cl^- > I^-$) obtained from ^{19}F n.m.r. studies.^{113,114} This result has been challenged recently by Riggs.⁶¹ A redetermination showed that the fairly broad Cls peak in the original spectrum was due to non-coincidence of the peak from the complex and an additional peak from contamination on the gold backing. The seriousness of this effect, which can occur when there are few carbon atoms in the sample being studied was only fully realised when a study of Zeise's salt was made (see Chapter III). In this present case it has now been shown that the peak maximum used for reference purposes, did not in fact correspond to the methyl carbons peak. Taking the

TABLE 2.2

(trans) Complex	Core Binding Energies (eV)		
	Pt4f _{7/2}	P2p _{3/2}	Cl2p _{3/2}
(ⁿ Bu ₃ P) ₂ PtCl ₂	72.3	130.7	198.1
(Ph ₃ P) ₂ PtHCl	71.9	131.0	197.3
(Me ₃ P) ₂ PtI ₂	71.8	130.5	- I3d _{5/2} 620.5
(Me ₃ P) ₂ Pt(CN) ₂	72.8	130.7	- N1s 398.6
(Ph ₃ P) ₂ PtMe ₂	71.6	130.6	-

TABLE 2.3

(cis) Complex	Core Binding Energies (eV)		
	Pt4f _{7/2}	P2p _{3/2}	Cl2p _{3/2}
(ⁿ Bu ₃ P) ₂ PtCl ₂	72.3	130.7	197.7
(Ph ₃ P) ₂ PtCl ₂	72.5	130.9	197.9
	72.4	130.7	197.8
	71.5	130.5	-

other component reverses the order as shown. To check this conclusion the spectrum of $\text{trans}-(\text{Me}_3\text{As})_2\text{PtI}_2$ was recorded using a thin film (from CHCl_3 solution) on carefully cleaned gold. The close similarity between complexes with arsine and equivalent phosphine ligands has been established (see Chapter IV) but a further comparison is given here.

TABLE 2.4

Complex	Core Binding Energies (Cls = 285.0 eV)				
	Pt4f _{7/2}	P2p _{3/2}	As3d _{5/2}	N1s	I3d _{5/2}
$\text{trans}-(\text{Me}_3\text{P})_2\text{Pt}(\text{CN})_2$	72.8	130.7	-	398.6	-
$\text{trans}-(\text{Me}_3\text{As})_2\text{Pt}(\text{CN})_2$	72.7	-	43.0	398.4	-
$\text{trans}-(\text{Me}_3\text{As})_2\text{PtI}_2$	71.8	-	42.6	-	620.7
$\text{trans}-(\text{Me}_3\text{P})_2\text{PtI}_2$	71.8	130.5	-	-	620.5

The first two lines of Table 2.4 illustrate the point; the metal BE and the BE of the nitrogen in the cyanide ligand is independent of the other ligands. Thus the coincidence of platinum and iodine BE's in the di-iodides indicates the previously reported platinum BE in $\text{trans}-(\text{Me}_3\text{P})_2\text{PtI}_2$ to be incorrect, the above value being much more consistent.

From the data in Table 2.4 it is apparent that the As3d_{5/2} BE and, though with lower significance, the P2p_{3/2} BE is lower for the cyanide complexes than for the iodides. The electron withdrawing demand of the CN⁻ ligand on the metal is such that some electron density is also removed from the arsine/phosphine ligands compared with the iodides. The fact that this effect is most marked for the

arsine ligand presumably reflects its higher polarisability.

The order of BE's for platinum in this series of trans complexes fits in with the most intuitively likely order - where the BE of the metal increases with increasing electronegativity of X and Y. These results are in very good agreement with recently published data⁶¹ on a series of complexes $(Et_3P)_2PtXY$ in which a linear correlation was found between platinum BE's and the sum of the 'effective' electronegativities of X and Y (calculated for polyatomic groups by taking the arithmetic average of individual Pauling atomic electronegativities).

The low BE of platinum in trans- $(Ph_3P)_2PtMe_2$ is reproduced in the chelate complex $(Ph_2P(CH_2)_2PPh_2)PtMe_2$, of necessity with cis configuration, shown in Table 2.3. This is the lowest BE observed for a Pt^{II} complex and illustrates the strong σ -donor properties of the CH_3 ligand. Replacement of the CH_3 group by any other ligand (X) increases the metal BE by either σ -withdrawing (electronegativity) effects (e.g. X = halogen) or through π -backbonding effects (e.g. X = olefin and, possibly, CN). The range of BE's observed for Pt^{II} complexes is thus about 1.3 eV.

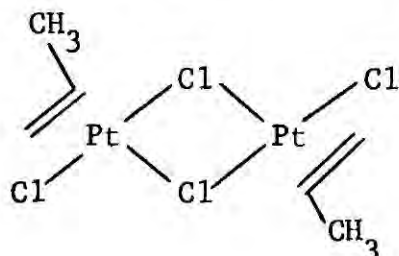
CHAPTER III

ESCA STUDIES OF SQUARE-PLANAR PLATINUM COMPLEXES (II)

CORRELATIONS WITH N.Q.R. STUDIES.

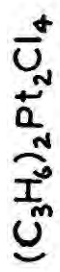
(i) N.q.r. CorrelationsIntroduction.

The search for olefin containing platinum complexes, for reasons discussed in the previous chapter, led to the study of the dinuclear complex $(C_3H_6)_2Pt_2Cl_4$ which has the structure:



Because of problems in obtaining a good thin coverage on gold it proved difficult to gain definitive information on the carbon BE's. However, the interesting feature which did emerge was the inequivalence of the bridging and terminal chlorines.

In square-planar platinum^{II} chlorides, some examples of which have already been discussed above, the Cl(2p) core levels appear as spin-orbit split (1.7eV) doublets in the ratio $2p_{1/2}:2p_{3/2} = 1:2$ the smaller $2p_{1/2}$ peak being seen as a fairly well resolved shoulder on the low KE (high BE) side of the total peak. In the Cl2p spectrum from this complex, however, no such shoulder can be seen and the peak is considerably broadened. In fact this peak can be satisfactorily deconvoluted into two normal Cl2p doublets with a separation of 1.1 eV (Fig. 3.1). The problem which now arises is the assignment of the two chlorine BE's. A qualitative correlation between Cl(2p) BE and ^{35}Cl n.q.r. frequencies ($^{35}\nu$) is to be expected¹¹⁵ and from the n.q.r. data^{116,117} on this complex ($^{35}\nu = 24.12$ (terminal), 15.95 (bridging) MHz) the higher BE Cl 2p peak can be tentatively assigned to the terminal chlorine. It is of interest, therefore, to



Mg $K\alpha$

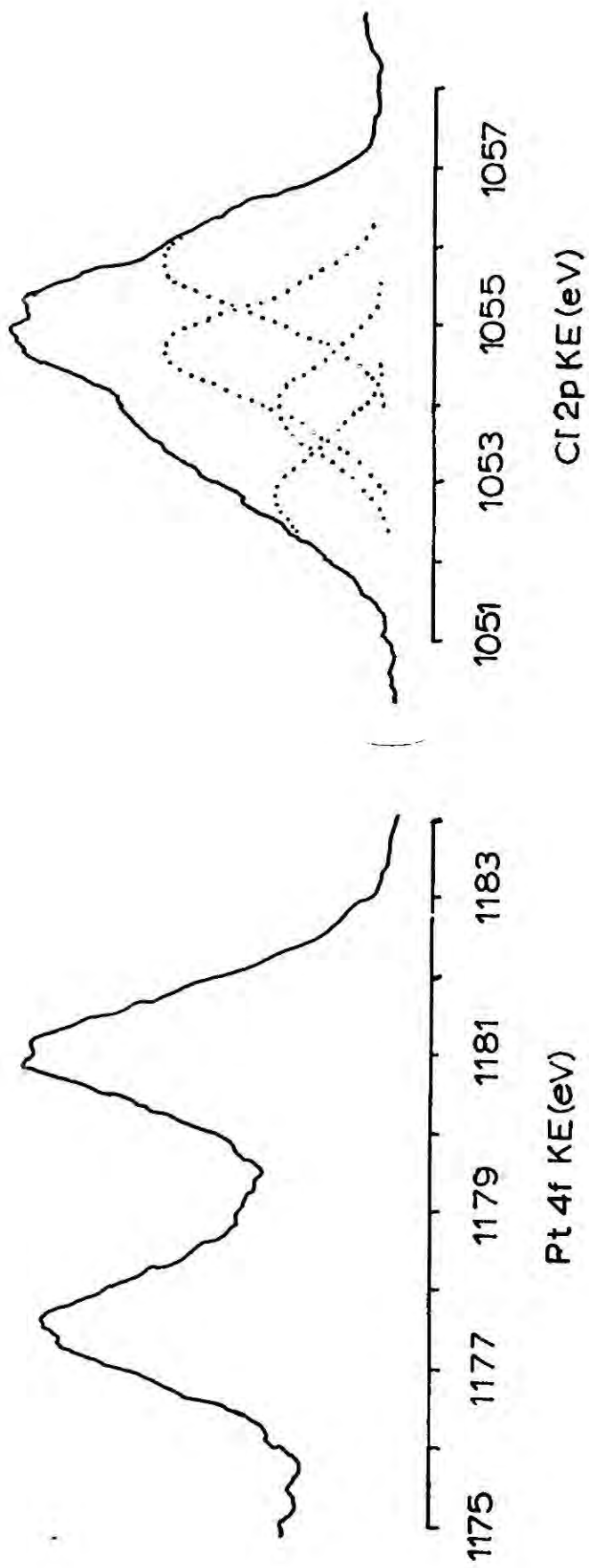


FIGURE 3.1

examine this correlation more closely.

^{35}Cl n.q.r. frequencies have recently been reported,^{116,118} for a number of complexes of the type L_2MCl_2 ($\text{M} = \text{Ni}^{\text{II}}, \text{Pd}^{\text{II}}$ and Pt^{II}) and for various dimeric Pt^{II} complexes with chlorine in terminal and bridging situations. ESCA data has been obtained on many of these complexes, in most cases using the same samples.

Experimental.

The procedures used were similar to those described in Chapter II. Samples were studied as thin films on a gold backing when solubilities in suitable solvents (CHCl_3 , CH_2Cl_2) were satisfactory and/or as powders pressed onto scotch tape. Relative B.E.'s obtained in either case were always within the estimated experimental error (± 0.2 eV) but sample charging had considerable and variable effect on the 'absolute' BE's. Thus, as before, attention is confined to those complexes which can be directly compared through use of an 'internal reference level' - again the Cls level from alkyl or aryl groups on polyatomic ligands (e.g. R_2S , R_3P), taken to be 285.0 eV.

Results and Discussion.

Table 3.1 gives the BE's of the various core levels measured for these complexes. Although it is the chlorine BE's which are to be expressly considered here, some brief comments can be made on the other BE data. In contrast to the series $(\text{R}_3\text{P})_2\text{PtXY}$, considered in the previous chapter, in which the effect of changing X and Y on the metal electron density was observed, the series L_2PtCl_2 contained in Table 3.1 illustrates the cis and trans influence of groups L on metal and chlorine BE's. It would appear

that the Cl^- ligands dominate the situation and that the central platinum atom mostly acts as an agent for electron transfer from L to Cl, its BE varying only slightly with L (the value for $\text{cis}-(\text{Et}_2\text{S})_2\text{PtCl}_2$ seems anomalously high). Thus the electron density around platinum is little different also for the dinuclear species $\beta-(^n\text{Pr}_3\text{P})_2\text{Pt}_2\text{Cl}_4$. As might be expected from the discussion in Section (iii) of Chapter II changing the bridging group from -Cl- to -SCN- in the latter complex significantly increases the platinum BE due to the greater electronegativity of the SCN ligand.

Table 3.2. collects the $\text{Cl}2p_{3/2}$ BE data for these same complexes and their associated ^{35}Cl n.q.r. frequencies ($^{35}\nu$). It is convenient at this point to consider theoretically the relationship between binding energies and n.q.r. frequencies.

In the electrostatic potential model developed by Siegbahn and co-workers,² shifts in core BE's may be related to the charge distribution by the equation

$$E^i = E_o^i + kq_i + \sum_{j \neq i} \frac{q_j}{r_{ij}} \quad (1)$$

where E_o^i is a reference level and the second term represents the potential from the charge at the atom considered. The third term is an intramolecular 'Madelung' type potential and accounts for the potential from charges in the rest of the molecule. In general the shift in BE of a given core level (e.g. $\text{Cl}2p_{3/2}$ considered here) is dominated by the charge on the atom concerned, the potential from other atoms being much smaller and opposite in sign. In the closely related series of molecules described here, therefore, the shifts in a given core level will in some measure reflect differences in charge distribution.

TABLE 3.1

Complexes	Core Binding Energies (eV)				
	Pt4f _{7/2}	Cl2p _{3/2}	P2p _{3/2}	S 2p _{3/2}	N1s
β -(ⁿ Pr ₃ P) ₂ Pt ₂ Cl ₄	72.1	198.5	130.6	-	-
		197.3			
β -(ⁿ Pr ₃ P) ₂ Pt ₂ (SCN) ₂ Cl ₂	72.9	198.3	130.9	162.9	399.9
cis-(ⁿ Bu ₃ P) ₂ PtCl ₂	72.3	197.7	130.7	-	-
trans-(ⁿ Bu ₃ P) ₂ PtCl ₂	72.3	198.1	130.7	-	-
cis-(Et ₂ S) ₂ PtCl ₂	72.7	197.9	-	164.3	-
trans-(Et ₂ S) ₂ PtCl ₂	72.3	198.1	-	164.4	-
(dipy)PtCl ₂	72.2	197.8	-	-	400.6
cis-(Ph ₃ P) ₂ PtCl ₂	72.5	197.9	130.9	-	-
trans-py ₂ PtCl ₂	72.1	197.9	-	-	401.1
trans-(Ph ₃ P) ₂ PtHCl	71.9	197.3	131.0	-	-

TABLE 3.2

Complex	35_{ν} a	$\text{Cl}2p_{3/2}$ B. E. b
$\beta\text{-}(\text{}^n\text{Pr}_3\text{P})_2\text{Pt}_2\text{Cl}_4$	22.36	198.5
	15.46	197.3
$\beta\text{-}(\text{}^n\text{Pr}_3\text{P})_2\text{Pt}_2(\text{SCN})_2\text{Cl}_2$	21.50	198.3
$\text{cis-}(\text{}^n\text{Bu}_3\text{P})_2\text{PtCl}_2$	17.84	197.7
$\text{trans-}(\text{}^n\text{Bu}_3\text{P})_2\text{PtCl}_2$	21.0	198.1
$\text{cis-}(\text{Et}_2\text{S})_2\text{PtCl}_2$	19.2	197.9
$\text{trans-}(\text{Et}_2\text{S})_2\text{PtCl}_2$	20.3	198.1
$(\text{dipy})\text{PtCl}_2$	18.98	197.8
$\text{cis-}(\text{Ph}_3\text{P})_2\text{PtCl}_2$	19.8	197.9
$\text{trans-py}_2\text{PtCl}_2$	19.62	197.9
$\text{trans-}(\text{Ph}_3\text{P})_2\text{PtHCl}$	-	197.3
$\text{trans-}(\text{PhMe}_2\text{P})_2\text{PtHCl}$	14.43	-

a Data taken from references 116 — 118 unless otherwise stated.

b Estimated accurate to ± 0.2 eV.

The Townes-Daily approximation^{119,120} leads to an expression for the ^{35}Cl n.q.r. frequency of the form

$$^{35}\nu = [(1-S)\sigma - \frac{1}{2}\pi] e^2 Qq_{\text{At}} / 2h \quad (2)$$

where chlorine employs a $3p_z$ orbital in a σ bond of covalent character σ and its $3p_x$ and $3p_y$ orbitals in π bonds of covalent character π . S is the degree of hybridisation of the $3s$ with the $3p_z$ orbital and $e^2 Qq_{\text{At}}/h$ is the quadrupole coupling constant for the free chlorine atom. Assuming that chlorine hybridisation changes for closely related complexes can be neglected (reference 116 and references therein) (i.e. $\Delta(1-S)=0$) and participation by chlorine in π -bonding is not significant (i.e. $\pi=0$) then (2) reduces to:

$$^{35}\nu = c\sigma \quad (3)$$

where c is a constant. Thus, decreasing population of the $3p_z$ orbital on chlorine (decreasing negative charge; increasing σ) gives increasing n.q.r. frequencies and, from equation (1) increasing BE's. In this series of complexes, therefore, a relationship might be expected between $^{35}\nu$ and $\text{Cl}_{2p_{3/2}}$ BE. Figure 3.2. shows a plot of n.q.r. frequency against BE.

The anticipated increase of $^{35}\nu$ with increase in $\text{Cl}_{2p_{3/2}}$ BE is clearly shown even though the change in BE is < 1.5 eV. Bearing in mind the many simplifications introduced in the above theory, the correlation is surprisingly good ($R^2 = 0.96$).

The two n.q.r. frequencies observed for $\text{trans-}(\text{}^n\text{Pr})_2\text{Pt}_2\text{Cl}_4$ fall at the extremes of the curve. It is reasonable to assign the higher frequency to the terminal Cl since this is in the same region as the other terminal chlorines in a dinuclear species. Also Fryer's correlation¹¹⁸ between $^{35}\nu$ and Pt-Cl bond length suggests that the higher frequency

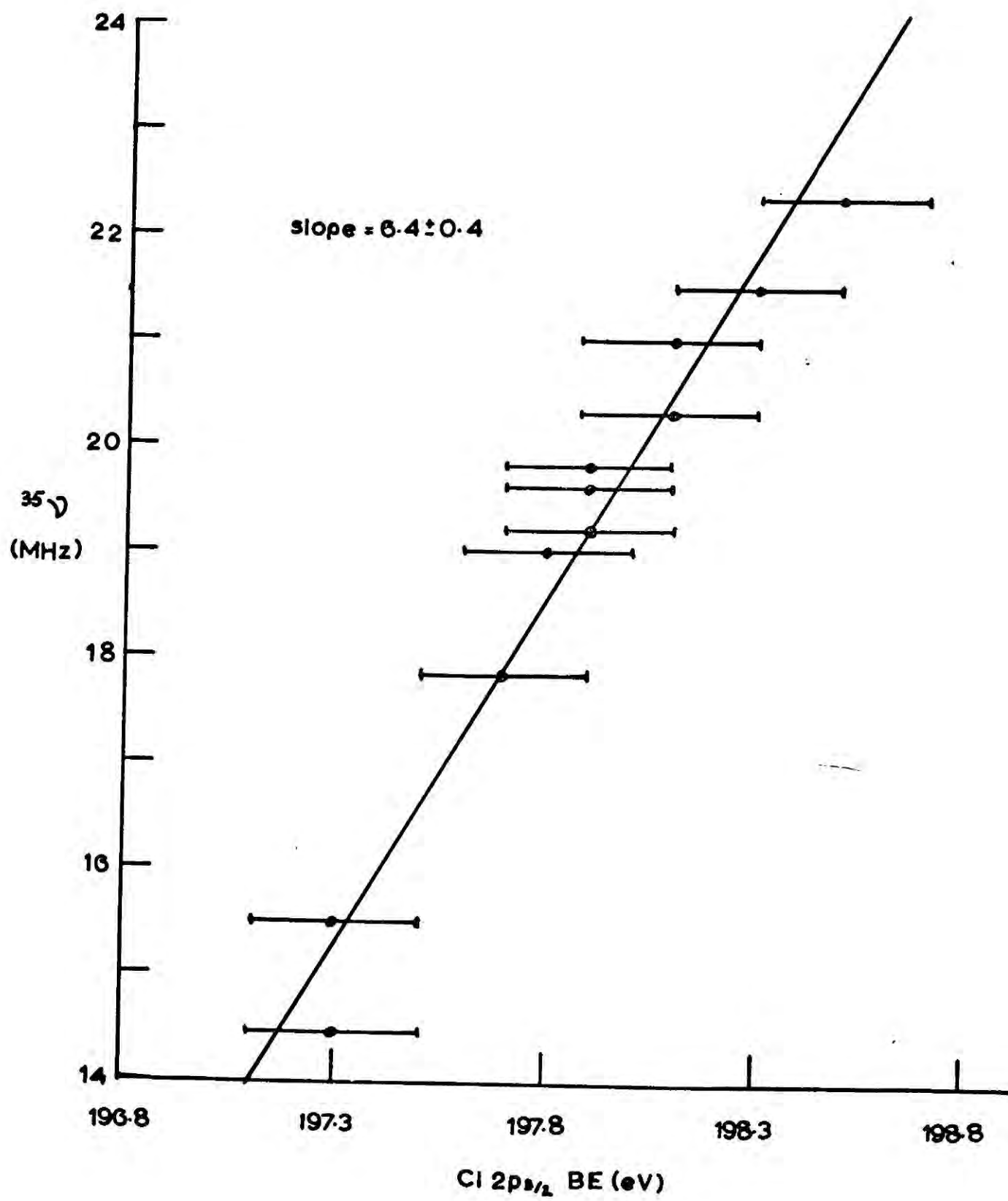


FIGURE 3.2

signal corresponds to the terminal Cl. This means that the bridging chlorines have the lower BE (higher negative charge) which implies that attachment to two Pt centres increases the electron drift towards chlorine.

Two recent studies^{59,60} have come to the opposite general conclusion regarding the relative electron densities at terminal and bridging halogens. The first⁶⁰ found the bromine BE in PdBr_2 (assumed⁶⁰ polymeric with all bridging bromines) to be 0.5 eV higher than in $(\text{Ph}_3\text{P})_2\text{PdBr}_2$ (terminal bromine) whilst the second⁵⁹ found the chlorine BE in PtCl_2 (again polymeric, bridging chlorines only) to be higher than in K_2PtCl_4 or K_2PtCl_6 . These comparisons may not be strictly valid, however, since n.q.r. data¹²¹ shows that the bridge frequencies in polymeric $\alpha\text{-PdCl}_2$ and $\beta\text{-PtCl}_2$ are 6-8 MH_3 higher than those in dimeric complexes, the latter giving lower values of 35ν than terminal chlorines as described above.

The above results indicate that within this closely related series of complexes, the chlorine BE gives a good indication of the effect of changes in overall electron density on the Pt-Cl bond (as paralleled in a more sensitive fashion by n.q.r. studies). The advantage of ESCA is that it gives information, in principle, on all other atoms in the molecule.

Before leaving this correlation it is worth returning to the propene complex mentioned at the beginning of this chapter. From the n.q.r. data and using the correlation in Fig. 3.2 the predicted $\text{Cl}2p_{3/2}$ BE's in this complex would be 197.4 eV for the bridging chlorines and 198.6 eV for the terminal chlorines - a relative shift of 1.2 eV which is in excellent agreement with the observed separation of 1.1 eV (Fig. 3.1). Referring the experimentally observed $\text{Cl}2p_{3/2}$ BE's to these predicted values and correcting the $\text{Pt}4f_{7/2}$ BE accordingly gives the predicted $\text{Pt}4f_{7/2}$ BE to be 72.3 (± 0.3) eV. This is not significantly different from the value for $(^n\text{Pt}_3\text{P})_2\text{Pt}_2\text{Cl}_4$ (Table 3.1) indicating that the electron distribution in the Pt-olefin bond might not be very different from that in the Pt-phosphine bond.

(ii) Zeise's salt and related complexes.Introduction.

The structure of, and electronic distribution in, Zeise's salt have been debated for many years. Apart from its historical significance, this complex is important because it demonstrates the high trans-effect of the ethylene ligand. The kinetic trans-effect in a large number of complexes can be correlated with the trans-influence which ligands exert in the ground state. It can reasonably be argued that a Syrkin-type description¹²² of the trans-influence in terms of σ -donation and rehybridisation of metal orbitals adequately accounts for the mass of data available for these complexes, even when ligands capable of π -bonding (e.g. phosphines)¹²³ are involved. In general the labilisation of the trans ligand is a result of bond weakening in the ground state. This is nicely shown by the n.q.r. work noted above and is supported by the above results.

Ethylene does not appear¹²⁴ to cause weakening of the Pt-N bond in trans-PtCl₂(Me₂NH)(C₂H₄) but its trans-effect is high. Thus previous attempts have been made to observe a ground state effect in Zeise's salt K[PtCl₃(C₂H₄)]·H₂O - as evidenced by some difference in the cis and trans Pt-Cl bonds. Until recently X-ray crystal structure data were inconclusive but it has now been shown¹²⁵ that the previously assumed space group was incorrect. The redetermined structure¹²⁵ gives the average length of the cis Pt-Cl bonds to be 2.305(7)Å which is equal to the Pt-Cl bond length in K₂PtCl₄.¹²⁶ The trans Pt-Cl bond length is 2.327(5)Å, i.e. longer by $\sim 4\sigma$. This could be indicative of trans weakening but the trans Cl interacts with four K⁺ ions (albeit with one only weakly) while the cis Cl's interact with one K⁺ ion and one H₂O molecule. The difference in environment of the trans Cl may

account for some of this lengthening relative to the other two Pt-Cl bonds.

The n.q.r. spectrum of Zeis's salt has been reported^{118,127,128} to consist of three main signals at about 20.4, 20.2 and 16.0 MHz (depending on temperature). The tentative conclusion¹²⁸ that these represent the cis (~ 20 MHz) and trans (16 MHz) chlorines respectively is strengthened by recent data¹²⁹ from related complexes with substituted olefins all of which exhibit signals in these two regions. Lattice effects (which cause the two signals at ~ 20 MHz) are not usually greater than 0.5 MHz. Since these two types of signal differ by ~ 4 MHz it is not unreasonable, on the basis of the above correlation, to expect a difference in the BE's of the cis and trans chlorines (of ~ 0.6 eV), if the n.q.r. data is reflecting a difference in electron population on the chlorines.

The complexes $M^+[LPtCl_3^-]$ ($M^+ = K^+, Pr_4N^+$; $L = C_2H_4, C_3H_6, Me_3P, Me_3As$) and $[M^+]_2[PtCl_4^{2-}]$ ($M^+ = K^+, Me_4N^+$) have been investigated by ESCA to check this and also to obtain a picture of the overall electron distributions.

Results and Discussion

All the samples were studied as powders on Scotch tape. The BE data are shown in Table 3.3. In examining these data a number of important points should be borne in mind. As discussed above charging effects demand caution in making comparisons between different complexes, especially since it has been found that sample charging can be more severe for ionic solids than for molecular ones. Thus each triplet of complexes is internally referenced either to the $K2p_{3/2}$ level or to the N1s level, from the respective cation, since it is assumed (with some experimental justification, see below) that these will not be greatly affected by the

TABLE 3.3

	Binding Energies		
	K2p _{3/2}	Pt4f _{7/2}	Cl2p _{3/2}
K ₂ PtCl ₄	294.8 ^a	73.9	200.3 ^b
K[(C ₂ H ₄) PtCl ₃]	294.8	74.5	200.4(2) 200.1(1) ^c
K[(C ₃ H ₆) Pt Cl ₃]	294.8	74.3	200.4(2) 199.6(1) ^c
	N1s	Pt4f _{7/2}	Cl2p _{3/2}
[Me ₄ N]PtCl ₄	404.1 ^a	73.5	199.5
[Pr ₄ N][Me ₃ PPtCl ₃]	404.1	73.7	199.8(2) 199.3(1) ^c
[Pr ₄ N][Me ₃ AsPtCl ₃]	404.1	73.7	199.72(2)199.3(1) ^c

a Relative BE's from a mixture of K₂PtCl₄ and (Me₄N)₂PtCl₄, see discussion.

b Estimated errors between samples \pm 0.2 eV.

Estimated errors within chlorine levels for a single complex \pm 0.1 eV.

c Deconvolutions were made using a Dupont 310 curve resolver. Figures in parentheses refer to relative ratios.

relatively small changes in the structure of the anion. In an attempt to reference both sets of complexes to the same BE scale an intimately ground mixture of K_2PtCl_4 and $(Me_4N)_2PtCl_4$ was studied so as to directly relate the K2p and N1s levels. The results of this experiment are worthy of extra comment..

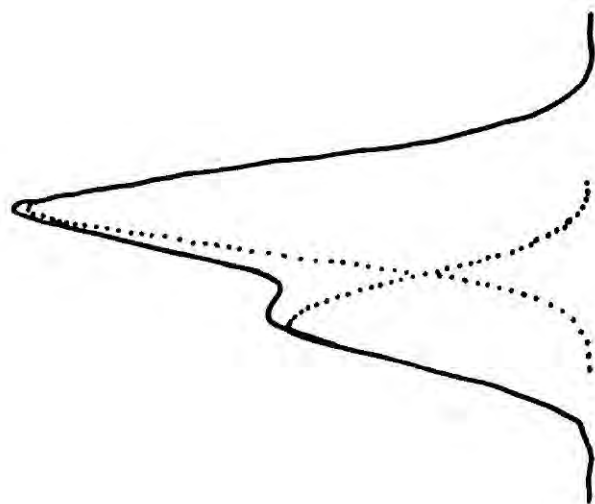
The chlorine 2p peak was broad and not resolved into the component $2p_{1/2,3/2}$ peaks (in contrast to the peaks from each complex investigated singly) and the $Pt4f_{5/2,7/2}$ doublet was likewise significantly broadened. By relating the integrated peak areas from spectra of the mixture and the individual components it was possible to show that the surface was stoichiometric (i.e. composed of an intimate mixture of microcrystallites of the two components) and to obtain the fraction of $PtCl_4^{2-}$ ions present from each salt (f_1 and f_2). Using linewidths and separations from the K_2PtCl_4 spectra the broad Pt(4f) and Cl(2p) spectra obtained from the mixture could be deconvoluted. The area ratios obtained were in very good agreement with f_1 and f_2 while the shifts indicated the Pt and Cl binding energies in K_2PtCl_4 to be higher than in $(Me_4N)_2PtCl_4$ by 0.7 and 0.9 eV respectively. The internal check of calculating the Pt(4f) and Cl(2p) BE's of each component in the mixture from a knowledge of the relative BE's of the reference N1s and K(2p) levels (of the cations) in the mixture and separately led to the same conclusion. A possible explanation of this effect is that the Madelung correction in equation (1), which in ionic crystals should be summed over the entire lattice, differs significantly for the two crystal lattices and thus has increased importance.

Any difference in the BE's of the cis and trans chlorines in $[LPtCl_3]^-$ will be manifested as a change in the line shape of the $Cl2p_{1/2,3/2}$

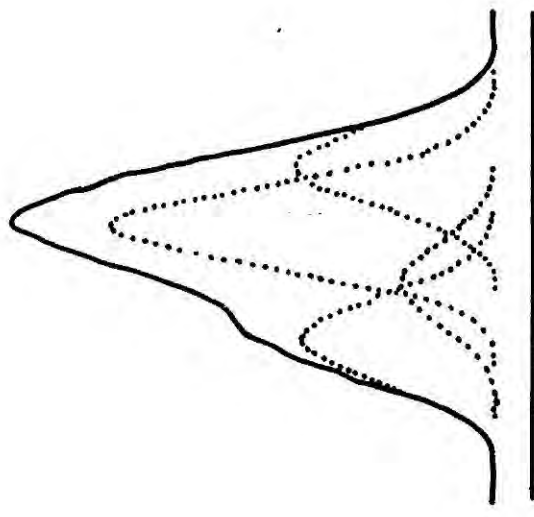
spin-orbital split doublet due to overlap of the two sets of peaks, as found for the dinuclear complexes with terminal and bridged chlorines. Differences in BE are expected to be less than in these cases, however, so it is important that the line shape for a single chlorine be well characterised. Since all the samples were highly pure and crystalline we do not consider line broadening effects due to sample inhomogeneity to make any contribution. Figure 3.3 shows the deconvoluted Cl2p_{1/2,3/2} doublet (area ratio 1:2) from K₂PtCl₄ (powder sample) in which all chlorines are equivalent; the separation is 1.65 (± 0.05)eV. As a check the same peaks were used to fit the Cl2p_{1/2,3/2} doublet from cis (nBu₃P)₂PtCl₂ studied as a very thin film on gold (under these conditions sample charging and inhomogeneity are minimised). No change in peak widths or separation was required to give an exact 1:2 match. This line shape is, therefore, taken as standard for a single chlorine.

All the [LPtCl₃]⁻ complexes studied gave Cl2p spectra which could not be fitted by a single doublet of standard line shape. The deconvoluted procedure adopted was to take two sets of standard doublets and fit these to the experimental peak shape. Only one fit in every case gave standard 2p_{1/2,3/2} separations in each doublet (1.7 eV) and a consistent separation of the two 2p_{1/2} and 2p_{3/2} peaks while at the same time satisfying the criteria of correct area ratios (1:2 in each doublet; overall 2:1 doublets for the two types). The consistent result for all four complexes indicates that the single chlorine has a lower BE than the other two chlorines. Two examples of the deconvoluted Cl2p peak are shown in Figure 3.3.

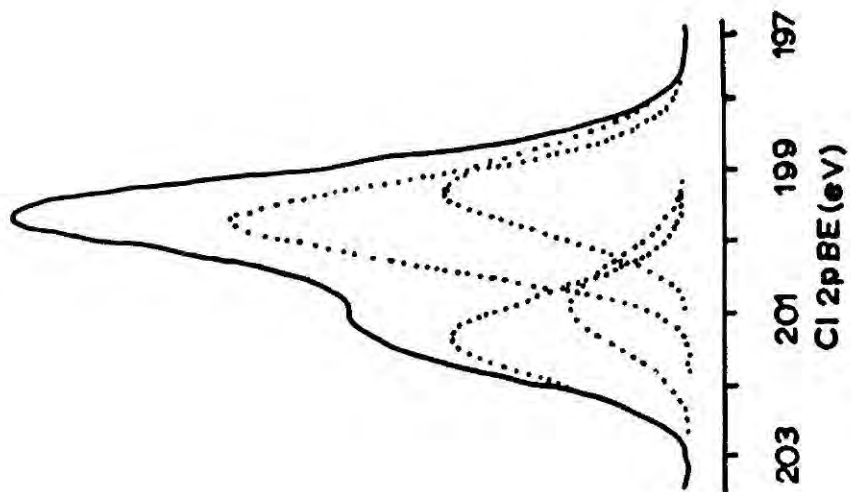
K_2PtCl_4
or $cis\text{-}(^nBu_3P)_2PtCl_2$



$K[(C_3H_5)_2PtCl_2]$



$[Pt_4N][Me_3AsPtCl_2]$



Cl 2p_{1/2}, 3/2

FIGURE 3.3

As indicated above a comparison cannot be meaningfully made between the absolute values of the data in the two halves of Table 3.3. However, the following points arise from a consideration of relative shifts where direct comparisons can be safely made:

(i) The effect of replacing one Cl^- ligand in $[\text{PtCl}_4]^{2-}$ by a neutral ligand L to give $[\text{LptCl}_3]$ is to split the remaining chlorine ligands into two differing types in the ratio 2:1 and these can, therefore, be assigned to the cis and trans positions respectively. Hence ESCA detects a ground state influence of L on the remaining ligands.

(ii) There is evidence that relative to PtCl_4^{2-} the BE of the cis chlorines is raised (decrease in negative charge) and that of the trans chlorine is lowered. This is in agreement with other ground state phenomena which relate to the trans-effect: increase in Pt-Cl bond length is accompanied by electron drift to chlorine.¹¹⁶ The correlation of chlorine BE with $^{35}\nu$ is again apparent since the single n.q.r. signal from K_2PtCl_4 is at 17.93 MHz while the two types of signal in $\text{K}[(\text{olefin})\text{PtCl}_3]$ are in the region of 16 and 20 MHz respectively.¹²⁹ Interestingly, these changes in electron density at chlorine are accompanied by a slight increase in BE of the central platinum which can only indicate some degree of $\text{Pt} \rightarrow \text{L}$ back donation. Significantly this effect is more noticeable when L = olefin and is greatest of all for ethylene.

In connection with this last point it is of obvious interest to gain some additional information on the electron distribution in the Pt-olefin bond. The main contributor to the Cls peak in the spectrum of Zeise's salt is the scotch tape backing (or possibly surface hydrocarbon) but a definite shoulder can be confidently assigned to the ethylenic carbons on the basis of its area ratio relative to the chlorine peak. The BE of

these carbons is ~ 283.4 eV which compares with an expected value of ~ 284.9 eV for the free ligand. These figures reveal a considerable electron transfer from metal to olefin, which result is understandable in terms of the Dewar-Chatt-Duncanson model⁸⁴ where the dominating feature is back donation from filled Pt d orbitals into π^* anti-bonding orbitals of the olefin. The 0.6 eV increase in Pt4f binding energy in going from $[\text{PtCl}_4]^{2-}$ to $[\text{PtCl}_3(\text{C}_2\text{H}_4)]^-$ is confirmatory information. The olefinic carbon BE is similar to that obtained previously for the neutral complex $(\text{Ph}_3\text{P})_2\text{Pt}(\text{C}_2\text{H}_4)$. The extra methyl carbons in $\text{K}[\text{PtCl}_3(\text{C}_3\text{H}_6)]$ are an additional contribution to the Cls peak from this complex and consequently no shoulder due to olefinic carbons is apparent although the breadth of the peak indicates that a qualitatively similar situation holds as for Zeise's salt.

In summary the cis and trans chlorines in $[\text{LPtCl}_3]$ have different electronic environments, the trans chlorine having the higher negative charge. Both cis and trans effects of L are discernable and the correlations with n.q.r. data indicate that these most probably arise through σ bonding mechanisms. Back bonding to the potential π -acceptors appears to occur, especially for olefinic ligands. These conclusions are in general agreement with those arrived at from semi-empirical LCAO-MO calculations on Zeise' salt itself.¹²⁷

In view of the fact, noted in Section (i), that a correlation between n.q.r. frequencies and BE's for chlorine is dependant on the species having very similar structures and geometries, it is interesting to compare the above results for square planar complexes with similar results for the octahedral case.

The ESCA spectra of K_2PtCl_6 were obtained for the powder pressed onto scotch tape. The spectra of K_2PtCl_4 and $K[PtCl_3 \cdot C_2H_4]$ described above had been obtained in similar fashion and the Cls peak from the backing tape (or adsorbed hydrocarbon) was seen to remain at constant separation (8.3eV) from the $K2p_{3/2}$ peak. This constituted the justification for referencing all levels in these and analogous complexes to the $K2p_{3/2}$ level. Since the same separation of Cls (backing) and $K2p_{3/2}$ peaks were observed in the spectra of K_2PtCl_6 it may be assumed that the $K2p_{3/2}$ BE is the same in this complex also. The observed BE's corrected for charging effects, are shown in Table 3.4.

TABLE 3.4

	Core Binding Energies (eV)			
	$K2p_{3/2}$	$Pt4f_{7/2}$	$Cl2p_{3/2}$	^{35}v
K_2PtCl_4	294.8	73.9	200.3	17.95 ^a
K_2PtCl_6	294.8	76.1	200.1	25.81 ^b 25.91 ^c

a ref 116, recorded at 0°C.

b ref 130, recorded at 23.5°C.

c ref 130, recorded at -75°C.

Clearly, as anticipated, the above $Cl2p_{3/2}$ B.E./ ^{35}v correlation has badly broken down because the n.q.r. signal for K_2PtCl_6 is ~ 8 MHz higher than

for K_2PtCl_4 whilst the chlorine BE's are similar, if not slightly lower for the former complex.

The 2.2 eV increase in BE of the central platinum atom in going from the Pt^{II} to the Pt^{IV} complex is intuitively reasonable and is in good agreement with values (2.4 eV) recently reported in the literature.^{59,61} The range of BE's for platinum from the results of this and the previous chapter is thus from 71.4 eV (Pt^0 , metal) to 76.1 eV ($Pt^{IV}Cl_6^{2-}$), i.e. ~ 1.2 eV per unit charge in formal oxidation state. The same conclusion has been arrived at in the most recent publications in this field.^{59,61,62.}

CHAPTER IV

STUDIES OF THE SURFACE ISOMERISATION OF $(\text{Ph}_3\text{P})_2\text{Pt}[\text{C}_2\text{Cl}_4]$ AND

RELATED COMPLEXES

(i) The Surface Isomerisation of $(\text{Ph}_3\text{P})_2\text{Pt}[\text{C}_2\text{Cl}_4]$ Introduction

The complex $(\text{Ph}_3\text{P})_2\text{Pt}(\text{C}_2\text{Cl}_4)$ was originally studied by ESCA as a member of the series $(\text{Ph}_3\text{P})_2\text{Pt}(\text{C}_2\text{X}_4)$ ($\text{X} = \text{H}, \text{Cl}, \text{F}, \text{CN}$) as discussed in Chapter II. The spectra obtained were of unexpected complexity, the most striking feature being the breadth of the Cl 2p peak which was expected to show the $2p_{1/2}, 2p_{3/2}$ resolution characteristic of chlorines in a single environment. It is known from X-ray diffraction work⁹² that this complex is somewhat unstable under X-irradiation and also, from purely chemical observations,^{132,132} that the complex is susceptible to isomerisation to the σ -vinyl derivative $(\text{Ph}_3\text{P})_2\text{PtCl}(\text{CCl}=\text{CCl}_2)$. It seemed of special interest, therefore, to study the behaviour of this complex under the conditions of the ESCA experiment in more detail.

Experimental

A number of different sample preparation procedures were used in this work and it is convenient to describe these as appropriate. Both Mg $K\alpha_{1,2}$ and Al $K\alpha_{1,2}$ exciting radiations were used; equivalent peaks are about 0.2 eV broader in the latter case, it being made clear below which X-ray source was used for particular experiments.

Results and Discussion

Preliminary runs on this complex were performed using the powder pressed onto scotch tape and also in the form of a thin layer deposited onto a cleaned gold backing from solution in CH_2Cl_2 (spectrosol grade). In both cases the chlorine $2p_{1/2,3/2}$ peak was very

broad and unresolved although the peak shapes differed somewhat. The Pt $4f_{5/2,7/2}$ doublet from the powder sample also seemed less well resolved than in the case of the spectrum from the thin film sample. A number of runs indicated the reproducibility of these effects. For comparison purposes the ESCA spectra of the isomeric complex $(\text{Ph}_3\text{P})_2\text{Pt}(\text{Cl}(\text{CCl}=\text{CCl}_2))$ were taken, also in the form of a thin film on gold from CH_2Cl_2 solution. The similarity of the Cl 2p spectra was immediately apparent.

Fig.4.1 shows the spectra obtained from pure $(\text{Ph}_3\text{P})_2\text{PtCl}(\text{CCl}=\text{CCl}_2)$ as described. The Pt $4f_{5/2,7/2}$ doublet is well resolved while the Cl 2p peak can be resolved into two doublets (taken from the single chlorine $2p_{1/2,3/2}$ line shape discussed in Chapter III) in the area ratio 1:3. These arise from the single chlorine attached to the metal and the three indistinguishable chlorines in the perchlorovinyl ligand, respectively. The lower BE of the chlorine attached to the metal reflects its higher negative charge. BE's are shown in Table 4.1, estimated errors being ± 0.2 eV.

Spectra observed for $(\text{Ph}_3\text{P})_2\text{Pt}(\text{C}_2\text{Cl}_4)$ studied as a thin film on gold (from CH_2Cl_2 solution) are identical with those from the vinyl complex. The spectra from this complex in powder form are more complicated. The chlorine 2p peak cannot be adequately fitted by a pair of doublets as above, but it is well fitted if an additional doublet is superimposed (Fig.4.2). Further, the Pt 4f peak for the powder sample can be resolved into two doublets (Fig.4.2). This suggests that two platinum complexes are giving rise to the observed spectra. As shown in Table 4.1 the BE of one type of Pt and the 1:3



Mg K α

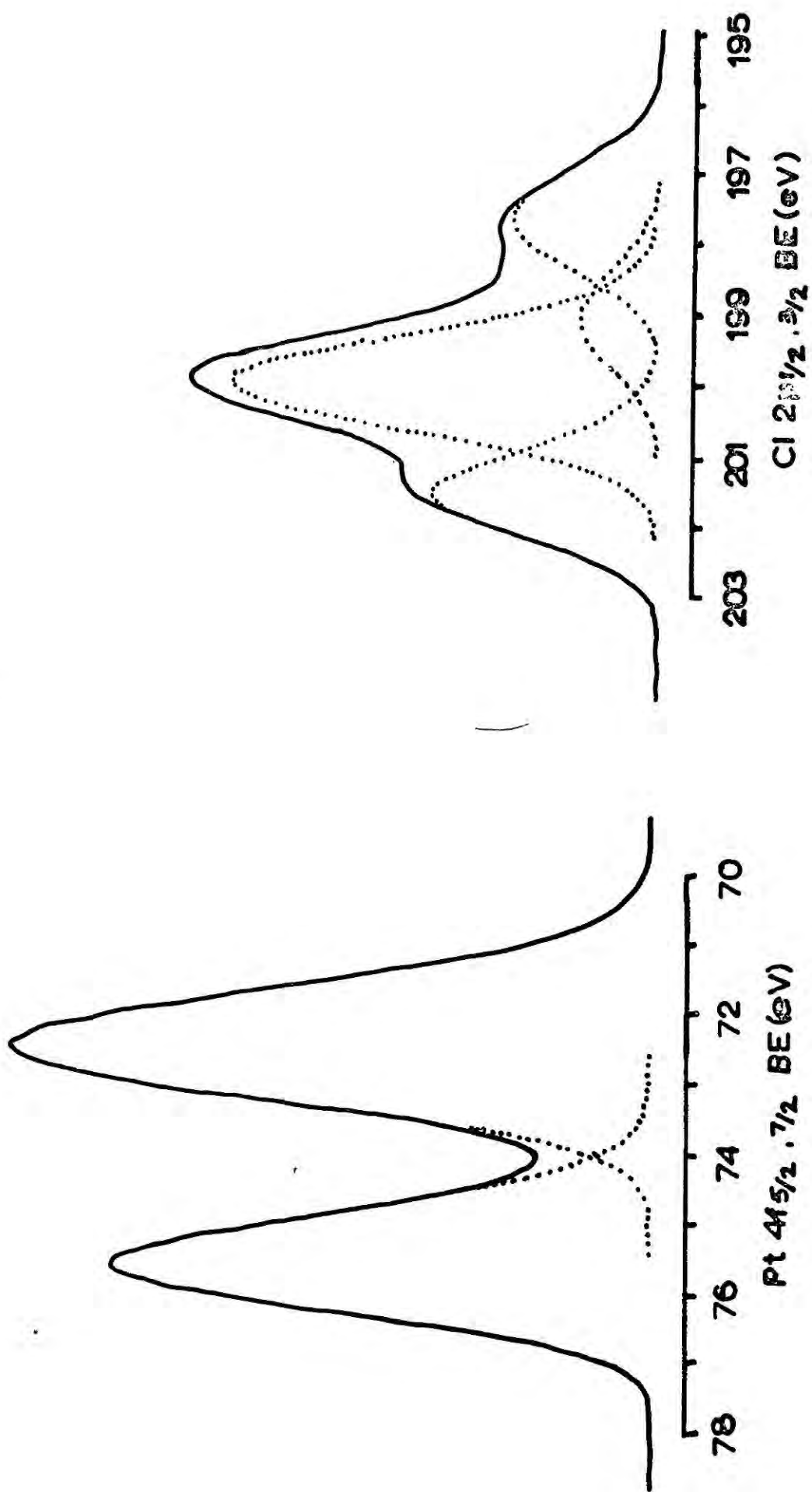


FIGURE 41



Mg K α

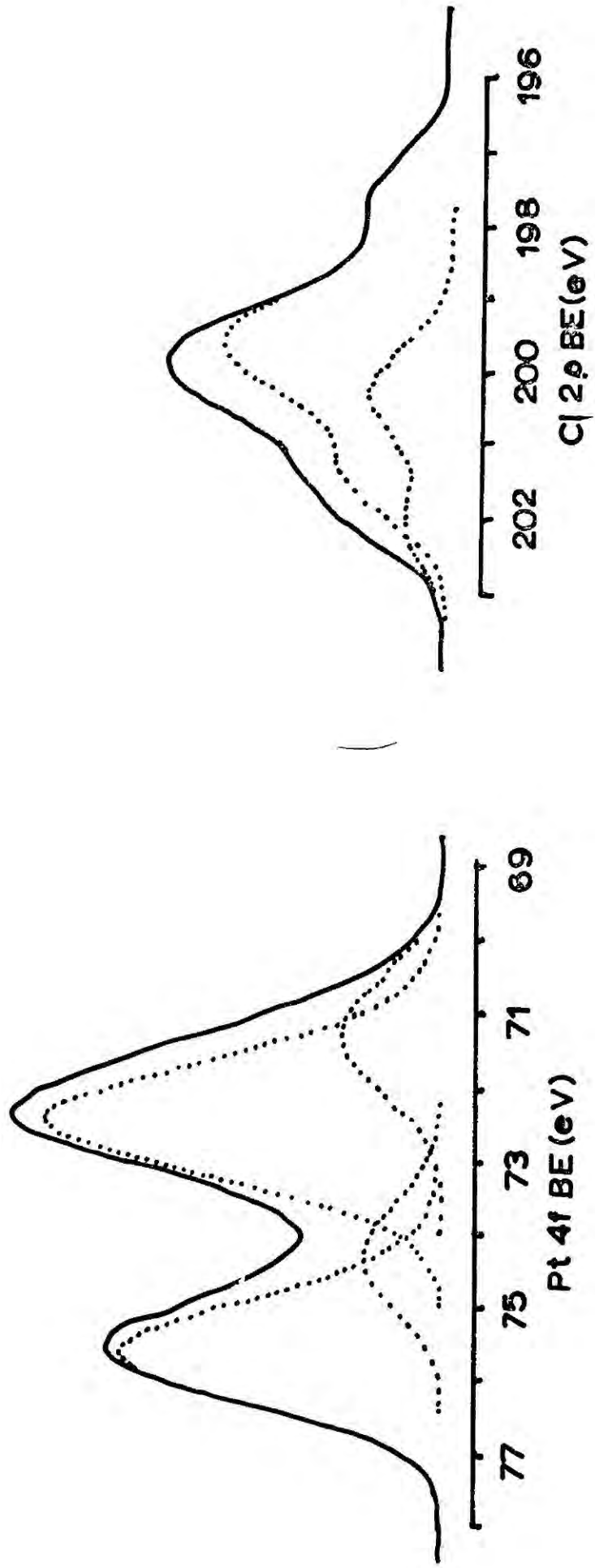


FIGURE 42

Cl pair coincide with those in $(\text{Ph}_3\text{P})_2\text{PtCl}(\text{CCl}=\text{CCl}_2)$ and the olefin complex run as a thin film. The single Cl doublet remaining and the other type of Pt could reasonably be ascribed to the expected spectra of $(\text{Ph}_3\text{P})_2\text{Pt}(\text{C}_2\text{Cl}_4)$. The contribution to the total peak areas from these peaks turns out to be the same ($\sim 24\%$) in each case which lends support to this interpretation.⁸⁷ However, the Pt $4f_{7/2}$ BE attributed to the metal in $(\text{Ph}_3\text{P})_2\text{Pt}(\text{C}_2\text{Cl}_4)$ (71.2 eV) is inconsistent with the weight of evidence (Chapter II and ref.89) suggesting that a value of ~ 72.5 eV would be more appropriate. In fact the BE for Pt $4f_{7/2}$ electrons in Pt metal is close to 71.2 eV which suggests, as observed in other samples, decomposition to give free metal. This is unlikely, however, because the effect is apparently absent for thin film samples. These deconvolutions for the powder sample spectra might just be a fortuitous result, the spectra being naturally broadened due to different surface characteristics for the powder sample relative to the thin film.

Whatever the meaning of this extra breadth in peaks from powder samples of $(\text{Ph}_3\text{P})_2\text{Pt}(\text{C}_2\text{Cl}_4)$, there can be little doubt that the observed spectra are due mainly to $(\text{Ph}_3\text{P})_2\text{PtCl}(\text{CCl}=\text{CCl}_2)$. Because the ESCA technique only samples the top 50 \AA or less, (Mg or Al $K\alpha$ radiation) these results would be obtained if there existed a surface layer of the vinyl isomer on the crystals of the olefin complex. Infrared spectra of analytically pure samples of each complex showed no bulk contamination of the olefin complex by the vinyl isomer, as evidenced by the complete absence of a Pt-Cl stretch band at $\sim 310 \text{ cm}^{-1}$ (characteristic of the vinyl isomer).

Infrared spectra were recorded for samples at each stage of the ESCA experiment on $(\text{Ph}_3\text{P})_2\text{Pt}(\text{C}_2\text{Cl}_4)$ in an attempt to gain more information. The important regions (Pt-Cl stretch, $250\text{-}500\text{ cm}^{-1}$) of these spectra are collected in Fig.4.3. Dissolution in CH_2Cl_2 and recrystallisation as a thin film on clean gold had no effect on the infrared spectrum of the pure complex. This is not unexpected since it is necessary to reflux the olefin complex in ethanol to effect isomerisation.¹³¹ After irradiation for ~ 1 hr in the spectrometer the infrared spectrum of the recovered material showed the growth of a very weak band at $\sim 310\text{ cm}^{-1}$. This effect was greater for the thin film sample than for the powder sample. The former also indicated the emergence of a band at $\sim 1550\text{ cm}^{-1}$ ($\nu_{\text{C}=\text{C}}$ found in the vinyl complex, but not the olefinic precursor).

It would appear, therefore, that a layer of the vinyl isomer is formed photochemically on the surface of the olefin complex. This might occur, to a limited extent, during preparation and subsequent standing; but it is certainly accelerated by X-irradiation and is fairly extensive when the surface area of the material is high (as in the thin film, where 'pure' vinyl-type spectra are observed).

In passing it might be mentioned that the Pt $4f_{7/2}$ BE in $(\text{Ph}_3\text{P})_2\text{PtCl}(\text{CCl}=\text{CCl}_2)$, and the Cl $2p_{3/2}$ BE for chlorine attached to platinum, are the same, within experimental error, as the values in Table 2.3 for cis-bis(diphosphine)platinum dichlorides which indicates that the electronegativity of the perchlorovinyl ligand is very similar to that of chlorine itself.

Before discussing possible mechanisms for the isomerisation reaction the results from similar investigations on related complexes will be presented.

Caption for Fig. 4.3

- (a) Pure $(\text{Ph}_3\text{P})_2 \text{PtCl}(\text{CCl} = \text{CCl}_2)$
- (b) Pure $(\text{Ph}_3\text{P})_2 \text{Pt}(\text{C}_2\text{Cl}_4)$
- (c) $(\text{Ph}_3\text{P})_2 \text{Pt}(\text{C}_2\text{Cl}_4)$ after thin film formation from CH_2Cl_2 on gold.
- (d) $(\text{Ph}_3\text{P})_2 \text{Pt}(\text{Cl}_2\text{Cl}_4)$ after X-irradiation (powder sample).
- (e) $(\text{Ph}_3\text{P})_2 \text{Pt}(\text{C}_2\text{Cl}_4)$ after X-irradiation (thin film sample).

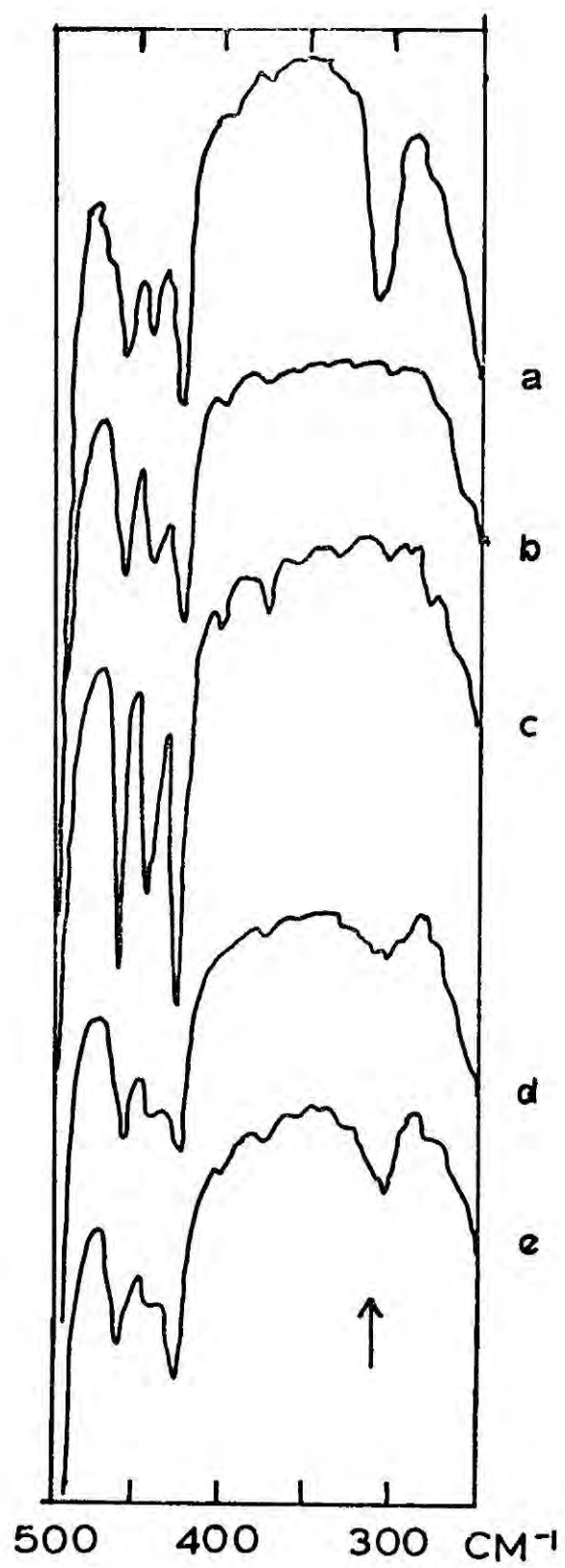


FIGURE 4.3

(ii) Surface isomerisation of $(\text{Ph}_3\text{As})_2\text{Pt}(\text{C}_2\text{Cl}_4)$ and $(\text{Ph}_3\text{As})_2\text{Pt}(\text{C}_2\text{HCl}_3)$

The spectra of $(\text{Ph}_3\text{As})_2\text{PtCl}(\text{CCl}=\text{CCl}_2)$, as a thin film on gold, are virtually identical to those from the analogous phosphine complex. The relevant BE's, again referenced to the phenyl carbons at 285.0 eV, are given in Table 4.1, and these are also almost identical to those from the phosphine complex as might have been expected from the comparison of arsine and phosphine complexes in Chapter II.

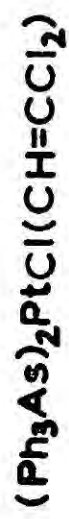
The continuous scan mode used in this work involves the combination of scan rate and rate meter time constant such that the peak shape is not distorted as it is recorded. Recordings of the Cl 2p peak from a powder sample of $(\text{Ph}_3\text{As})_2\text{Pt}(\text{C}_2\text{Cl}_4)$ made deliberately with high scan rate directly after activating the X-ray beam indicated that this complex might be isomerising slightly more slowly than the phosphine analogue, but the spectra obtained initially under the correct (much slower) scan conditions always appeared very similar to those of the vinyl isomer - in particular the low BE of the Cl 2p peak showed the tell-tale hump of the chlorine bound to metal. Thus changing phosphine ligands to arsine equivalents has no effect on the isomerisation of these tetrachloroethylene complexes.

The trichloroethylene complex $(\text{Ph}_3\text{P})_2\text{Pt}(\text{C}_2\text{HCl}_3)$ is very difficult to isolate due to its facile isomerisation to $(\text{Ph}_3\text{P})_2\text{PtCl}(\text{CH}=\text{CCl}_2)$ ^{131,133} but the arsine analogue can be obtained in the crystalline state. Since the vinyl complex has now only two chlorines in the organic ligand compared with three for the previously studied vinyl complexes the isomerisation of $(\text{Ph}_3\text{As})_2\text{Pt}(\text{C}_2\text{HCl}_3)$ offers the chance to check the conclusions, based on deconvolutions of complex Cl 2p spectra, drawn from the results from isomerisation of the tetrachloroethylene complexes.

The spectra of $(\text{Ph}_3\text{As})_2\text{PtCl}(\text{CH}=\text{CCl}_2)$ are shown in Fig.4.4, the BE's are included in Table 4.1. The complex was studied in powder form because it was completely insoluble in CH_2Cl_2 or CHCl_3 . The Cl 2p peak shows the low BE shoulder of the Pt-Cl chlorine but with the expected relative increase in intensity relative to $(\text{Ph}_3\text{As})_2\text{PtCl}(\text{CCl}=\text{CCl}_2)$. An attempted deconvolution for two types of chlorine in the ratio 2:1 gives a slightly disappointing fit compared with the 3:1 fit for the perchlorovinyl complexes. This may be due to slight impurity of the sample or to the presence of trapped CH_2Cl_2 (from preparation) in the lattice. Both types of chlorine in this complex have slightly lower BE's than in the perchlorovinyl analogue while the Pt $4f_{7/2}$ BE and the As $3d_{5/2}$ BE of the arsine ligand are the same. This reflects the lower electronegativity of $-\text{CH}=\text{CCl}_2$ compared with $-\text{CCl}=\text{CCl}_2$ (lower BE for Cl-Pt in the former complex) and the decreased competition for electron density of the chlorines in the vinyl ligand (two chlorines in $-\text{CH}=\text{CCl}_2$ versus three in $-\text{CCl}=\text{CCl}_2$).

TABLE 4.1

	Core Binding Energies (eV)			
	Pt $4f_{7/2}$	Cl $2p_{3/2}$		As $3d_{5/2}$
$(\text{Ph}_3\text{P})_2\text{PtCl}(\text{CCl}=\text{CCl}_2)$	72.3	197.7(1)	199.9(3)	-
$(\text{Ph}_3\text{As})_2\text{PtCl}(\text{CCl}=\text{CCl}_2)$	72.1	197.7(1)	199.9(3)	42.7
$(\text{Ph}_3\text{As})_2\text{PtCl}(\text{CH}=\text{CCl}_2)$	72.2	197.5(1)	199.6(2)	42.8



Mg K α

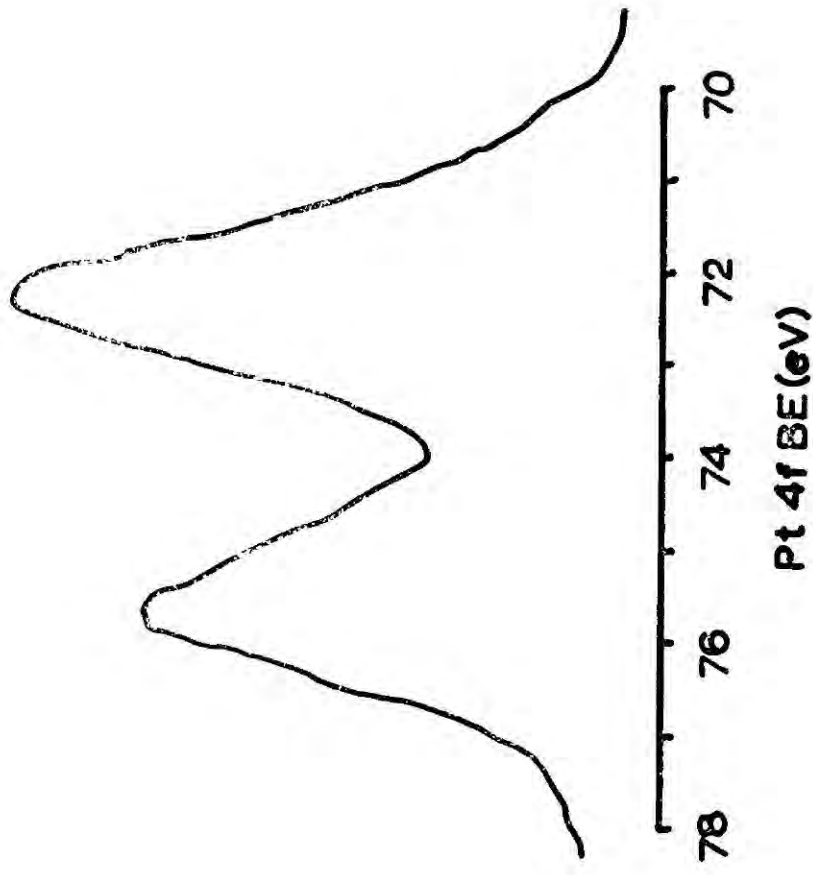
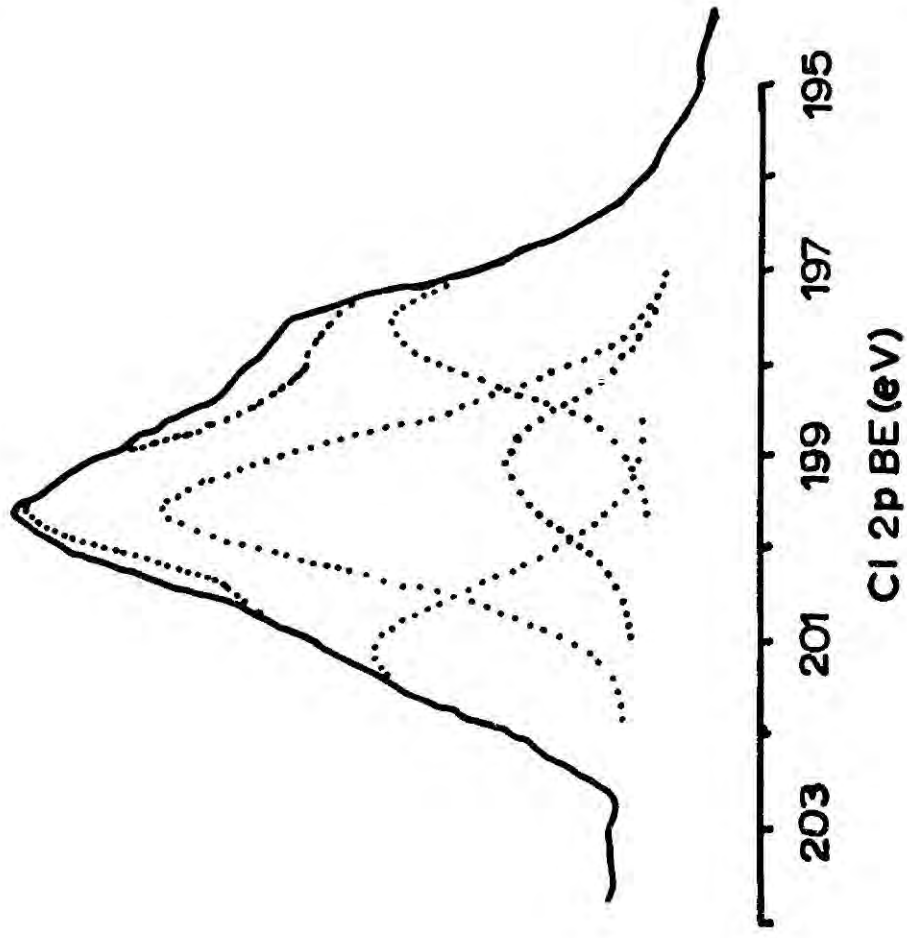


FIGURE 4.4

Spectra from a powder sample of $(\text{Ph}_3\text{As})_2\text{Pt}(\text{C}_2\text{HCl}_3)$ taken immediately after switching on the X-ray beam are identical to those from $(\text{Ph}_3\text{As})_2\text{PtCl}(\text{CH}=\text{CCl}_2)$. The surface isomerisation of this complex would therefore appear to be very rapid under X-ray bombardment. After longer periods of irradiation the Cl 2p and Pt 4f peaks began to broaden probably due to sample decomposition.

Infrared spectra of these complexes were again recorded to follow the surface/bulk effect of isomerisation. Unfortunately the Pt-Cl stretch region is masked by vibrational modes of the triphenyl arsine ligands; however, there are other diagnostic features available.¹³⁴ $(\text{Ph}_3\text{As})_2\text{PtCl}(\text{CCl}=\text{CCl}_2)$ gives a medium band at $\sim 810 \text{ cm}^{-1}$ which is absent in the spectrum of $(\text{Ph}_3\text{As})_2\text{Pt}(\text{C}_2\text{Cl}_4)$. The spectra in this region for these two pure complexes are shown in Fig.4.5 together with the spectrum from $(\text{Ph}_3\text{As})_2\text{Pt}(\text{C}_2\text{Cl}_4)$ recovered after 45 mins. irradiation. This latter spectrum exhibits a weak band at about 810 cm^{-1} indicating that a very similar situation pertains to that found for the triphenylphosphine analogue, namely that irradiation affects the bulk of the sample (as monitored by i.r. spectra) very little but the surface layers (as monitored by ESCA) undergo complete isomerisation to the vinyl complex.

Similarly, $(\text{Ph}_3\text{As})_2\text{PtCl}(\text{CH}=\text{CCl}_2)$ gives a strong band at $\sim 840 \text{ cm}^{-1}$ whereas $(\text{Ph}_3\text{As})_2\text{Pt}(\text{C}_2\text{Cl}_3\text{H})$ has a broad weak band at $\sim 845 \text{ cm}^{-1}$. The latter gives a medium band at 785 cm^{-1} which is absent in the vinyl isomer spectrum. The relevant regions of these spectra are shown in Fig.4.6 together with the spectrum from $(\text{Ph}_3\text{As})_2\text{Pt}(\text{C}_2\text{HCl}_3)$ after irradiation for about 40 mins. The lowering in intensity of the 785 cm^{-1} peak in this latter spectrum is marked as is the accompanying

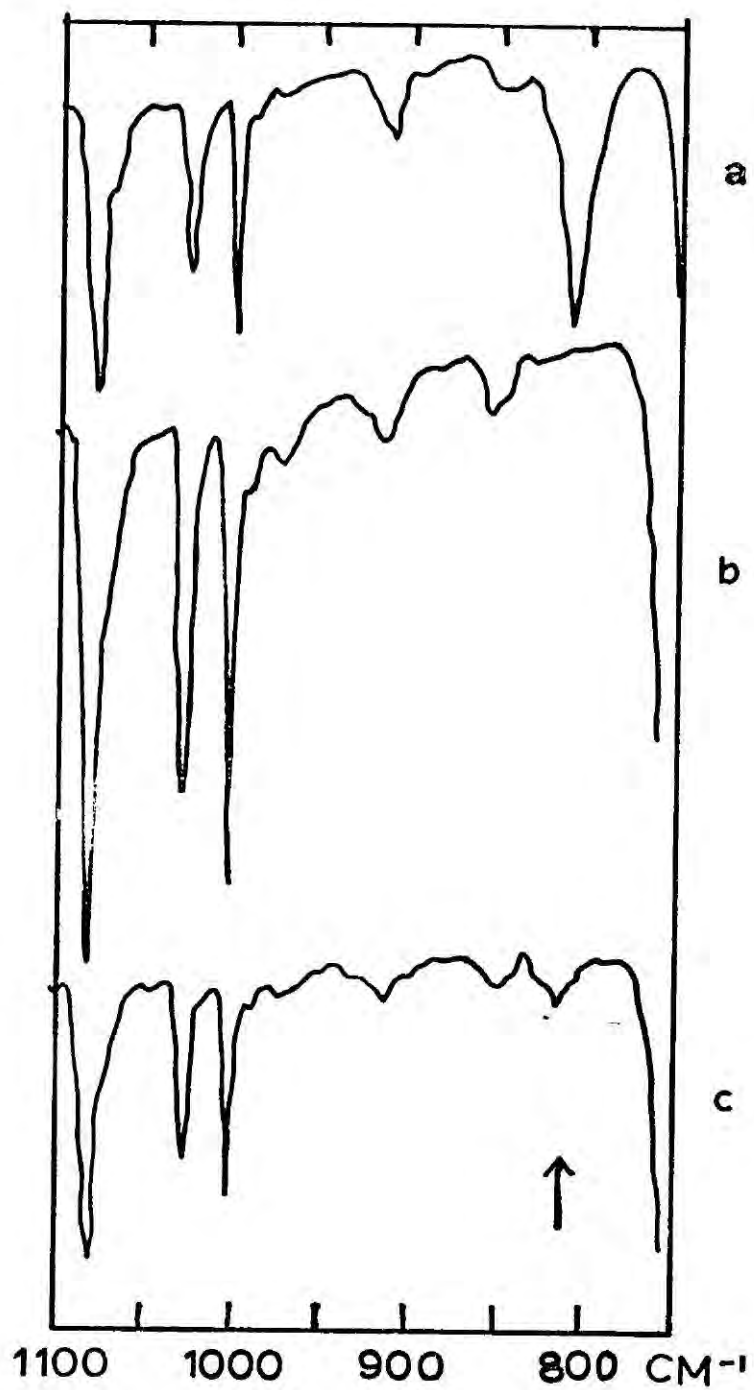


FIGURE 4.5

- (a) pure $(\text{Ph}_3\text{As})_2 \text{Pt Cl}(\text{CCl} = \text{CCl}_2)$
- (b) pure $(\text{Ph}_3\text{As})_2 \text{Pt}(\text{C}_2\text{Cl}_4)$
- (c) $(\text{Ph}_3\text{As})_2 \text{Pt}(\text{C}_2\text{Cl}_4)$ after γ -irradiation

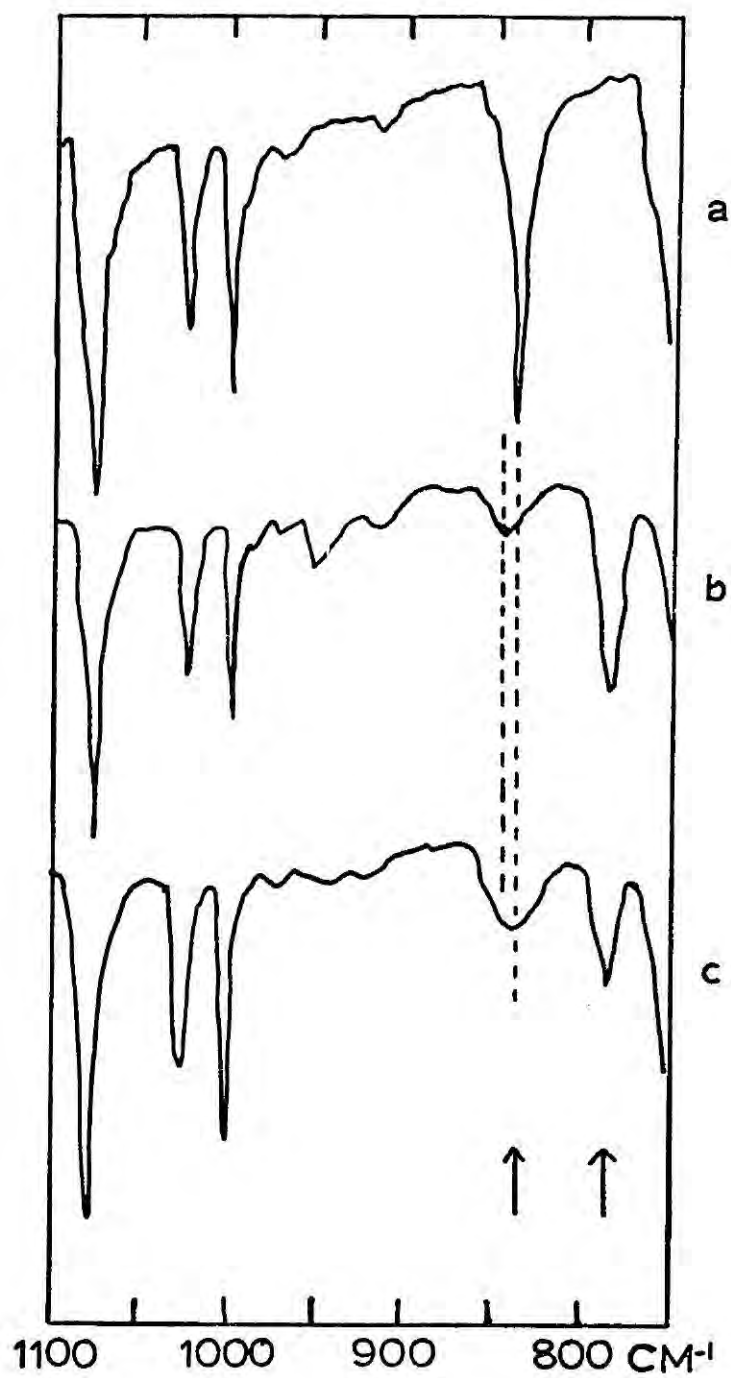


FIGURE 4.6

- (a) pure $(\text{Ph}_3\text{As})_2 \text{Pt Cl} (\text{CH} = \text{CCl}_2)$
- (b) pure $(\text{Ph}_3\text{As})_2 \text{Pt} (\text{C}_2\text{HCl}_3)$
- (c) $(\text{Ph}_3\text{As})_2 \text{Pt} (\text{C}_2\text{HCl}_3)$ after X -irradiation

increase in breadth and intensity of the peak centred at $\sim 840\text{cm}^{-1}$ (note the shift of the peak maximum from $845 \rightarrow 840\text{ cm}^{-1}$). Compared with the tetrachloroethylene complexes it would appear that isomerisation of the trichloroethylene complex occurs to a greater extent since the i.r. results show considerable isomerisation of the bulk to have occurred. Since similar sized samples were used in all these investigations this indicates a greater ease of isomerisation of the trichloroethylene complex under X-rays which is in accord with chemical and kinetic information on the triphenylphosphine analogues.^{131,133}

(iii) Attempts to obtain ESCA spectra for unisomerised $(\text{Ph}_3\text{As})_2\text{Pt}(\text{C}_2\text{Cl}_4)$

There are several indications from the work described above that at room temperature complexes $\text{L}_2\text{Pt}(\text{ol})$ ($\text{ol} = \text{C}_2\text{Cl}_4, \text{C}_2\text{Cl}_3\text{H}$) are slightly more stable with respect to isomerisation when $\text{L} = \text{Ph}_3\text{As}$ rather than $\text{L} = \text{Ph}_3\text{P}$. Accordingly, $(\text{Ph}_3\text{As})_2\text{Pt}(\text{C}_2\text{Cl}_4)$ was chosen for attempts to obtain spectra of the pure isomer. A brief comment by Seigbahn et al.¹ suggests that freezing techniques can be useful for studying compounds which tend to decompose under normal ESCA conditions, consequently attempts were made to study a thin film of the complex at low temperatures.

To avoid the possibility of solvent (CH_2Cl_2) interference after forming a thin film sample (normally, at ambient temperatures, any trapped solvent is quickly pumped off) an unchlorinated solvent was required. $(\text{Ph}_3\text{As})_2\text{Pt}(\text{C}_2\text{Cl}_4)$ is just soluble enough in acetone for thin film formation on gold although the coverage is less good than when CH_2Cl_2 is used as solvent. Such a sample was prepared and, after placing in the spectrometer, was cooled down to -110°C and maintained

at this temperature. Condensation of contaminants (mainly water vapour) in the spectrometer housing is not a problem at this temperature since this begins at $\sim -130^{\circ}\text{C}$ (this was checked by a quadrupole mass spectrometer connected directly into the spectrometer). The results suggested that the complex was indeed stable under these conditions since chlorine 2p peak shapes were more like the 'single chlorine' peak shape and no low BE peak (due to Pt-Cl) was observed. When the sample was allowed to warm-up to ambient temperature the Cl 2p spectrum again resembled that from the vinyl isomer (Fig.4.7). This behaviour was reproduced with fresh samples. The observed BE's, referenced as usual to Cls = 285.0 eV, are shown in Table 4.2

TABLE 4.2

	Core Binding Energies (eV)		
	Pt 4f _{7/2}	Cl 2p _{3/2}	As 3d _{5/2}
(Ph ₃ As) ₂ Pt(C ₂ Cl ₄) (-110 ^o C)	72.4	200.6	42.7
C ₂ Cl ₄ (-80 ^o C)	-	202.2	-

Also shown is the Cl 2p_{3/2} BE for C₂Cl₄ studied as a thin condensed film on gold at -80^oC.

It is satisfying to find that the platinum BE compares well with the predicted value of ~ 72.5 eV from the results on other olefin complexes (Chapter II). In comparing the chlorine BE for free and complexed C₂Cl₄ it is assumed that any charging correction for the C₂Cl₄ data will be small; also since this data cannot be internally



Al K α

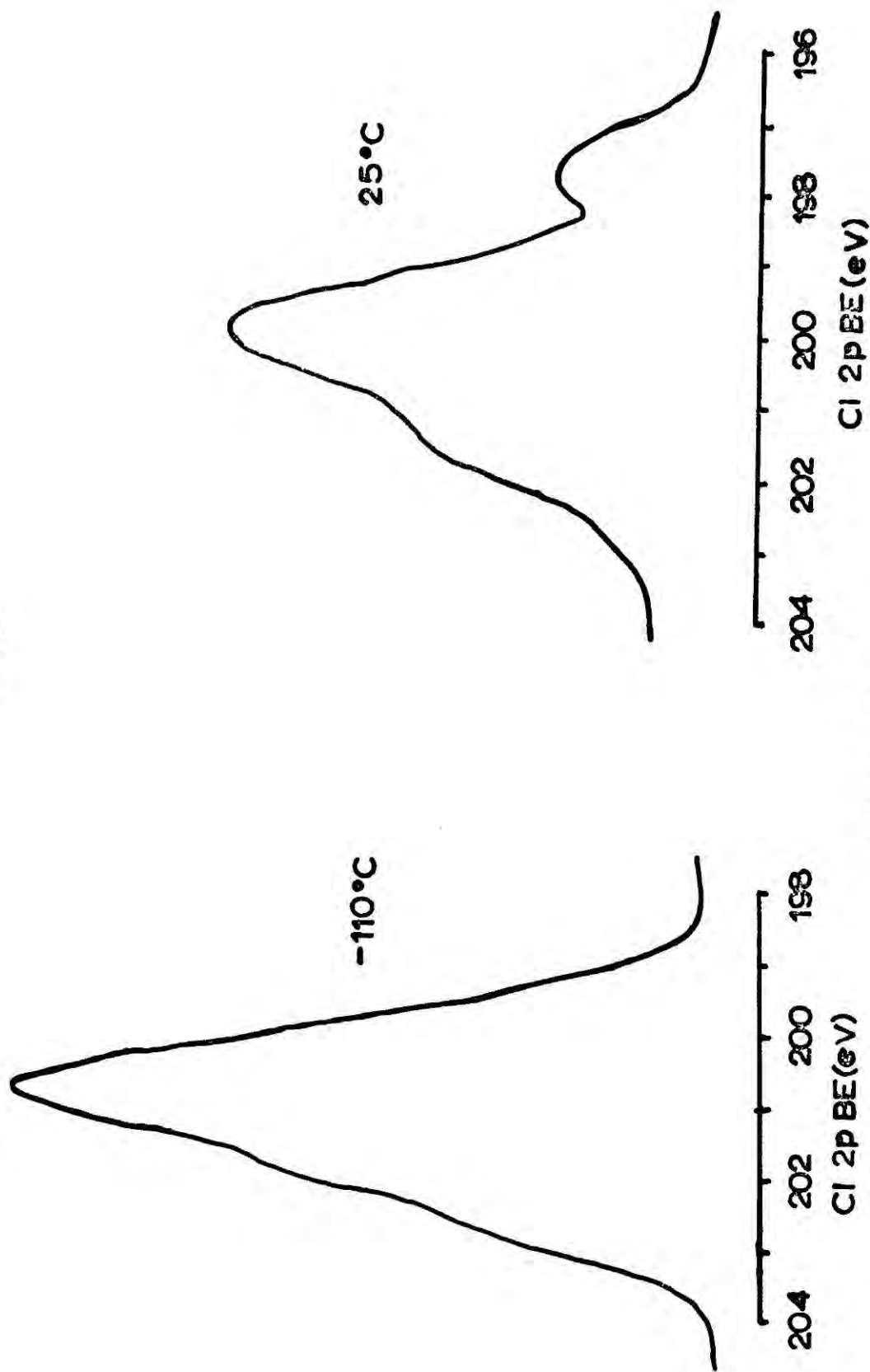


FIGURE 4.7

referenced to that of the complex the relative error in comparing the data is higher than usually quoted. Even if this is as high as ± 0.5 eV it is apparent that there is a significant decrease in the chlorine BE when C_2Cl_4 becomes complexed. This increase in electron density can only be accounted for if there is a marked degree of electron transfer from metal to ligand; these results, therefore, constitute further direct evidence for the validity of the Dewar-Chatt-Duncanson model⁸⁴ discussed in Chapter II.

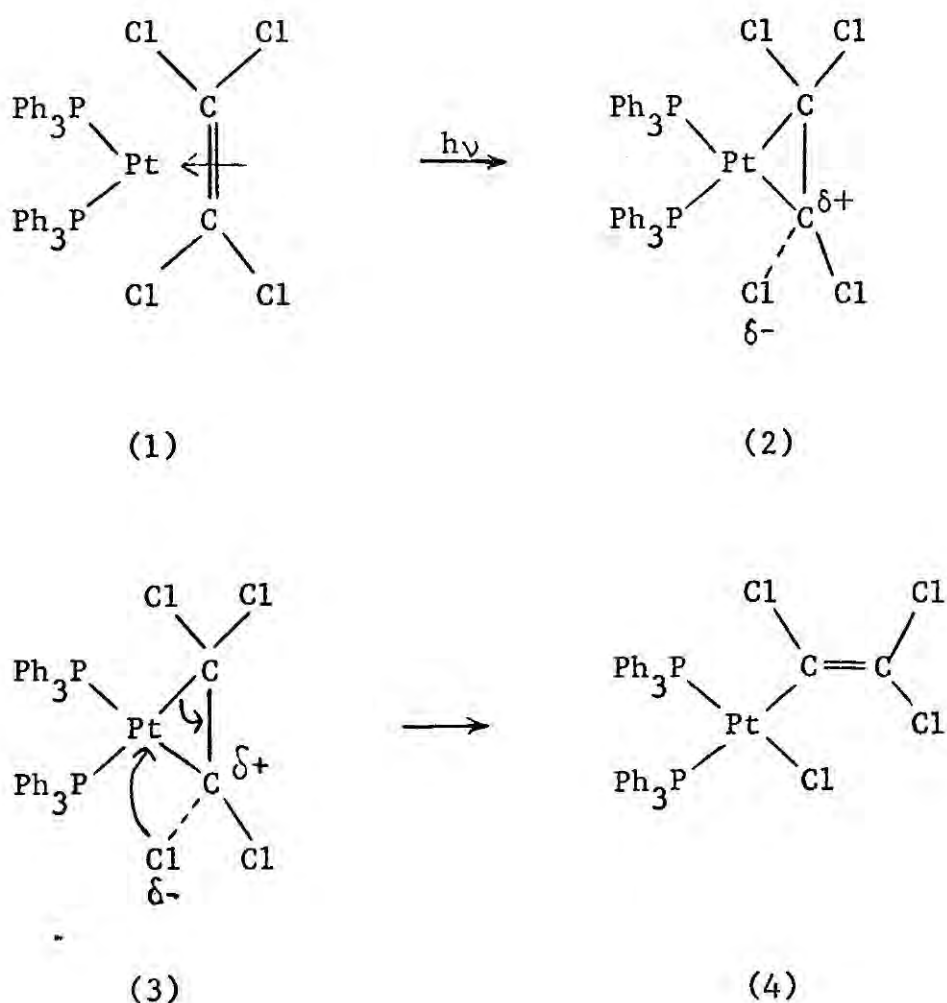
(iv) Mechanisms of Isomerisation

Detailed results are available in the literature concerning the isomerisation of $(Ph_3P)_2Pt(C_2Cl_4)$ and $(Ph_3P)_2Pt(C_2HCl_3)$ in hydroxylic solvents (e.g. alcohols.^{132,133,135}) Careful i.r. studies on the vinyl complexes formed indicate¹³⁶ that these have the cis configuration of phosphine ligands, although isomerisation to the thermodynamically favoured trans arrangement is easily effected by heating in benzene to $\sim 110^\circ C$ (in a sealed tube), and in those vinyl complexes which are formed directly from reaction of $(Ph_2MeP)_4Pt$ with olefin the stereochemistry is invariably trans.¹³⁷

The two mechanisms for isomerisation of $(Ph_3P)_2Pt(C_2Cl_4)$ to cis- $(Ph_3P)_2PtCl(CCl=CCl_2)$ which are consistent with preparative¹³¹ and kinetic^{132,135} data are a synchronous intramolecular process and a rate-determining ionisation to $[(Ph_3P)_2Pt(CCl=CCl_2)]^+$ and Cl^- , possibly associated as an ion-pair, followed by rapid formation of a platinum to chlorine bond and a platinum to carbon σ -bond. The kinetic details are more consistent with the latter variation but indicate that in the case of $(Ph_3P)_2Pt(C_2HCl_3)$ isomerisation the intramolecular process plays a much more important role despite the fact that formation of the

proposed ion-pair $[(\text{Ph}_3\text{P})_2\text{Pt}(\text{CH}=\text{CCl})]^+\text{Cl}^-$ is easier, which would explain the greater speed of reaction.

In the solid state the extreme case of ion-pair formation (aided in polar solution) is unlikely to be realised, however, the precedent for an intramolecular mechanism involving in the first instance stretching (weakening) of a carbon-chlorine bond fits nicely; this first step could occur photochemically and, in the surface layers, be aided by the presence of adsorbed water molecules (by analogy with the solution reaction):-



The predicted stereochemistry would thus be a cis configuration of phosphine ligands. The very small differences in i.r. spectra of the cis- and trans-isomers of vinyl complexes, however, makes it impossible to infer anything about the stereochemistry of the vinyl complexes formed during X-irradiation of the olefinic isomers from inspection of the i.r. spectra taken after irradiation.

The same type of mechanism is presumed to operate for the triphenylarsine analogue and for the trichloroethylene derivative, with preferential initial excitation of the C-Cl bond of the =CHCl group.

CHAPTER V

ESCA STUDIES OF SOME TRANSITION METAL CARBONYL COMPLEXES

CONTAINING ORGANO-NITROGEN LIGANDS.

A series of transition metal carbonyl derivatives containing organonitrogen ligands, prepared in this University (Dr H.R. Keable and Dr M. Kilner), offered the possibility of applying the experience gained from the previous studies of platinum complexes to problems concerning structural and bonding modes in these complexes. Some of the results have already been included in Dr H.R. Keable's Ph.D. Thesis (University of Durham, 1972).

(i) Introduction

The range of BE's for N1s core levels in commonly encountered situations is fairly large (around 10 eV)^{48,138} hence significant shifts may be anticipated upon co-ordination of ligands through nitrogen. Two ligand systems, the methyleneamino ($R_2C:N-$)¹³⁹ and the aza-allyl/allene (R_2CNR_2)¹⁴⁰ groups, have been investigated and each has the possibility of bonding in various ways. Two forms of the complex $[\pi-C_5H_5W(CO)_2\{(p\text{-tolyl})_2CNC(p\text{-tolyl})_2\}]$ have been isolated which are thought to differ only in the nature of attachment of the organonitrogen group to the metal. The para-substituents of the aryl groups have a profound effect on the course of the reactions involving methyleneamino derivatives and these electronic effects together with structural forms adopted by the ligands have been investigated by ESCA.

(ii) Experimental

Spectra were excited using $MgK\alpha_{1,2}$ radiation, the samples being studied as powders pressed onto double sided scotch tape. Even though the percentage of nitrogen in some compounds is very low satisfactory spectra were always obtained.

Corrections for charging effects, not greater 1eV in most cases, were made as follows. All compounds contained *p*-tolyl or *p*-CF₃C₆H₄- groups which dominate their Cls spectra. PhCH₃ and PhCF₃, studied as thin condensed films on gold, under which conditions charging effects are minimised (< 0.3 eV), gave the following binding energies:-¹⁴¹

PhCH₃: Cls (centroid) = 285.0 eV

PhCF₃: Cls (centroid) = 286.3 eV (Ph), 293.8 eV (-CF₃),
Fls = 690.8 eV.

Under these conditions and those used for this investigation the Au4f_{7/2} level at 84.0 eV BE, used as reference, had a halfwidth of 1.15 eV. The Cls centroid for compounds with *p*-tolyl groups was, therefore, referenced to 285.0 eV and the Fls peak for the compounds with *p*-CF₃C₆H₄- groups referenced to 690.8 eV. For the latter compounds the Cls peaks arising from -C₆H₄- and -CF₃ groups then occurred at 286.1 eV and 293.8 eV(BE's) respectively in satisfactory agreement with the values from PhCF₃. The time independent nature of the spectra and visual examination of the samples after removal from the spectrometer indicated that radiation damage was insignificant.

(iii) Results and Discussion

(a) Qualitative Discussion.

The complexes studied fall into two groups: methyleneamino complexes $\pi\text{-C}_5\text{H}_5\text{M}(\text{CO})_2\text{N:CR}_2$ and aza-allyl/allene complexes $\pi\text{-C}_5\text{H}_5\text{M}(\text{CO})_2[\text{R}_2\text{CNR}_2]$ (M = Mo, W; R = *p*-tolyl and *p*-CF₃C₆H₄-). Their experimental BE's and those of free ligand model compounds are given in Table 5.1.

TABLE 5.1

Molecular Core binding energies in eV

	Cl _{1s}	F _{1s}	N _{1s}	Mo3d _{5/2}	W4f _{7/2}
$\pi\text{-C}_5\text{H}_5\text{Mo}(\text{CO})_2\text{NC}(\text{p-toly1})_2$	285.0	-	398.4	229.0	-
$\pi\text{-C}_5\text{H}_5\text{W}(\text{CO})_2\text{NC}(\text{p-toly1})_2$	285.0	-	398.8	-	31.6
$\pi\text{-C}_5\text{H}_5\text{W}(\text{CO})_2\text{NC}(\text{p-CF}_3\text{C}_6\text{H}_4)_2$	286.1*	690.8	399.8	-	32.3
$(\text{p-toly1})_2\text{C:NH}$	285.0	-	398.7	-	-
$(\text{p-CF}_3\text{C}_6\text{H}_4)_2\text{C:NH}$	286.3*	-	400.1	-	-
$\pi\text{-C}_5\text{H}_5\text{Mo}(\text{CO})_2[(\text{p-toly1})_2\text{CNC}(\text{p-toly1})_2]$	285.0	-	400.0	228.4	-
$\pi\text{-C}_5\text{H}_5\text{Mo}(\text{CO})_2[(\text{p-CF}_3\text{C}_6\text{H}_4)_2\text{CNC}(\text{p-CF}_3\text{C}_6\text{H}_4)_2] (\text{A+B})^+$	286.1*	690.8	401.0	229.3	-
$\pi\text{-C}_5\text{H}_5\text{W}(\text{CO})_2[(\text{p-toly1})_2\text{CNC}(\text{p-toly1})_2] (\text{B})^+$	285.0	-	400.1	-	31.0
$\pi\text{-C}_5\text{H}_5\text{W}(\text{CO})_2[(\text{p-toly1})_2\text{CNC}(\text{p-toly1})_2] (\text{A+B})^+$	285.0	-	400.1	-	31.2
$(\text{p-toly1})_2\text{C:NCHPh}_2$	285.0	-	398.8	-	-

* Cl_{1s} (CF₃) at 293.8 eV.+ Isomeric forms in the solid state, see discussion.
Estimated error in binding energies ± 0.3 eV.

An interesting feature of the spectra from molybdenum complexes is the close proximity of the N1s and Mo3p_{3/2} levels. This latter core level is less convenient for accurate study than the 3d_{5/2} level because of its greater inherent linewidth, however, the spectra in this region give an immediate picture of the nitrogen and molybdenum BE's and allow relative shifts to be measured without the error imposed by corrections to reference levels. This point is illustrated in Fig. 5.1.

It is clear that in going from the methyleneamino complex to the aza-allyl/allene complex that the increase in N1s BE is accompanied by a decrease in the BE of the metal core levels. This suggests that the electron density increases at the metal atom and decreases at the nitrogen of the ligand on replacing the methyleneamino by the aza-allyl/allene group.

In the two complexes shown the $\pi\text{-C}_5\text{H}_5\text{Mo(CO)}_2\text{-}$ moiety can be thought of as being bonded to the three electron donors $(p\text{-tolyl})_2\text{C:N-}$ and $(p\text{-tolyl})_2\text{CNC}(p\text{-tolyl})_2$ respectively. The bonding aspects will be discussed in more detail below, but the peak separations show directly that this description must, at least, be a reasonable approximation. The shifts in Mo BE's shown by 3p_{3/2} level are mirrored by the more accurately measurable Mo3d_{5/2} level quoted in Table 5.1.

It is apparent from the metal and N1s BE's that the shifts in going from one complex of Mo to its analogue in the W series are not significantly different. Moreover, the shifts in BE's for each metal in going from $\pi\text{-C}_5\text{H}_5\text{M(CO)}_2\text{NC}(p\text{-tolyl})_2$ to $\pi\text{-C}_5\text{H}_5\text{M(CO)}_2[(p\text{-tolyl})_2\text{-CNC}(p\text{-tolyl})_2]$ type complexes are the same (ca 0.6 eV). This result may be expected in view of the fact that the atomic radii of the two metals are very similar due to the lanthanide contraction.

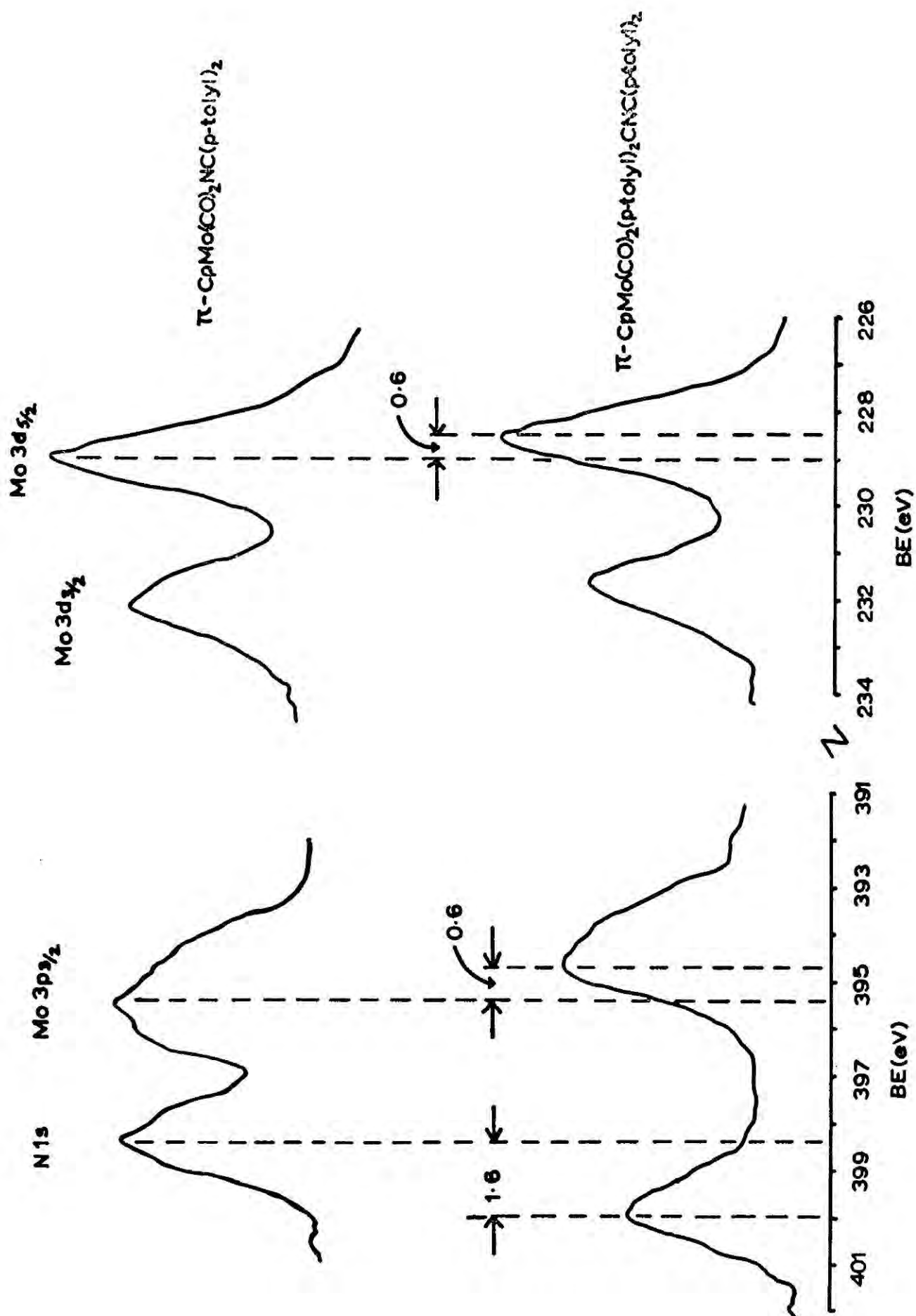


FIGURE 5.1

The long range effects of changing the p-substituents on the aryl groups can be readily seen in both methyleneamino and aza-allyl/allene complexes. Changing CH_3- to CF_3- would be expected to lower the electron density at nitrogen and the metal, through the powerful electron withdrawing influence of the p- CF_3 group; indeed, the N1s BE's in both types of complex are seen to increase by 1eV while the metal BE's increase significantly also. Such electronic effects in aza-allyl/allene complexes have been inferred from correlations of carbonyl stretching frequencies with the electronic properties of the para-substituents as indicated by their Hammett σ -constants.¹⁴² Table 5.2 collects the metal BE's and solid state carbonyl stretching frequencies, while Fig. 5.2 correlates these two parameters (using the higher of the two ν_{CO} values). The parallel trends show that the correlation is independent of the metal which is further indication of the very close similarity between complexes of Mo and W. Since both methyleneamino and aza-allyl/allene complexes are used in this correlation the good fit obtained offers direct evidence for the widely accepted belief that carbonyl groups exert a strong stabilising effect in complexes of metals in low formal oxidation states through dissipation of excess electron density on the central metal atom. There is no good theoretical reason why such correlations should be linear but since both measurements monitor to a lesser or greater extent the electronic environment of the metal atom a definite trend would be expected.

(b) Methyleneamino complexes

A large variety of data has already been accumulated in order to resolve the question of bonding in complexes involving the methyleneamino ligand $\text{R}_2\text{C}=\text{N}-$ which could either act as a one or three electron donor

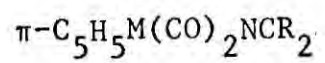
TABLE 5.2

W complexes	W4f _{7/2} B.E. (eV)	ν_{CO} (KBr)(cm ⁻¹) ^a
$\pi\text{-C}_5\text{H}_5\text{W}(\text{CO})_2\text{NC}(\text{p-tolyl})_2$	31.6	1938, 1838
$\pi\text{-C}_5\text{H}_5\text{W}(\text{CO})_2\text{NC}(\text{p-CF}_3\text{C}_6\text{H}_4)_2$	32.3	1956, 1869
(B) $\pi\text{-C}_5\text{H}_5\text{W}(\text{CO})_2[(\text{p-tolyl})_2\text{CNC}(\text{p-tolyl})_2]$	31.0	1931, 1830
Mo complexes	Mo3d _{5/2} B.E. (eV)	
$\pi\text{-C}_5\text{H}_5\text{Mo}(\text{CO})_2\text{NC}(\text{p-tolyl})_2$	229.0	1949, 1855
$\pi\text{-C}_5\text{H}_5\text{Mo}(\text{CO})_2[(\text{p-tolyl})_2\text{CNC}(\text{p-tolyl})_2]$	228.4	1936, 1836
(A+B) $\pi\text{-C}_5\text{H}_5\text{Mo}(\text{CO})_2[(\text{p-CF}_3\text{C}_6\text{H}_4)_2\text{CNC}(\text{p-CF}_3\text{C}_6\text{H}_4)_2]$	229.3	1958, 1873 ^b

a data from refs. 149,152

b mean of frequencies from two isomers: 1963, 1880 and 1954, 1866cm⁻¹

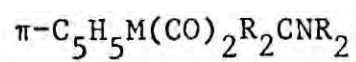
Caption for Fig. 5.2



a : M = W, R = p-tolyl

b : M = W, R = p-CF₃C₆H₄

c : M = Mo, R = p-tolyl



d : M = W, R = p-tolyl

e : M = Mo, R = p-tolyl

f : M = Mo, R = p-CF₃C₆H₄

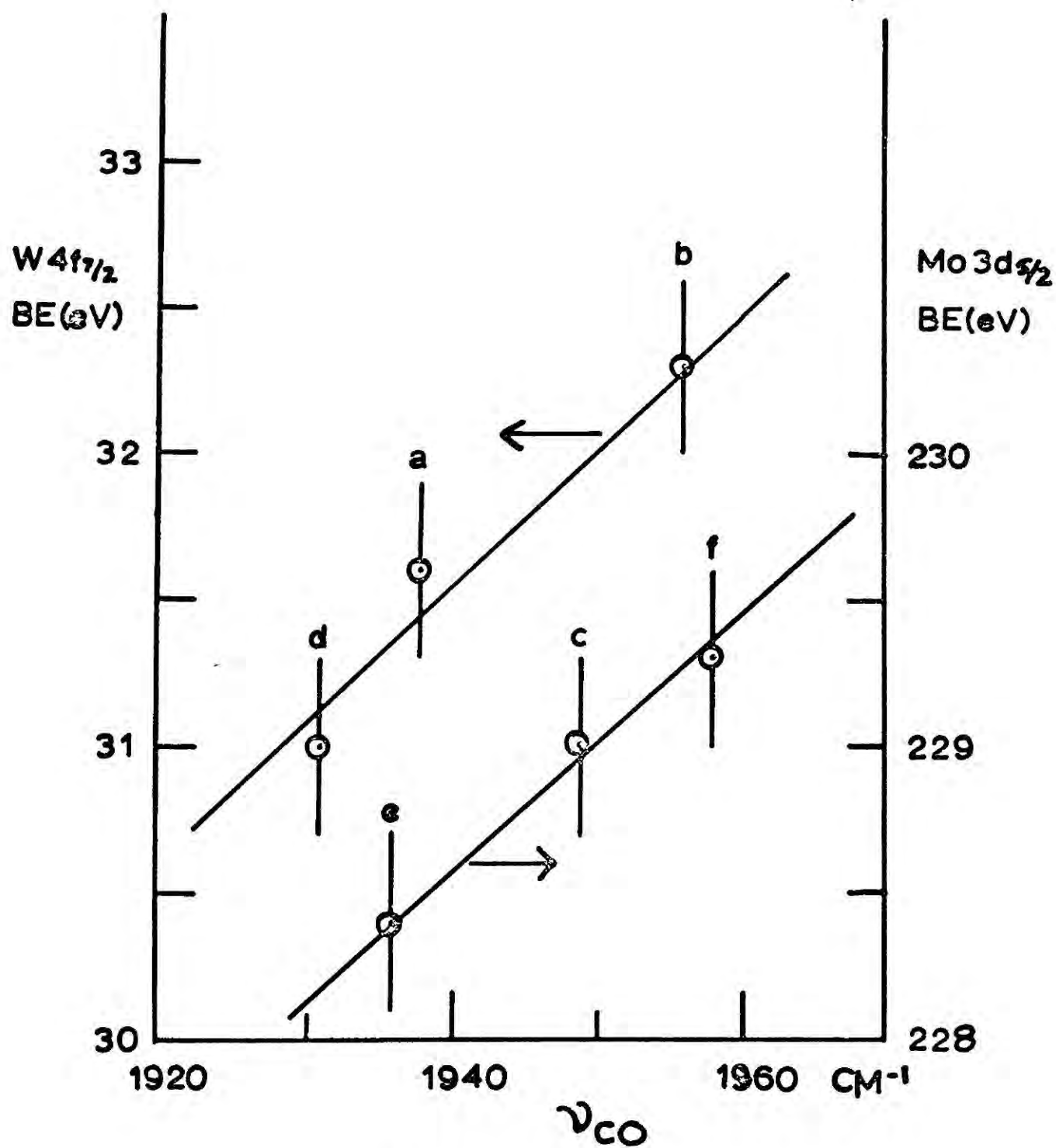


FIGURE 5.2

(bent or linear M-N-C skeletons respectively) depending on the involvement of the nitrogen lone pair. Variable temperature ^1H and ^{19}F nmr spectra for the complexes with $\text{R} = \text{tBu}$,^{143,144} p-tolyl ¹⁴² and $\text{p-CF}_3\text{C}_6\text{H}_4$ ¹⁴² respectively (the aryl groups having fairly low steric requirements) strongly suggest a linear M-N-C skeleton. X-ray diffraction data for $\pi\text{-C}_5\text{H}_5\text{Mo(CO)}_2\text{NCtBu}_2$ ¹⁴⁵ showed a virtually linear skeleton and considerable multiple bonding in the M-N bond, although a model indicated that this may be due to steric requirements of the ligand and not solely due to electronic effects. C=N stretching frequencies for complexes in which $\text{R} = \text{tBu}$ are not appreciably lowered from those of the free methyleneamine as might be expected if back donation were significant. Methyleneamino groups bound linearly to the main group metals and metalloids¹⁴⁶ where $d_\pi \rightarrow \pi^*$ back donation is not possible (eg. Be, B, Al, Si) or unlikely (eg. Ga) show significant increases in ν_{CN} but as the co-ordinating element becomes heavier this increase becomes smaller¹⁴⁷ and the small charges for transition metal complexes are in keeping with this trend. Hence σ and $p_\pi\text{-}d_\pi$ donation processes which tend to increase ν_{CN} may be effectively balanced by $d_\pi \rightarrow \pi^*$ back bonding. In the complexes studied here the C=N frequencies are obscured by ring vibrations of the aryl groups so this information is lacking.

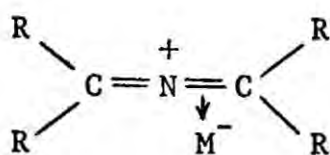
Referring to the relevant figures in Table 5.1 it is apparent that there is no statistically significant alteration of the Nls BE's of the methyleneamines on replacing the hydrogen by a transition metal. This is equivalent to saying that the electron density on nitrogen is virtually unaltered which suggests that either the lone pair is not involved in bonding or that the π -donor and π -acceptor tendencies of the ligand are effectively balanced. The fact that long range electronic effects are efficiently transmitted from para-positions on the aryl groups via

nitrogen and the metal to the carbonyl groups argues the presence of a conjugated π -system and, therefore, favours the latter explanation. It is therefore likely that for all types of R group in $R_2C:N-$ ligands the M-N-C skeleton will be linear as a result of maximum overlap of the nitrogen lone pair (in a p orbital) with suitable metal d orbitals. Back donation ($d_{\pi} \rightarrow \pi^*$) can then increase synergically with this increase in $p_{\pi}-d_{\pi}$ bonding.

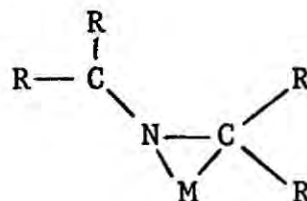
(c) Aza-allyl/allene complexes

The aza-allyl/allene ligand is thought to act as a three electron donor (thus fulfilling the inert gas rule for the metal), on the basis of a) the failure to add a further neutral 2-electron donor such as triphenylphosphine or even CO under conditions of high temperature and pressure,¹⁴⁸ and b) the low carbonyl frequencies indicating dissipation of high charge build-up on the metal as described above.

For the complexes studied, $\pi-C_5H_5M(CO)_2[R_2CNCR_2]$ (M = Mo, W; R = p-tolyl, p-CF₃C₆H₄) two isomers exist in the solid state (forms A and B). The possible nature of these isomers and the isolation of form A (M = Mo, R = p-tolyl) (1) and form B (M = W, R = p-tolyl) has been discussed previously.¹⁵⁰ The crystal structure of (1) shows that the ligand adopts the aza-allene bonding mode;¹⁴⁵ The observed molecular geometries¹⁴⁵ and interatomic distances are not inconsistent with either of the extreme bonding modes (Figure 5.3).



(a)



(b)

Figure 5.3

The first (Figures 5.3(a)), involves transfer of an electron to the metal leaving a positively charged ligand which is isoelectronic with the allenes; the ligand then acts as a two electron mono-olefin type donor. The second (Figure 5.3(b)) would imply bonding of the aza-allene radical, $R_2C=N-CR_2$, via a metal-carbon bond and σ -donation of the nitrogen lone pair, resulting in formation of an essentially σ -bonded three membered ring.

The bonding situation illustrated in Fig 5.3(a) would be expected to be similar to that found in transition metal allene complexes involving σ -donation from the ligand and $d_{\pi} \rightarrow \pi^*$ back donation. The similarity of C-C bond lengths for the 'free' and complexed ligands, and their slight deviation from the normal olefinic C-C distance,¹⁵⁰ in such complexes indicates that the latter process has little effect on the coordinated C-C bond length. The metal-carbon bond distances in such complexes tend to be slightly longer than those in metal alkyls. In the aza-allene complex the co-ordinated C-N bond length is that of the single bond and the Mo-N and Mo-C distances are slightly shorter than single bonds. Back donation must, therefore play a significant role. This is only to be expected for the postulated positively charged ligand and a parallel could be drawn between this ligand and TCNE which, as a poor σ -donor and very strong π - acceptor, displays almost single C-C bond distances in its complexes.¹⁵¹ The C-N bond lengths also indicate more extensive back donation than in the corresponding methyleneamino complexes (see above). The flow of electron density to the ligand could balance, if not exceed, initial transfer of an electron to the metal, in view of the reduction of the co-ordinated C-N bond order to one.

For this bonding mode, therefore, the nitrogen BE would not be expected to differ greatly from that of the free ligand while the metal BE might compare with that found for the corresponding methylamino complex where donation to and from the metal appear to balance also.

In the other bonding mode the more effective Mo-N bonding would take place with the nitrogen lone pair occupying an orbital of near sp^2 hybridisation, with most of the electron density directed towards the metal. The Mo-N and Mo-C distances imply a degree of back donation. This may occur for the Mo-N bond by $d_{\pi} \rightarrow \pi^*$ donation into the orthogonal π^* orbitals of the unco-ordinated C=N system, but for the structure shown in Fig. 5.3(b) there would be no π^* orbitals available for back donation on the unco-ordinated carbon atom. A less extreme structure than that shown, in which some π character is given to the co-ordinated C-N bond must be invoked to fit the observed structural parameters. The net result is still likely to be one in which a build-up of electron density occurs on the metal, at the expense of the nitrogen.

Consider now the BE data given in Table 5.1. The N1s BE (400.0 eV) for $\pi\text{-C}_5\text{H}_5\text{Mo}(\text{CO})_2\{(\text{p-tolyl})_2\text{CNC}(\text{p-tolyl})_2\}$ is 1.3 eV greater than in $\pi\text{-C}_5\text{H}_5\text{Mo}(\text{CO})_2\text{NC}(\text{p-tolyl})_2$ and 1.2 eV greater than in $(\text{p-tolyl})_2\text{C=NHPH}_2$. The latter may be taken as a reasonable model for the free aza-allene ligand since as far as the N1s BE is concerned there is expected to be little difference between $(\text{p-tolyl})_2\text{C=N-CHPh}_2$ and $(\text{p-tolyl})_2\text{C=N-CPh}_2$. Such increases in BE indicate a considerable relative reduction of electron density at nitrogen. There is also a significant increase in the metal electron density in going from the methyleneamino to the

aza-allene complex (0.6 eV decrease in BE). This data suggests that bonding of the aza-allene group to Mo involves a greater degree of electron donation from ligand to metal than is apparent in the analogous methyleneamino complexes, rather than the predominantly metal-ligand back donation process implied by the structure shown in Fig. 5.3(a). This is good evidence for the direct involvement of the nitrogen lone pair in bonding as described above for a less extreme case of Fig. 5.3(b).

The structure of the 'form B' isomer is as yet unknown, though the similarity of the infrared spectrum to that of the common type in solution¹⁵² suggests that the ligand may adopt the aza-allylic arrangement. No significant broadening of the N1s or Mo3d peaks from a sample containing approximately equal quantities of A and B isomers of $\pi\text{-C}_5\text{H}_5\text{W}(\text{CO})_2\{(\text{p-tolyl})_2\text{CNC}(\text{p-tolyl})_2\}$ with respect to the pure B form was detected so it can be confidently predicted that whatever structure is adopted the electron distribution is essentially the same in both A and B forms.

Similar isomeric forms are thought to exist for the complexes $\pi\text{-C}_5\text{H}_5\text{Mo}(\text{CO})_2\{(\text{p-CF}_3\text{C}_6\text{H}_4)_2\text{CNC}(\text{p-CF}_3\text{C}_6\text{H}_4)_2\}$ (M = Mo, W).¹⁵² The Mo compound contains approximately equal proportions of the two isomers and these cannot be separated by fractional crystallisation. Broadening of the Mo3p and 3d peaks is significant, whereas the N1s peak has the same half-width as found in all other spectra (1.7-1.8 eV). This may be an artifact due to differential charging effects but this is considered to be very unlikely since the isomers crystallise as an intimate mixture. The difference between the higher frequency ν_{CO} signals for the two forms is 8 cm^{-1} in this complex compared with only $\sim 3\text{ cm}^{-1}$ for the complex with p-tolyl groups (by analogy with the data from the W

complex which has been isolated in both isomeric forms). From the BE/ν_{CO} correlation (Fig. 5.2) it may be deduced that a BE difference large enough to give detectable line broadening would only be expected for the case where $\Delta\nu_{CO} \geq 8 \text{ cm}^{-1}$.

PART II

CHAPTER VI

SOME INVESTIGATIONS OF THE PLATINUM-ETHYLENE-HYDROGEN
SYSTEM.

(i) General Introduction.

The eventual aim of this work was the examination of a typical catalytic system by ESCA in order to assess the potential of the technique for giving information on the nature of adsorbed species, catalytic sites, and surface coverage. The system chosen was the supported platinum-ethylene-hydrogen system for the following reasons.

- a) The platinum-olefin-hydrogen system has been extensively studied in the past in a variety of ways, giving rise to a large body of data.
- b) The metal catalyst in the supported state is much more amenable to study, in general, than the other high surface area preparation - the evaporated metal film. In particular, silica supported metals can be conveniently used for i.r. studies of adsorbed species.
- c) Platinum is highly convenient for ESCA studies because of the high photoionisation cross-section of the 4f core levels.
- d) Under normal, mild, conditions the hydrogenation of ethylene over platinum is superficially very simple giving ethane as the only product.

Notwithstanding this latter statement, Selwood¹⁵³ has remarked: "No problems in surface chemistry have been more hotly debated than the adsorption and hydrogenation mechanisms for ethylene; and few debates have resulted in such meagre conclusions". This remark serves to illustrate the underlying complexity of the system.

The available information, pertaining mainly to the possible nature of the adsorbed species and the mechanism of hydrogenation is largely contained in two thorough reviews written during the last ten years.^{154,155}

In choosing this system as being representative of the very large and important class of olefin hydrogenation reactions catalysed by metals a sweeping simplification of the number of variables is made. Thus the nature of the olefin (geometric and electronic effects relating to size and nature of substituent groups) is removed from consideration together with the attendant problems of multiple reaction pathways and the reasons for possible selectivity (an area which has recently been reviewed¹⁵⁶). The great variation in behaviour of different metals when catalysing a given reaction¹⁵⁵ is similarly bypassed. Even so, the single metal has been used to carry out the reaction in a variety of forms: (i) macroscopic forms (wires, foils, granules); (ii) microscopic forms (powders by chemical reaction, smokes, skeletal powders, colloidal suspensions, blacks, condensed metal films); (iii) supported forms, where the metal in varying concentrations is dispersed to a varying degree in another more or less inert substance (usually an irreducible metal oxide or salt). Within each category there is scope for infinite variation. Even with metal in simple wire form the exact surface structure will depend on the precise metallurgical history of the sample and it is factors such as this which bedevil the achievement of reproducibility of behaviour in reaction systems catalysed by metals.

Owing to this wide variation in the form and method of preparation of catalysts used for investigations of the system to be considered it is difficult to estimate the reliability of comparing data from studies

involving different experimental techniques. It is also a feature of surface studies in general, and catalyst studies in particular, that because of the complexity of methods and instrumentation involved it is uncommon for data to be derived from a single system by more than one technique. Thus it was considered necessary to characterise the catalyst to be used for ESCA studies by applying the most commonly used techniques to a study of its behaviour in the system with ethylene and hydrogen. These techniques are:

- (i) derivation of kinetic parameters e.g. orders of reaction and activation energies,
- (ii) investigation of the pattern of deuteration of product ethanes* and deuterium incorporation in the ethylene starting material in the reaction of ethylene with deuterium, using mass spectrometry,
- (iii) transmission i.r. studies of chemisorbed species produced by ethylene adsorption and their reaction with hydrogen.

Hopefully, a further outcome of these studies would be an indication of the reliability of data using these techniques with different catalytic preparations.

In the following sections of this chapter the experimental procedures are described and the results obtained using each technique discussed in conjunction with related data published by other workers.

* In the following discussion ethane is used as the generic term for the various deuterated ethanes ($C_2H_nD_{6-n}$).

(ii) Kinetic Studies

(a) Experimental.

The apparatus consisted of two distinct sections: (1) the vacuum-line/reaction vessel system and (2) the glc separation and detection system.

The vacuum-line/reaction vessel system

This is shown diagrammatically in Fig. 6.1. The apparatus, with the exception of the calibrated leak valve, was of all glass construction. Greased taps were kept to a minimum to avoid sample contamination as far as possible; Young valves were consequently preferred as the standard tap. Gas pressures between 1-760 torr were measured by means of a mercury manometer and from 1- 10^{-7} torr by means of a Penning gauge. The pumping system consisted of a conventional two-stage set-up comprising a rotary pump capable of giving a backing pressure of $< 10^{-3}$ torr with liquid N_2 in the cold traps and a mercury diffusion pump capable of reaching $< 10^{-6}$ torr. Full details of the equipment are given at the end of this section.

The reaction system, overall capacity ~ 200 ml, consisted of a cylindrical pyrex glass reaction vessel, attached to the line through a water-cooled B-24 greased joint, with a thermal cycle loop of 2mm glass tubing. The limb of this loop furthest from the reaction vessel was wound over its length with heating tape and its temperature maintained at $\sim 120^\circ C$ to assist diffusion of reactants and products around the system and to ensure sample homogeneity. Over the temperature range used for reactions no problems of sample inhomogeneity arose (total gas pressures were rarely greater than 200 torr), the system having been well tested

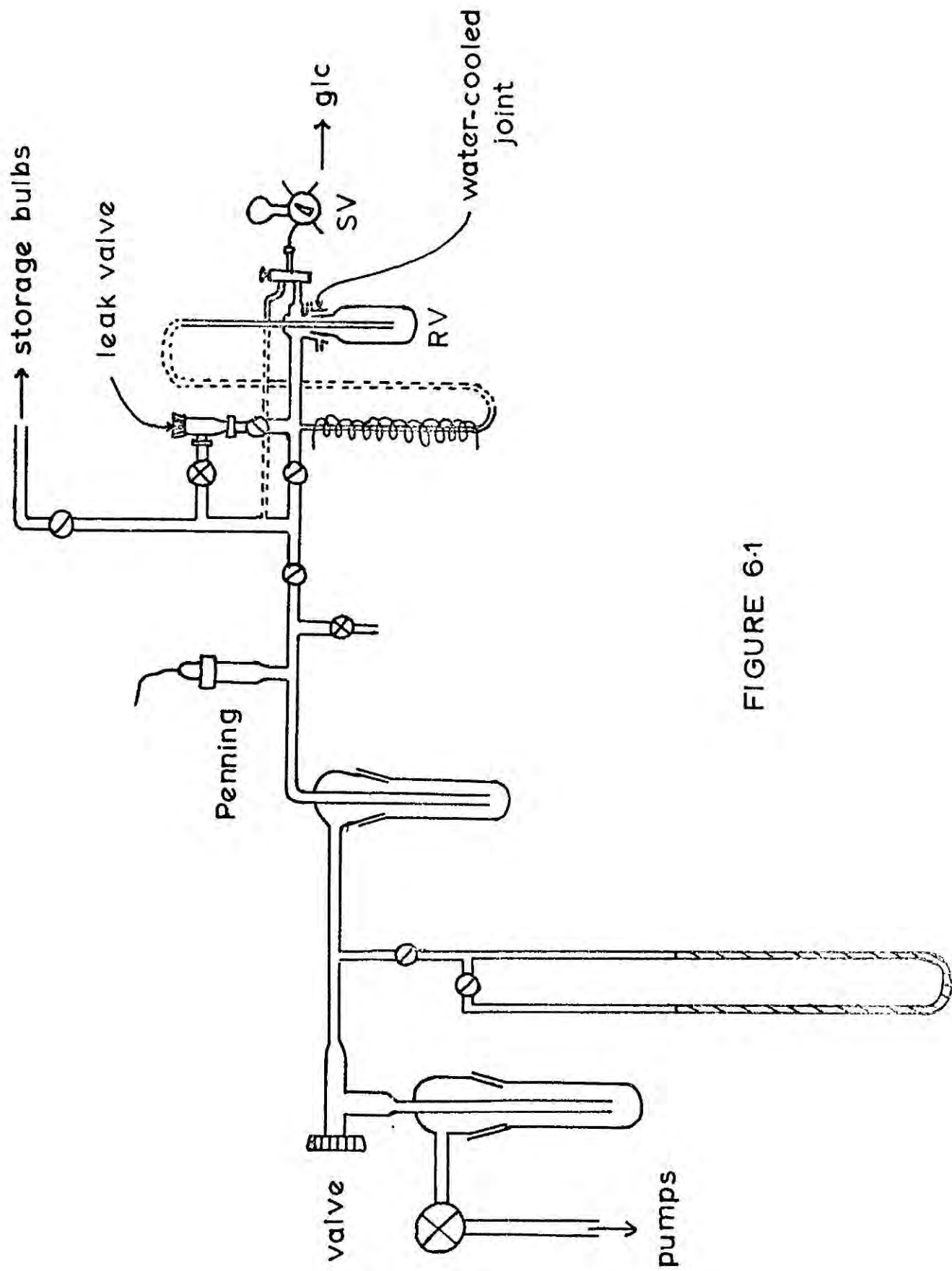


FIGURE 6.1

initially with N_2/CO_2 mixtures, at various temperatures and pressures, with this factor in mind.

Reactant gases could be added to the vessel in sequence, using the calibrated leak valve, or premixed by expansion into the vessel from the vacuum line. The reaction temperature (if above ambient) could be regulated by means of a furnace designed to fit around the reaction vessel almost up to the water-cooled connecting joint. A 'Eurotherm' controller was used to control the temperature of the furnace and the reaction vessel temperature measured accurately by use of a chromel-alumel thermocouple, fastened against its base (ie by the catalyst), with a 'Copricon' potentiometer. Temperatures below ambient were achieved by placing a slush bath, at the required temperature, around the reaction vessel - the exact temperature being measured in the same way.

Sampling to the glc system was carried out directly through a 2ml Pye sample valve connected to the reaction vessel system as shown in Fig. 6.1 and, in more detail, in Fig. 6.2. By means of the two-way tap the sample loop could be evacuated (to $< 10^{-3}$ torr) via the vacuum line and then filled by connection to the reaction vessel. The dead space between the two-way tap and the sample loop was reduced to ~ 1 ml by using capillary glass tubing of minimal length and a Pye $3/16$ " capillary connection to effect the glass-sample valve union. The union was made vacuum tight by encapsulation in 'glyptol'.

glc separation and detection.

The glc system is shown schematically in Fig. 6.3. The column used for separating the ethane product from unreacted hydrogen and ethylene was 2' x $3/16$ " of silica gel (B.D.H. chromatographic grade,

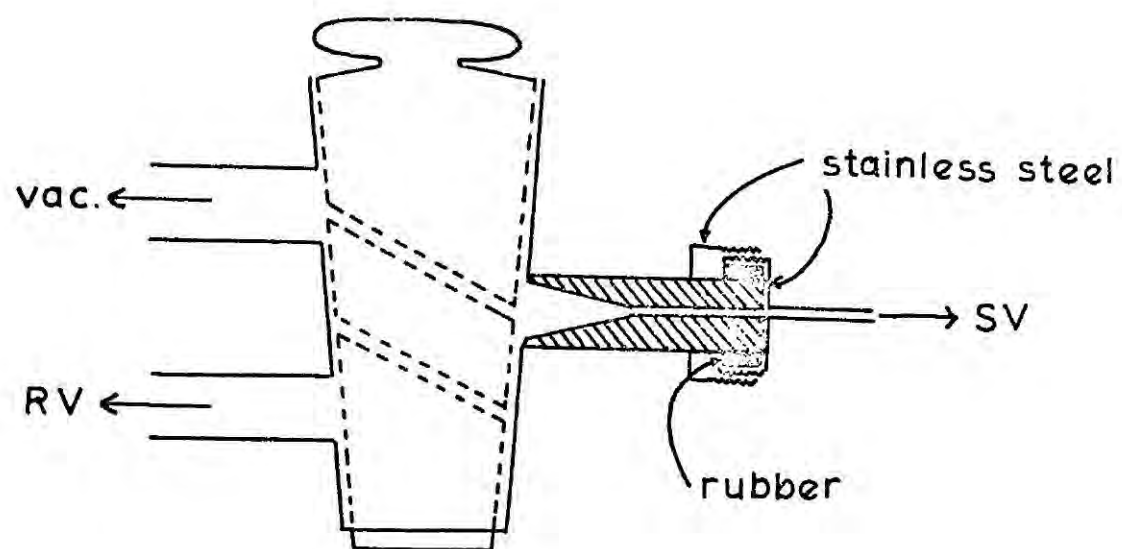
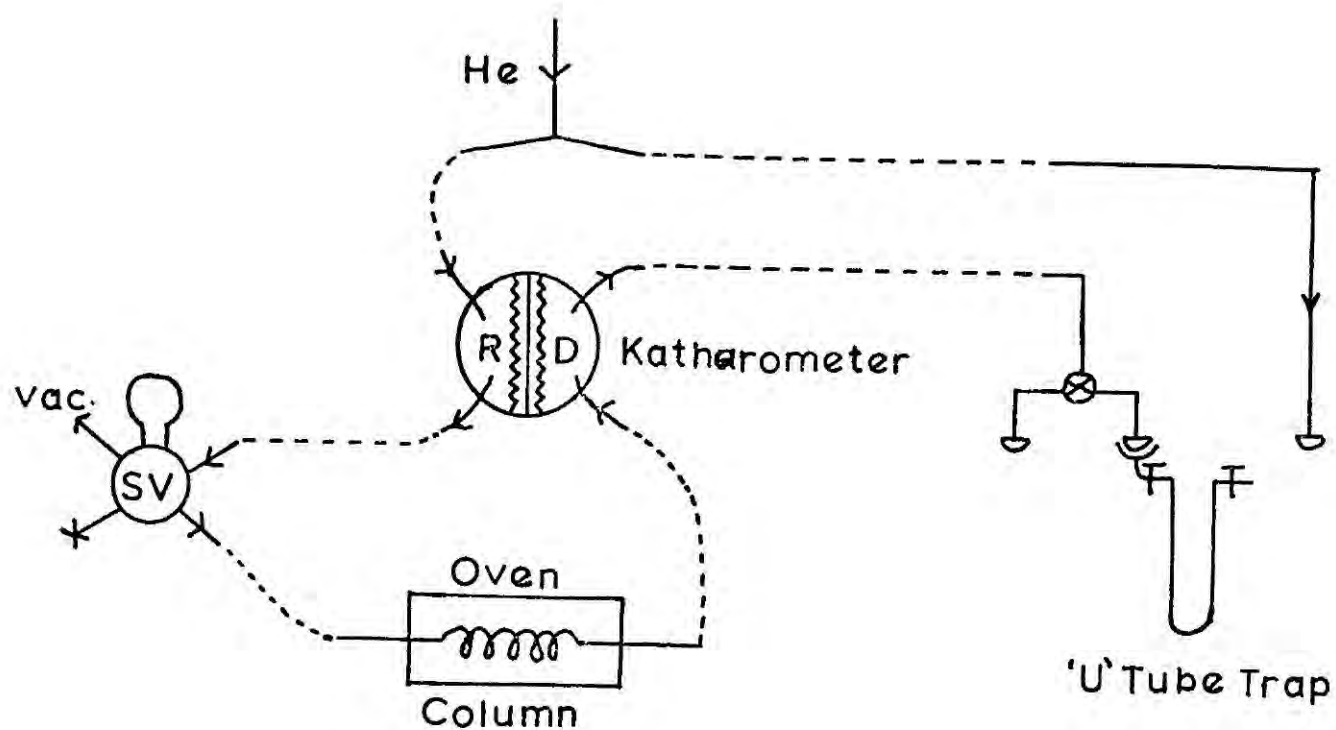
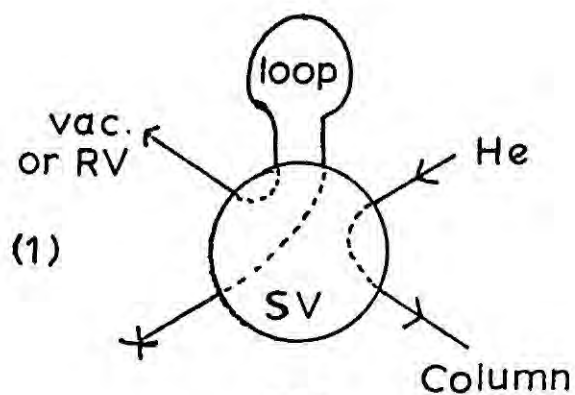


FIGURE 6.2

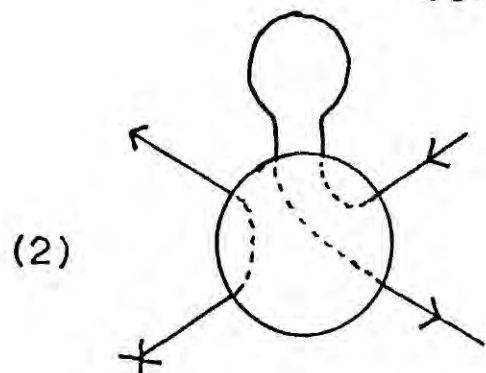


R=Reference , D=Detection

FIGURE 6.3



(i) loop to vac. then,
(ii) to RV



contents of loop
to column

FIGURE 6.4

60-120 mesh). The pressure drop across this column was very small so by adopting the configuration shown (Fig. 6.3), viz. passing the carrier stream (He) through the reference side of the katharometer detector before sweeping the sample and thence through the detection side, the necessity of balancing columns was obviated. The two operating modes of the sample valve, chosen simply by a two-position switch are shown schematically in Fig. 6.4.

It is customary in such glc systems to incorporate both column and katharometer in the same oven. The microcatalytic equipment used (see below) was ideal in most respects for the chosen application but required a capillary column. Consequently the column was housed in a separate oven to that containing the microkatharometer, the distance between the two being kept to a minimum within the constraints of the apparatus geometry (< 30 cms of stainless steel capillary tubing). An advantage so gained was the freedom to run the katharometer at its optimum temperature for sensitivity while maintaining the column at its optimum temperature for separation of components in the gas stream.

Using a He flow-rate of 20 mls/min (pressure = 5 p.s.i.) as recommended for the equipment the other variables for the column (length and temperature) were chosen so that: (1) the separation between elution times for C_2H_6 and C_2H_4 was great enough to allow efficient trapping of both fractions separately (necessary for the mass spectrometric work described in Section (iii)) but (2) the total elution time was < 10 mins so that sampling could be reasonably frequent. Consequently a $2' \times \frac{3}{16}''$ silica column, as described above, was operated at $45^\circ C$. A typical record of the separation properties of this system is shown in Fig. 6.5.

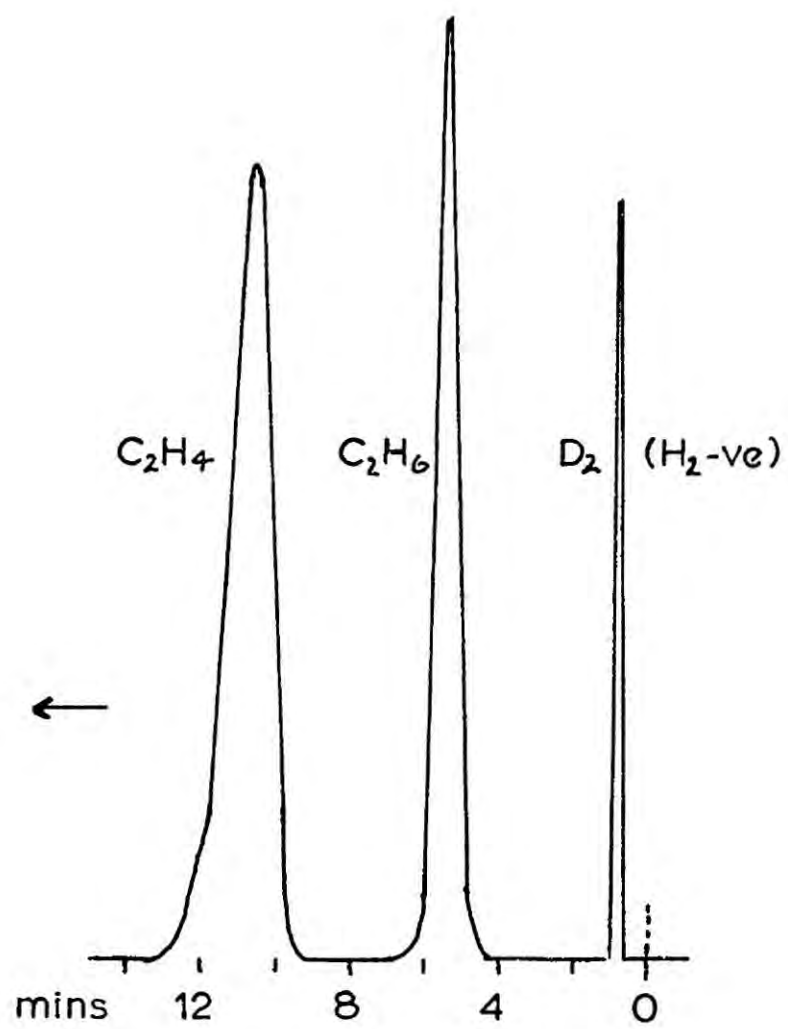


FIGURE 6.5

By placing known pressures of a gas in the reaction vessel and measuring the height of the recorded peaks, calibration curves for peak height vs. partial pressure of H_2 , C_2H_4 and C_2H_6 in the system were constructed. Reactions were studied by monitoring the formation of ethane and deriving initial rates of reaction. In most cases the partial pressure region of the calibration curve used fell on the initial linear portion so that graphs of the ethane peak height against time could be used directly to derive initial rate parameters (see later). Repeated samples gave highly reproducible glc peaks (to within 1%); since the sample taken was only $\sim 1\%$ of the total and usually no more than five samples were taken in any given run, the effects of sample removal on subsequent calculations was ignored.

Equipment details:

Rotary pump - A.E.I. 'Metrovac' type.

Diffusion pump - Edwards 'Speedivac' (Hg) type.

Gas sample valve - Pye Series 104 (2 ml capacity).

Katharometer - Servomex Microkath. Mk 158.

Katharometer oven - Servomex I.O. 199.

Oven controller - Servomex T.C. 201.

Katharometer bridge control - Servomex G.C. 197.

Column oven - Griffin and George glc oven.

Recorder - Honeywell (Brown Electronik) chart recorder, model 64B.

Reactants.

Ethylene (British Oxygen Corp. C.P. grade) was transferred directly from a cylinder to a storage bulb, previously evacuated to 10^{-6} torr,

and thoroughly degassed by several freeze-pump-thaw cycles but not otherwise purified. Hydrogen (B.O.C., C.P. grade) was similarly stored and maintained at liquid nitrogen temperature so that when admitted to the reaction vessel any possibility of contamination by trace amounts of water was greatly reduced. Both reactants, as used, were shown to be impurity free by glc and mass spectral analyses. Ethane (Matheson C.P. grade) used for calibration purposes was treated in exactly the same way as the ethylene and similarly shown to be impurity free within the limits of detection. Oxygen (B.O.C., C.P. grade) used for catalyst pretreatment was similarly stored but not otherwise treated.

The catalyst.

The material to use as the platinum support was dictated by the wish to perform infrared studies of hydrocarbon species adsorbed on the catalyst. Silica, by virtue of its high transmission properties, is ideally suited for this role. Of the many varieties of silica produced, 'Aerosil' (Bush, Beech and Bailey Ltd.) was chosen because of its particularly high transmission properties for infrared, its high surface area ($380\text{m}^2\text{ gm}^{-1}$) and because, even when loaded with quite high percentages of metal, it can readily be pressed into thin discs which are reasonably robust.

Because of the variety of studies to be performed on the catalyst, the precise metal loading was subject to several considerations. For all investigations a high dispersion (aided by the high surface area of the chosen support) was desirable. For ESCA work as high a loading as possible was required to give at least adequate spectral intensities. For IR work a balance had to be struck between sufficient surface area of metal to adsorb enough material to give adequate IR bands (in the C-H stretch region) and the competing loss of transmission with increase in metal concentration.

From this last consideration the upper limit to metal loading is probably $\sim 15\%$,¹⁵⁷ while for catalysts prepared by chloroplatinic acid impregnation and reduction the achievable dispersion begins to level off above $\sim 10\%$.¹⁵⁸ A 12% Pt/SiO₂ catalyst was therefore prepared and found to have good properties for IR work and acceptable Pt4f peak intensities (from ESCA) in preliminary investigations.

The structure and activity of supported metal catalysts has been extensively studied by Moss and co-workers with particular reference to the Pt/SiO₂ system (refs 158,159 and refs contained therein). This work has resulted in quite detailed understanding of those factors which influence the characteristics of the catalyst during preparation and subsequent use, and has established reliable 'recipes' for obtaining catalysts with maximum dispersion (minimum crystallite size) for a given metal concentration. The following method of preparation of the catalyst used in this work is based on these data.^{158,159}

Catalyst preparation

1 gm of chloroplatinic acid, H₂PtCl₆.xH₂O (Johnson-Mathey, stated 40% Pt) was dissolved in approximately 5 ml distilled water in an evaporating basin. 2.93gm Aerosil SiO₂ were added and the whole stirred while slowly evaporating off the excess water. The remaining dry powder (pale yellow) was dried in an air oven ($\sim 110^{\circ}\text{C}$) for 23 hrs. and reduced in a 1% H₂/N₂ stream for 2 hrs. at 150°C during which the powder turned yellow-brown and then black. When reduction appeared complete the catalyst was further treated with flowing H₂(pure) for 30 mins at the same temperature.

Analysis of the product gave a Pt content of 12.2%. Electron micrographs revealed a mean Pt crystallite size of $\sim 50\text{\AA}$ and the total catalyst surface area was found to be $330\text{ m}^2\text{ gm}^{-1}$ by the nitrogen adsorption method.

Description of experiments and results

There have been two previous reports^{160,161} of the main kinetic parameters for ethylene hydrogenation over supported platinum. In both cases the reaction was followed by noting the change in total pressure macrometrically (possible mercury poisoning of the catalyst was stated not to be a problem). Reactants were usually added consecutively, ethylene first, though the order was found not to affect the catalyst's performance. The results obtained were:

$$1) \quad -dp/dt = k[H_2]^{1.2}[C_2H_4]^{-0.5}$$

$$(E_a = 9.9 \pm 0.5 \text{ Kcal mole}^{-1} \text{ (T = 0-50}^\circ\text{C) (ref 160)}$$

$$2) \quad -dp/dt = k[H_2]^{1.0}[C_2H_4]^{-0.3}$$

$$(E_a = 15 \pm 2 \text{ Kcal mole}^{-1} \text{ (T = 0-40}^\circ\text{C) (ref 161)}$$

No comment has been made by the common authors on the significant differences in these results which indicates the necessity for a closer re-examination of the system.

For kinetic work the 12% Pt/SiO₂ catalyst was far too active so two dilute forms were prepared by grinding the catalyst with the required amount of support material (Aerosil) to give dilutions of x 20 and x 50 respectively.

The procedures described for the above determinations were closely followed in a series of preliminary experiments. The catalyst (typically 10 mgms of the 20 x diluted batch) was reduced in situ using 50 torr H₂ for 30 mins at 200°C. After evacuation to $\sim 10^{-5}$ torr and the return to room temperature a known pressure of ethylene was added, followed by

hydrogen addition via the leak valve. The reaction was followed as described above. Reproducible behaviour under identical starting conditions could not be achieved, irrespective of whether the catalyst was merely evacuated or reactivated by heating in H_2 between runs. If the system was only evacuated between runs then the activity, as measured by the initial rate of ethane production, fell systematically. In order to remove the possibility that prior exposure to ethylene might cause catalyst poisoning the remaining experiments were performed using the technique of premixing the reactants in the desired ratio and expanding them into the evacuated reaction vessel.

It has been suggested¹⁵⁸ that observed 'activation energies' (E_a values) greater than the accepted 8-10 kcal mole⁻¹ are to be expected for catalysts of low metal content used at temperatures $> -80^\circ C$ because of poisoning due to the formation of carbidic residues on the metal. To check this and to obtain orders of reaction runs were performed on a deliberately deactivated catalyst.

Determination of E_a for a deactivated catalyst

15 mgms of the 20 x diluted catalyst was subjected to a series of runs, under the following standard conditions, until the activity had fallen to the point of reproducibility. Initial partial pressures were 50 (± 2) torr of C_2H_4 and H_2 and the reaction temperature gradually raised to $60^\circ C$, as the activity fell, to give conveniently measurable rates. When the activity was constant a series of standard runs was carried out at various temperatures between $60-120^\circ C$. After each run the temperature was stabilised at that to be used for the next run before evacuating the vessel to 10^{-5} torr. A blank run on 17 mgms of pure Aerosil under

the same conditions, apart from higher temperature (150°C), gave an ethane peak on the glc recorder just detectable ($\ll 1\%$ conversion) after 3.5 hrs. Any contribution to the catalyst activity from the support can, therefore, be completely neglected under any of the conditions used in these experiments. Typical plots of increase in ethane partial pressure with time are shown in Fig. 6.6; extrapolation of the plot to zero partial pressure does not coincide with zero time because: (i) the onset of reaction does not coincide with the arbitrary $t = 0$ chosen (the time of opening the tap for expansion into the reaction vessel), (ii) the time for product to diffuse initially to the sample valve region is finite and (iii) there may in any case be a significant induction period.¹⁶⁰ The observed initial rates ($k \text{ torr } (\text{C}_2\text{H}_6) \text{ min}^{-1}$) for the various temperatures are shown in Table 6.1.

$T(^{\circ}\text{K})$	$1000/T \text{ (deg}^{-1}\text{)}$	$10k(\text{torr min}^{-1})$	$\ln(10k)$
343	2.92	0.533	-0.629
357	2.80	1.91	0.647
369	2.71	4.95	1.599
378	2.64	9.72	2.274
392	2.55	30.0	3.401

TABLE 6.1

An Arrhenius plot of $\ln(10k)$ vs $10^3/T$ gives a good straight line whose slope $(-E_a/R) = 10.6 \times 10^3 \text{ deg}^{-1}$ (Fig. 6.7). Hence $E_a = 21 \text{ kcal mole}^{-1}$. The error, arising mainly from accuracy of initial pressure measurement and uncertainty in actual catalyst temperature is estimated to be $< 5\%$,

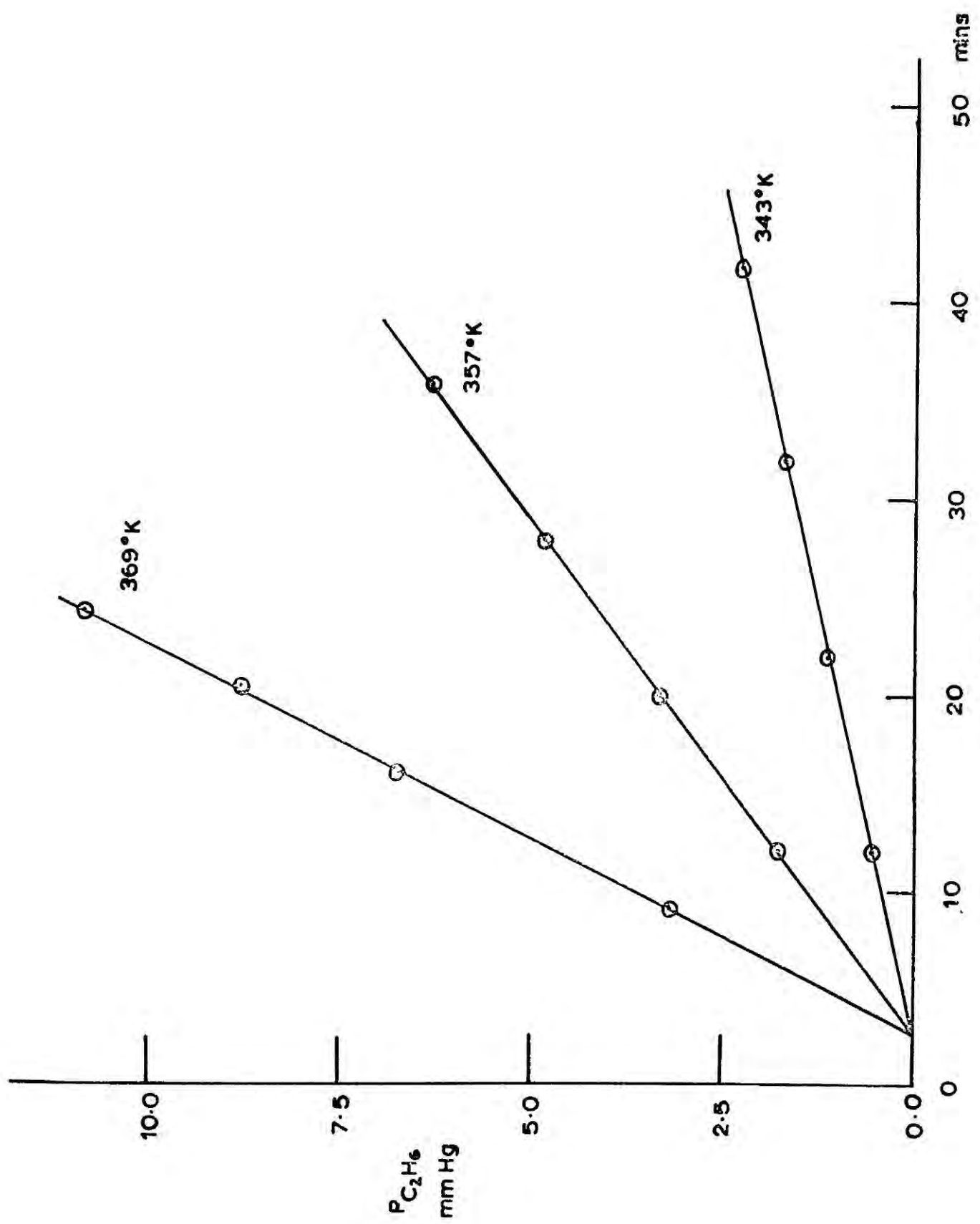


FIGURE 6.6

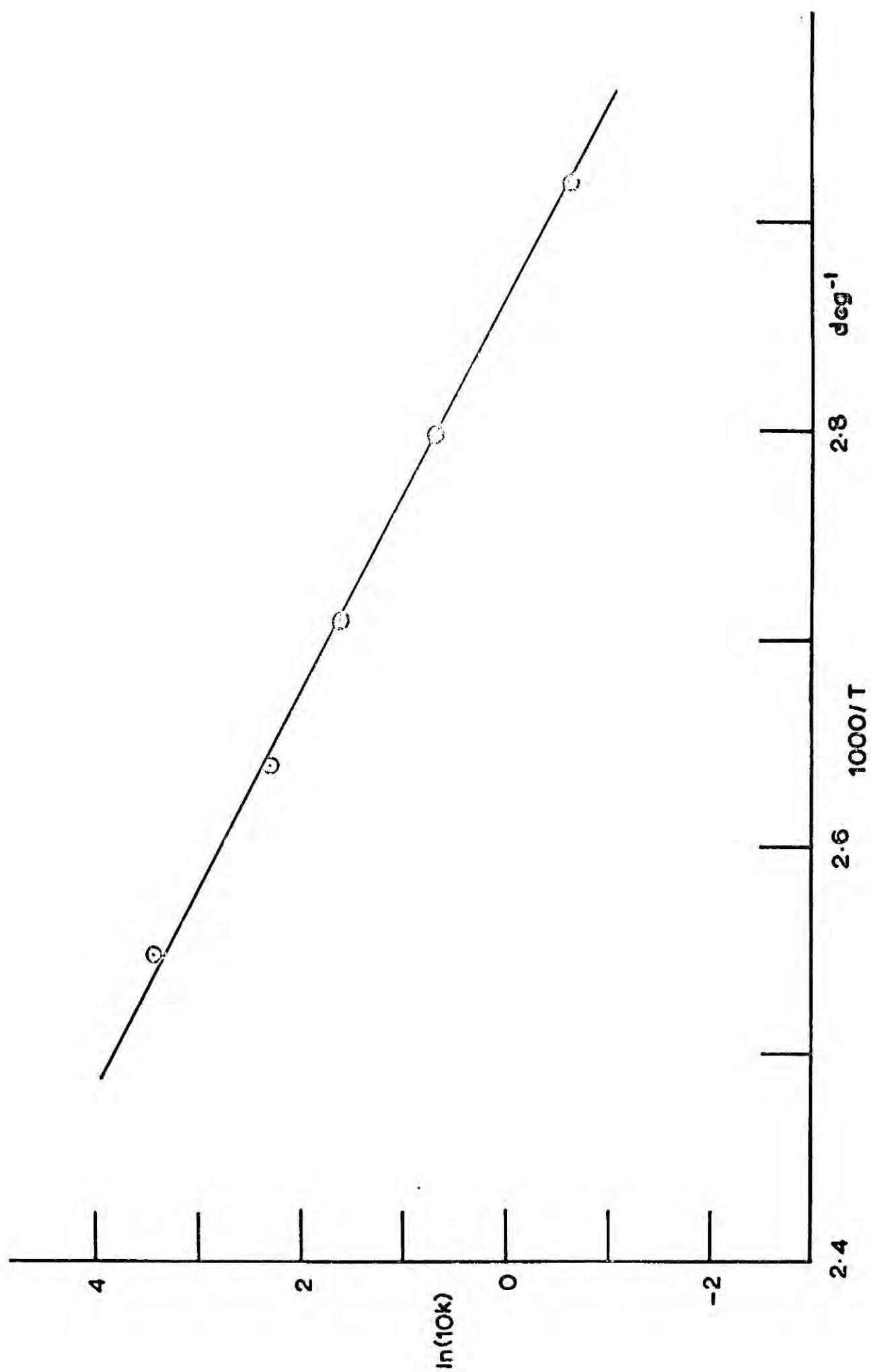


FIGURE 6.7

giving $E_a = 21 \pm 1$ kcal mole⁻¹. This value is, as anticipated, much higher than (at least double) the accepted value of ~ 9 kcal mole⁻¹ mentioned above. The reasons for this are discussed in section (i)c below.

Determination of orders of reaction for a deactivated catalyst

(i) Order in H₂.

The same catalyst charge as used above was retained for a series of runs at 60°C. The ethylene partial pressure was kept constant at 53 ± 1 torr while the hydrogen partial pressure was varied from 20-160 torr. The system was merely evacuated between runs to 10^{-5} torr, the runs being performed in random order to obviate trends (such as the continuing very slow loss of catalyst activity). Initial rate plots were obtained directly in terms of C₂H₆ glc peak height (at these low pressures, proportional to partial pressure). The results are shown in Table 6.2.

run no.	k (\propto torr min ⁻¹)	log k	PH ₂ (torr)	log PH ₂
3	1.11	0.0453	28	1.447
1	2.06	0.314	55	1.740
5	2.99	0.476	76	1.881
2	4.13	0.616	114	2.057
4	5.57	0.746	160	2.204

TABLE 6.2

A plot of log k vs log PH₂ gives a good straight line (Fig. 6.8) of slope 1.0 ± 0.05 , the order of reaction in H₂.

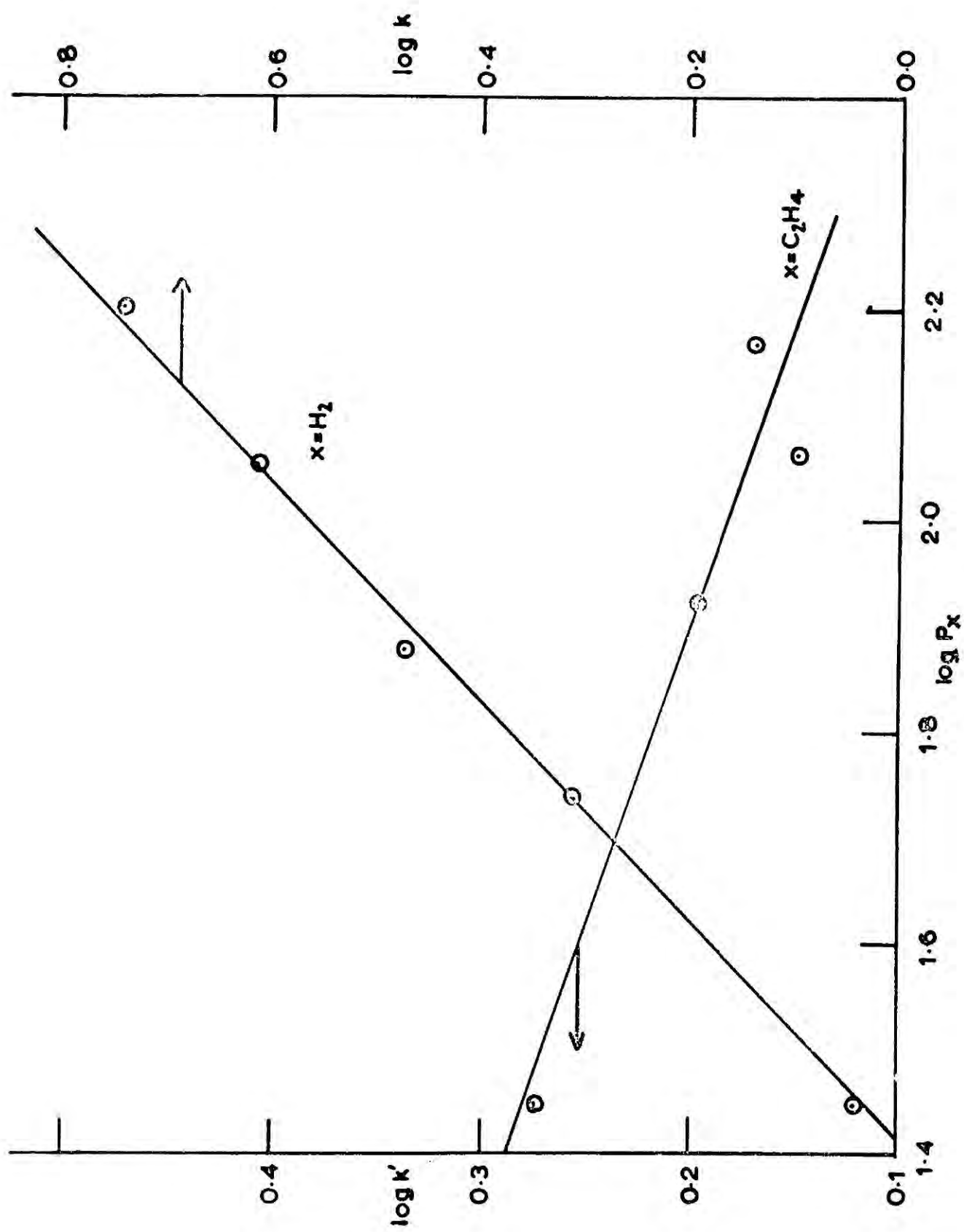


FIGURE 6.8

(ii) Order in C_2H_4 .

This time the partial pressure of hydrogen was kept constant at ~ 50 torr while the ethylene partial pressure varied between 20-150 torr. All reactions were carried out as above, in random order, at $60^\circ C$. It was found difficult, because of the premixing method used, to achieve the requirement of constant H_2 partial pressure with great accuracy. However, this was corrected for by taking into account the effect of this variation (assuming order in $H_2 = 1.0$ as found) on the initial rate. Table 6.3 gives the initial rate data ($k \propto \text{torr min}^{-1}$) and the calculated values adjusted to $P_{H_2} = 50$ torr (k').

run no.	P_{H_2} (torr)	k	k'	$\log k'$	$P C_2H_4$ (torr)	$\log P C_2H_4$
1	57	2.14	1.88	0.274	28	1.447
3	52	1.64	1.58	0.199	84	2.068
4	52	1.48	1.42	0.149	117	1.924
2	45	1.33	1.48	0.170	148	2.170

TABLE 6.3

A plot of $\log k'$ vs. $\log P C_2H_4$ is shown in Fig. 6.8. A rough straight line through the points has a slope of ~ -0.2 . This result is highly uncertain and probably reflects the poisoning action of high ethylene partial pressures plus the magnification of the P_{H_2} correction in $\log k'$. The order in C_2H_4 is thus -0.2 ± 0.1 .

The rate equation is thus: $\text{rate} = k[H_2]^{1.0}[C_2H_4]^{-0.2}$ which is in good agreement with the above mentioned result of Bond and co-workers for Pt supported on alumina,¹⁶¹ the latter also having a highly uncertain value for the order in C_2H_4 (-0.3 ± 0.1). Both sets of data differ from the earlier results of Bond¹⁶⁰ and will be discussed further below.

Investigation of catalyst regeneration methods

The preliminary kinetic studies described above revealed the inability of traditional hydrogen reduction methods to restore the lost activity observed after a kinetic run. Such methods have been used in i.r. work (see Section (iv)) to provide 'clean' metal surfaces by removal of surface carbide-like residues left after hydrocarbon adsorption. The need to find a surface cleaning treatment for ESCA work being especially important, it was decided that an investigation of the possibility of burning off carbidic residues with oxygen would be worthwhile.

The catalyst charge which had been used for all the above kinetic parameters investigations was retained and treated as follows. Firstly, the catalyst was heated under 200 torr O_2 for 1 hr. at $200^\circ C$ and then evacuated (at $200^\circ C$) to $< 10^{-5}$ torr. Secondly, it was treated under equivalent conditions with H_2 (to remove adsorbed O_2) and evacuated. Thirdly, it was allowed to cool to $23^\circ C$ under 50 torr of fresh H_2 and finally evacuated. A run under standard conditions (50 torr of each reactant at room temperature) gave a dramatic increase in rate over that previously observed. A repeat reaction after evacuation had an initial rate some 40% lower and a further run after O_2/H_2 regeneration at $200^\circ C$, as before, gave a rate which was too fast to measure properly. Using a fresh charge of 5mgms of 50 x diluted 12% Pt/ SiO_2 and performing repeat runs it was found that the regeneration procedure carried out at $300^\circ C$ was capable of completely re-activating the catalyst (only 50 torr of O_2/H_2 was now used in the consecutive treatments).

The actual activity was now probably a function of the achievable vacuum ($\geq 10^{-6}$ torr) and fluctuated about a high mean value to the extent

that a redetermination of the orders of reaction was not possible under the conditions previously employed. However, an approximate value for the activation energy was attempted.

Determination of E_a for a 'clean' catalyst.

5 mgms of 50 x diluted catalyst was pretreated as above and similarly treated in between subsequent runs, the catalyst being allowed to reach the required temperature while standing under 50 torr of fresh H_2 . In all runs the initial partial pressures were 50 ± 2 torr in each reactant the temperatures used covering $0-50^\circ C$ in random order. Relative initial rates (k) based on increase in C_2H_6 peak height with time ($\alpha \text{ torr min}^{-1}$) are shown in Table 6.4.

run no.	$T^\circ K$	$1000/T \text{ deg}^{-1}$	$k(\alpha \text{ torr min}^{-1})$	$\ln k$
2	273	3.66	0.35	-1.05
4	283	3.535	0.62	-0.48
1	295	3.39	1.65	0.50
6	296	3.38	2.32	0.84
3	308	3.24	4.8	1.57
5	319	3.14	13.6	2.61

TABLE 6.4

An Arrhenius plot of $\ln k$ vs. $10^3/T$ gave a reasonable straight line (Fig. 6.9) of slope $-6.4 \times 10^3 \text{ deg}$.

$$\therefore -\frac{E_a}{R} = -6.4 \times 10^3 \quad \text{or} \quad E_a = 12.8 \text{ kcal mole}^{-1}$$

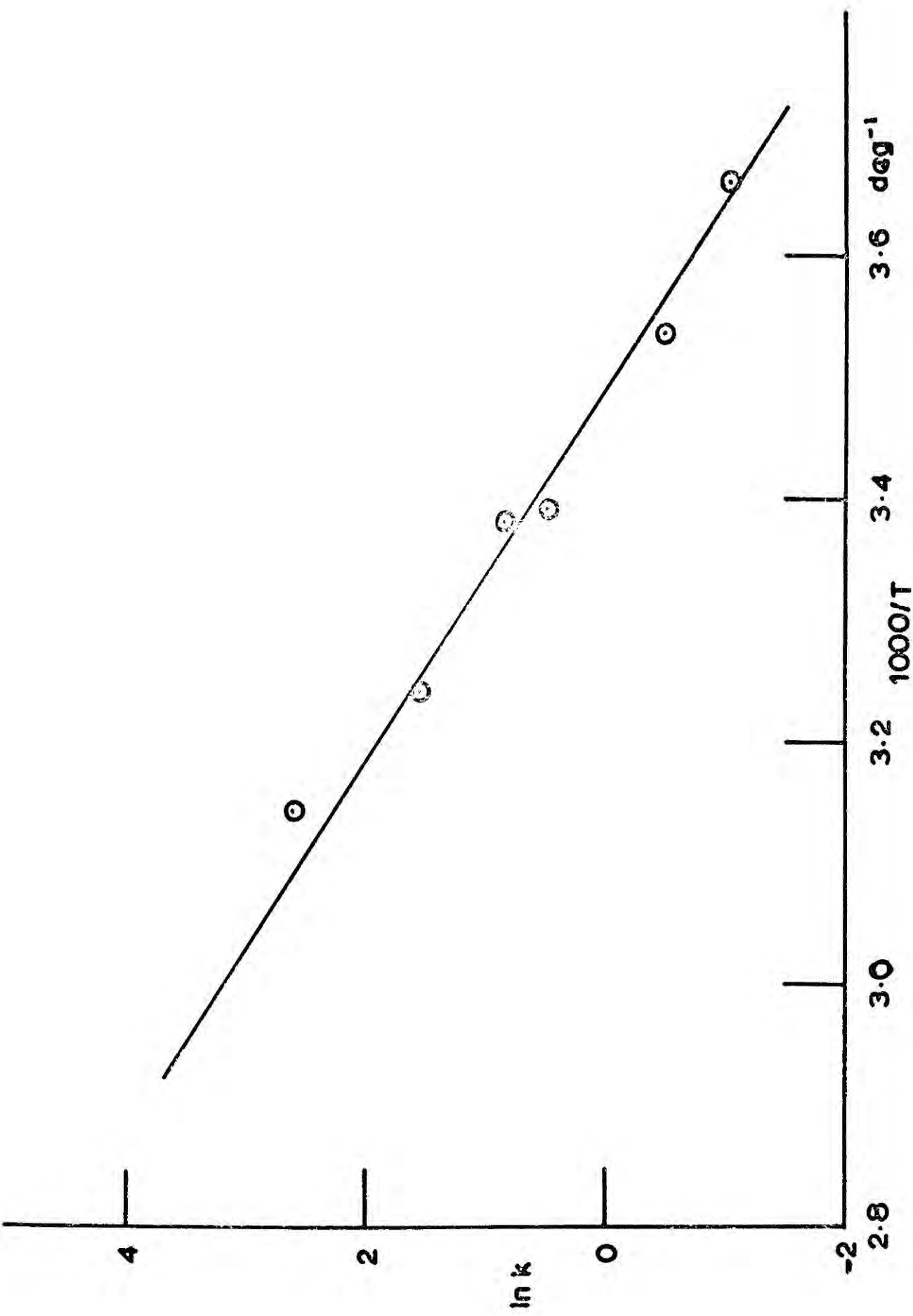


FIGURE 6.9

The scatter of the plot is greater than in the previous one (Fig. 6.7) because of the previously found difficulty with reproducibility (eg runs 1 and 6 in Table 6.4) and because the much faster rate of reaction leads to greater errors due to the sensitivity to sample removal timing and the estimation of initial rates. From the graph $E_a = 13 \pm 2 \text{ kcal mole}^{-1}$, which is lower than the value obtained from the deactivated catalyst by ca. 8 kcal mole^{-1} .

(c) Discussion.

Since the completion of this work, new data on the Pt/SiO₂-ethylene-hydrogen system has been published by Schlatter and Boudart.¹⁶² These authors also found great variations in activity of the catalysts used depending on the pretreatment conditions and ascribed this to the presence of carbonaceous material in the support material (SiO₂) which could desorb during reductive H₂ treatment to be reabsorbed by the Pt, with poisoning effects. The work had also been carried out partly to check the reported value of E_a , for this same reaction, of 17-20 kcal mole⁻¹ by Sinfelt and Lucchesi¹⁶³ which seemed anomalously high. Using low temperatures for reactions (-50°C) and hydrogen pretreatment Schlatter and Boudart obtained E_a values of ca. 9 kcal mole⁻¹ and zero order dependence on ethylene partial pressure. Deactivation during runs was not found to be significant either. However, they also found that treating the catalyst with air at 300°C prior to a run always gave a marked increase in activity (measured in terms of the turnover number, N_t) which they concluded was the result of removal of the support contamination mentioned earlier. A value of

N_t (the number of ethylene molecules converted per surface Pt atom per sec.) was quoted for standard conditions of 23 torr C_2H_4 and 152 torr H_2 for a 0.05% Pt/ SiO_2 catalyst (air treated at $300^\circ C$) at $25^\circ C$ of 4.92 sec^{-1} . Unfortunately, the metal surface area of the catalyst used in the work described here has not been measured so a value for the turnover number cannot be calculated accurately. However, an approximate minimum value can be estimated assuming 100% dispersion. For the standard pressures used by Schlatter and Boudart¹⁶² the result is $N_t \approx 4 \text{ sec}^{-1}$ (see Appendix I for the calculation) at $23^\circ C$. Since the actual dispersion will be somewhat lower than 100% it is obvious that the two results are in close agreement; it is also worth noting that they are comparable to the values obtained from Pt films (Beeck, unpublished work quoted in ref 162) - a result long anticipated¹⁶⁴ but not previously observed in practice for this system.

The marked drop in activation energy noted for the oxygen treated catalyst is in accord with the above mentioned conclusions of Schlatter and Boudart concerning the effect of inherent poisons on the catalyst. Whereas a value of $21 \text{ kcal mole}^{-1}$ for the deliberately deactivated catalyst compares with $17-20 \text{ kcal mole}^{-1}$ reported by Sinfelt and Lucchesi¹⁶³ for an unintentionally contaminated catalyst, the much lower value of $13 \text{ kcal mole}^{-1}$ for the 'clean' (oxygen pretreated) catalyst compares with values ranging from $9-11 \text{ kcal mole}^{-1}$ quoted in ref 162. It is worth noting that these latter values were frequently obtained at much lower temperatures

(-80° to 0°C) under which conditions poisoning of the Pt either by transfer of contaminants from the support material or from retention of ethylenic residues would be expected to be reduced, leading to lower E_a values. It seems likely that the negative orders in C_2H_4 for the reaction accompany use of a contaminated catalyst not at low ($< -50^{\circ}\text{C}$) temperatures.¹⁶⁰⁻¹⁶² On the other hand this work demonstrates that even for a 'clean' catalyst the activity drops during a run at room temperature by about 40% and that high temperature H_2 treatment is incapable of restoring the original activity. It is suggested that this is due to poisoning of Pt sites by ethylenic residues and this is in accord with recent results obtained from radiochemical studies¹⁶⁵⁻¹⁶⁷ on the behaviour of ethylenic species retained by supported Pt.

Discussion of the mechanistic implications of this kinetic data is deferred until Section v, while the relevance of oxygen cleaning treatments to the questions of particle size and support effects is further discussed in conjunction with mass spectrometric results in the next section (iiie).

(iii) Mass Spectrometric studies of ethylene deuteration.

(a) Introduction.

Early use of deuterium enriched hydrogen as a tracer for investigating the mechanism of ethylene hydrogenation over Ni^{168,169} indicated that exchange processes occurred concurrently with the addition reaction but the analytical probe used (thermal conductivity measurements on the 'hydrogen' gas) permitted only a determination of

the average D-content of the products. The use of i.r. to study deuterium distributions in the products gave additional information but had limited sensitivity and application.¹⁷⁰ The technique of using pure D₂ and measuring deuterium distributions by mass spectrometry found its first application in the study of ethylene 'hydrogenation' (over Ni) in 1950¹⁷¹ with similar studies of metal catalysed olefin deuteration quickly following.^{160,172-174} The technique has been extensively used to study exchange of hydrocarbons with D₂ over metals, an area recently reviewed.¹⁷⁵

There have been only two such studies^{160,161} of the deuteration and exchange of ethylene over Pt catalysts. The first¹⁶⁰ involved a study of the reaction over various types of supported Pt. Samples were analysed, at either 50 or 100% conversion, by brominating part of the sample (to remove ethylenes) and analysing both parts to obtain the ethane distributions directly and the ethylenes by difference. The second¹⁶¹ used a Pt/Al₂O₃ catalyst with the less crude analytical procedure of separating the products by glc and analysing ethanes and ethylenes separately. The aim of the work described below was to check the reproducibility of these data and hopefully to extend the method to acquire new data to help with mechanistic interpretations.

(b) Experimental

The apparatus described above was modified so that the ethane and ethylene fractions could be collected after glc separation for analysis by mass spectrometry, as shown schematically in Fig. 6.3. The 'U' tube traps were constructed from 1 mm capillary tubing, to ensure rapid flushing by the He carrier gas, with a total length

between two 2mm taps of ca. 30cm. Each carried an S.13 socket for rapid connection to a S.13 ball joint fixed to the outlet (1 mm stainless steel capillary tubing) from the katharometer. Since two fractions were collected from each glc sample both 'U' tubes were He flushed and by placing a 'Dewar' of liquid N₂ around a trap about 30 secs before a fraction emerged from the glc column each fraction could be collected with very high efficiency, in a separate tube, without any contamination from the other fraction. The collected fractions could be kept air-free for considerable periods at -196°C (Apiezon 'N' being used to grease the taps of the 'U' tubes) but in practice were analysed within an hour. D₂ (Matheson C.P. grade) was used as described above for H₂.

The Edwards mass spectrometer used for the analysis was already set up to follow static reactions directly via a capillary leak from a reaction vessel/vacuum line system. This was modified so that the contents of a 'U' tube could be expanded into a small volume adjacent to the capillary leak through an S.13 ball joint to which the 'U' tube traps could be readily attached as previously described. The leak rate into the mass spectrometer was about 5%/hr. The advantages of this method of collecting and analysing samples over on-line glc/m.s. are: (1) the opportunity to perform repeated slow scans to give greater accuracy and (2) the sample is homogeneous; this may not be the case with glc/m.s. if there is some separation of the different isotopes during glc. This factor also leads to higher accuracy.

(c) Analysis

Analysis of both ethylene and ethane samples was carried out using 16V electrons. The ethane fragmentation pattern was very sensitive to the filament condition and the precise voltage of the

electron beam, ethylene much less so. Typical fragmentation patterns, expressed as percentages of the parent peak (M) were (approximately):

m/e	31	30	29	28	27	26
C_2H_6	2	100	24	204	-	-
C_2H_4			2	100	1	2

the 2% (M + 1) peak arising from the natural deuterium abundance. Hence, only fragments due to the loss of one or two H/D atoms need to be considered in ethane analyses and the accuracy attainable does not warrant inclusion of the (M + 1) contribution. When ethane samples were being analysed a fragmentation pattern for C_2H_6 was always obtained for analysis purposes. This was unnecessary for ethylene analyses but in this case, since contribution from the parent peak only was significant, accuracy was much greater and due account had to be taken of natural deuterium occurrence in C_2H_4 . A computer programme was written to convert relative peak heights from a sample of mixed deuterioethanes into the percentages of each component. The theory behind this and the programme itself are described in Appendix II.

(d) Description of experiments and results.

A series of preliminary experiments using approximately equal initial partial pressures of D_2 and C_2H_4 (~ 50 torr) indicated that at low conversions the trapped ethane samples produced sufficient gas pressures in the mass spectrometer for reasonably intense peaks to be observed and, hence, reliable distribution patterns to be calculated. They also showed that while ethylene exchange is very low ($< 1\%$) the concentration of ethylene- d_1 (C_2H_3D) increases linearly

with time. Because of this the ethane distributions measured at various conversions between 5 and 25% were the same within experimental error. Initial distributions are a more sensitive test of mechanism than distributions measured at high conversions since the latter represent an average of many pressure ratios if not exactly equal initially.

Effect of partial pressures.

The effect of varying the partial pressures of C_2H_4 and D_2 were studied in a series of runs at $23^\circ C$ using ~ 10 mgms of the 50 x diluted catalyst batch pretreated with O_2 , then H_2 as described above. Ethane and ethylene samples were analysed at low conversions. Table 6.5. gives the ethane distributions and Table 6.6 indicates the proportion of ethylene- d_1 in the total ethylene samples and the values normalised to 10% conversion for comparison.

$P D_2$	$P C_2H_4$	$P D_2/P C_2H_4$	d_0	d_1	d_2	d_3	d_4	d_5	d_6	% Conv.
36	200	0.2	26.4	28.6	26.2	9.4	4.9	3.5	1.0	5
45	50	0.9	14.7	30.1	29.5	12.7	7.4	3.7	1.8	11
200	46	4.3	3.5	32.9	35.0	14.7	7.4	4.2	2.1	10

TABLE 6.5

$P_{D_2}/P_{C_2H_4}$	% Conv.	% ethylene-d ₁	% ethylene-d ₁ at 10% conv.
0.2	5	0.7	1.4
0.9	11	0.45	0.4
4.3	10	0.35	0.3

TABLE 6.6

Hence increasing the initial D_2/C_2H_4 pressure ratio increases the deuterium incorporation in the product ethane, ie the percentages of ethanes d_1 - d_6 increase at the expense of ethane- d_0 . Ethylene exchange is suppressed at the same time.

Effect of temperature

In an exactly similar series of experiments the relative partial pressures were kept the same ($P_{D_2} = P_{C_2H_4} = 50$ torr) while the reaction temperature varied. These results are analogously presented in Tables 6.7-8.

T ^o C	% ethanes							% Conv.
	d ₀	d ₁	d ₂	d ₃	d ₄	d ₅	d ₆	
23	14.7	30.1	29.5	12.7	7.4	3.7	1.8	11
105	11.4	27.8	31.7	14.3	7.8	4.8	2.1	26
152	12.6	30.7	26.4	14.8	8.4	4.9	2.2	29
200	8.0	32.0	26.5	17.2	10.0	4.8	1.6	21

TABLE 6.7

T°C	% conv.	% ethylene-d ₁	% ethylene-d ₁ at 10% conv.
23	11	0.45	0.4
105	26	4.4	1.7
152	29	6.2	2.1
200	21	5.7	2.7

TABLE 6.8

The increase in temperature does not have a marked effect on the ethane distributions, the percentage of higher ethanes increasing only slightly - possibly as a result of the very noticeable increase in ethylene exchange rate.

These results agree both qualitatively and, where comparison is possible, quantitatively very well with those obtained earlier for a Pt/SiO₂ catalyst.¹⁶⁰ The only discrepancy is the rather high percentages of ethane-d₂ found in the latter work but this could easily be due to the use of excess D₂ and analysis at much higher conversions (50 or 100%). The mechanistic implications of these results are discussed in Section (V).

Support and diluent effects.

Some years ago an isolated report by Sinfelt and Lucchesi¹⁶³ presented kinetic evidence for hydrogen 'spillover' in this system. These workers noted a very significant increase in rate of ethylene

hydrogenation when their Pt/SiO₂ catalyst was intimately mixed with Al₂O₃ but no significant effect on dilution with further SiO₂. They concluded that atomic hydrogen formed by H₂ dissociation on Pt enters 'spilled over' onto the Al₂O₃ which then acted as the hydrogenation catalytic agent with greater turnover than Pt itself. As mentioned above, it was in this work that E_a for ethylene hydrogenation over the Pt/SiO₂ catalyst was found to be 17-20 kcal mole⁻¹. In his original work on patterns of ethylene deuteration and exchange over supported Pt Bond¹⁶⁰ noted differences in addition patterns for different supports and although ethylene exchange was noted to be very low variations were found in this process too although figures were not quoted. The following experiments aimed to use the ethylene deuteration/exchange patterns as a probe for investigating these results further.

As previously, runs were carried out using equal partial pressures of ethylene and deuterium (usually 100torr) and samples of ethylene and ethane analysed at low conversions. Results were obtained from four catalysts, using 4-70 mgms, at 23°C.

- 1) 12% Pt/SiO₂ diluted x 20 with SiO₂ as used above. Aerosil SiO₂.
- 2) 0.1% Pt/SiO₂ prepared similarly.
- 3) 0.1% Pt/Al₂O₃ prepared similarly. Ketjen CK300 Al₂O₃.
- 4) 50:50 mixture of (2) and CK300 Al₂O₃. Prepared by grinding the constituents together.

Before each run the catalyst was subjected to the O₂/D₂ pretreatment procedure described above to give a 'clean' Pt surface,

under which conditions reaction rate for a given catalyst was proportional to the weight of catalyst, other conditions being identical.

The ethane distributions are collected in Table 6.9. Also shown are the relative initial rates (k_{rel}) calculated for unit weight of Pt in the catalyst. Since catalyst weights were very small, these values are correspondingly approximate but they have an important bearing on the following discussion. Fig. 6.10 shows the variation of ethylene- d_1 concentration with conversion for the four catalyst preparations.

catalyst	% ethanes							% conv.	k_{rel}
	d_0	d_1	d_2	d_3	d_4	d_5	d_6		
1	14.7	30.1	29.5	12.7	7.4	3.7	1.8	19	0.4
2	17.1	23.8	37.2	12.3	5.3	2.9	1.3	25	0.9
3	17.2	21.8	40.3	12.2	5.2	2.2	1.1	22	1.0
4	21.3	23.3	35.3	11.5	4.4	2.5	1.7	16	0.8

TABLE 6.9

(e) Discussion.

The difficulty of obtaining reliable ethane distributions is well known^{160,161} and, as shown in Appendix II, the comparison of calculated and observed peak heights for $m/e = 28$ and 29 , which the analysis makes possible, indicates that the values for % ethane- d_n

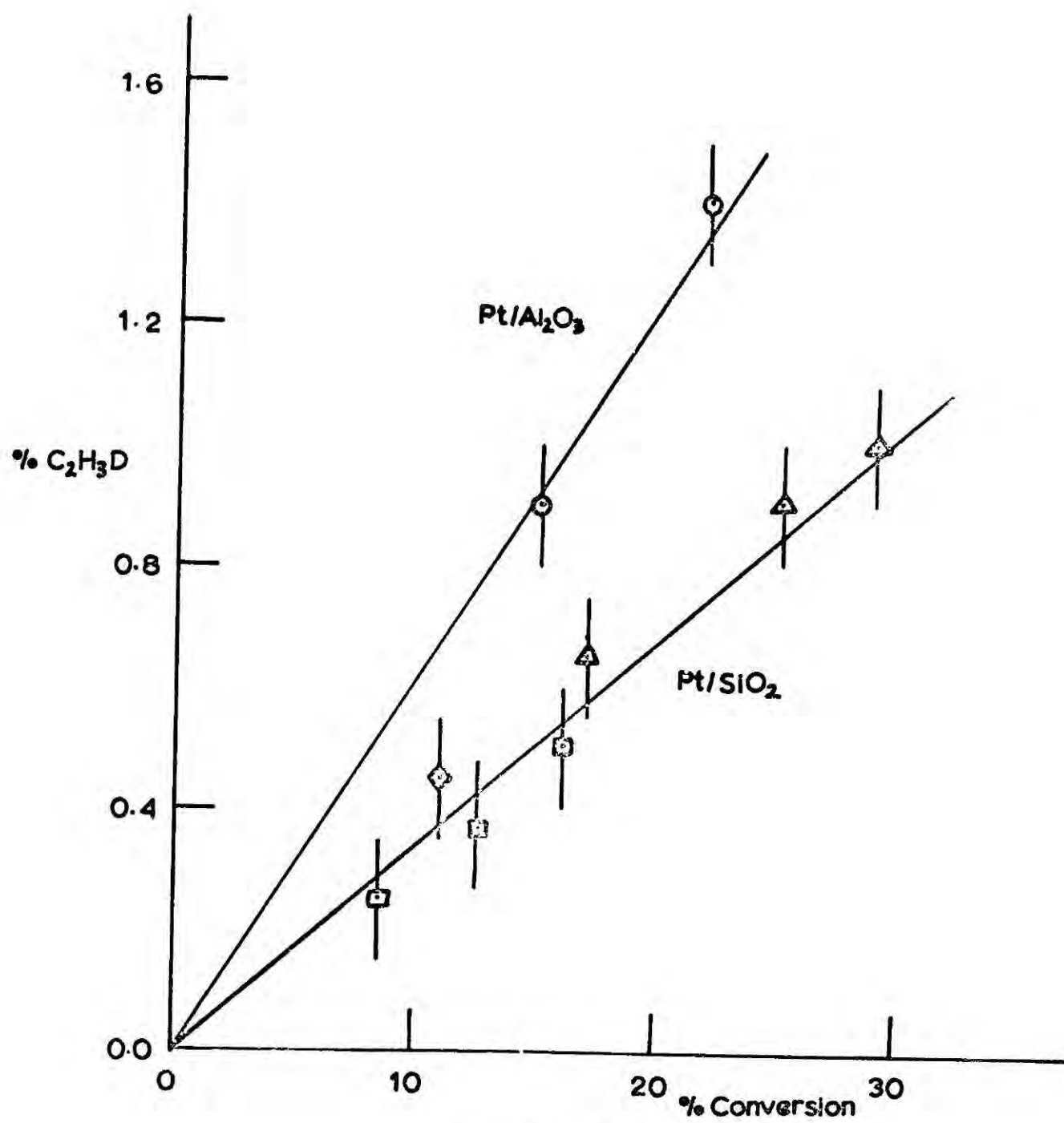


FIGURE 6-10

catalyst 1. \diamond
2. \triangle
3. \circ
4. \square

rapidly became increasingly inaccurate for $n = 2, 1$ and 0 . The results in Table 6.9 for catalysts (2)-(4) are very similar but differ slightly from (1). The reliability of the results from (1) is less than the rest, however, on the basis of the agreement between calculated and observed peak heights for $m/e = 28$ and 29 . There is certainly no significant difference between the results from catalysts (2)-(4).

In agreement with Bond¹⁶⁰ the amount of ethylene exchange over $\text{Pt}/\text{Al}_2\text{O}_3$ is significantly higher than over Pt/SiO_2 . The reason for this support effect is not yet understood but it is real as preliminary work with Pt on different supports consistently revealed widely differing ethylene exchange rates. This is an area which could fruitfully be investigated in more detail since it is fundamental to our knowledge of supported metal catalyst behaviour.

Of more immediate relevance to the present discussion is the lack of detectable difference between Pt/SiO_2 , $\text{Pt}/\text{SiO}_2 + \text{SiO}_2$ and $\text{Pt}/\text{SiO}_2 + \text{Al}_2\text{O}_3$ for ethylene exchange. The ethylene exchange probe is obviously sensitive enough to detect support effects; consequently if hydrogen spillover from metal to support occurs to promote ethylene hydrogenation on the support then a difference would be expected in the data from Pt/SiO_2 mixed with SiO_2 or Al_2O_3 . The absence of this difference, mirrored by the less sensitive ethane distributions, plainly indicates that the reaction takes place only on the metal and is, therefore, in disagreement with the proposal of Sinfelt and Lucchesi¹⁶³ concerning hydrogen spillover and reaction on the support. The detailed

kinetic work of Schlatter and Boudart¹⁶² discussed above and published since this work was completed also probed the 'spillover' evidence and for 'clean' catalysts found no difference in turnover number for ethylene hydrogenation over Pt/SiO₂ catalysts when undiluted or when diluted with SiO₂ or Al₂O₃. These authors concluded that the catalyst used by Sinfelt and Lucchesi was badly contaminated with carbonaceous material; this migrated to the Pt on H₂ activation (to give low activity) but was scavenged by added Al₂O₃ during this treatment, giving rise to an apparent increase in activity. The results in Table 6.9 show that the relative initial rates for catalysts (2)-(4) are the same to within 20%, which is probably within the level of approximation possible here. Even the very different catalyst (1) gives a value only about half these. Since all catalysts were subjected to oxygen cleaning treatment before runs these observations are in complete agreement with the more detailed kinetic data of Schlatter and Boudart¹⁶² on this system. As noted previously the very high E_a value obtained by Sinfelt and Lucchesi is also indicative of a contaminated catalyst.

In the past differences in specific activities of metals, supported or unsupported and prepared in various ways, as derived from kinetic measurements for a standard reaction have been used as evidence for the existence of support and particle size effects. Platinum has been particularly subject to such considerations¹⁷⁶. The above results indicate that in future it will be necessary to demonstrate that the metal surface has been effectively cleaned in order that artifacts of the type discussed above can be eliminated.

(iv) I.r. studies of the $C_2H_4-H_2-Pt/SiO_2$ system.(a) Introduction.

In general, the IR technique has been much more successfully used for the study of surface species than any other spectroscopic method. This is due partly to the fact that its comparatively long wavelength radiation is only weakly scattered by the surface interfaces so that transmission measurements are possible. For adequate sensitivity to adsorbed molecules high-area adsorbents are needed in the form of fine powders, solids with fine pores or porous discs pressed from powders. These also minimise radiation-scattering because the particles or pores are often considerably smaller than the i.r. wavelength. Pressed discs are especially convenient, when they can be made because of their high density and self-supporting nature. The accessible region of the spectrum is then determined by the absorption of radiation by the adsorbent. Extensive work has been carried out with high area oxides (eg SiO_2 , Al_2O_3 , $SiO_2-Al_2O_3$, ZnO), zeolites and oxide supported metals as adsorbents. The whole subject has been covered in books by Little¹⁷⁷ and Hair¹⁷⁸, and selected topics have been reviewed.^{179,180}

The ability of i.r. to detect surface species on supported metals was first demonstrated by Eischens, Francis and Pliskin in 1954¹⁸¹ for CO on SiO_2 supported Cu, Ni, Pt and Pd. Pliskin and Eischens later reported spectra for C_2H_4 on Ni/SiO_2 ¹⁸² and since then C_2H_4 has been studied, on SiO_2 -supported metals, in detail, mainly by Sheppard and co-workers.¹⁸³⁻¹⁸⁶ In these studies i.r. spectra were studied under static conditions by dosing the sample and removing gas-phase species.

Recently, Avery obtained spectra from C_2H_4/H_2 mixtures flowing over Pt/SiO₂ under catalytic conditions, although the observed kinetics indicated the reaction to be controlled by the rate of diffusion of C_2H_4 to the catalyst site.¹⁸⁰ Because of interpretational difficulties much of the data accumulated has yet to be published but a summary of the established information¹⁸⁰ is given now to aid the later discussion of the present results.

At a given temperature different spectra are obtained from C_2H_4 on Ni, Pd and Pt (it being understood from now on that any metal referred to in this context is SiO₂- supported). However, spectra for C_2H_4 on Ni at low temperatures are similar to those from C_2H_4/Pd at somewhat higher temperatures and to those from C_2H_4/Pt at higher temperatures still. The accessible i.r. frequency range is down to 1300 cm⁻¹; below this frequency SiO₂ absorbs very strongly. The main vibrational modes of hydrocarbons which can be studied are those of the νCH stretch ($\sim 3100-3000\text{cm}^{-1}$ for (sp²)C-H; $\sim 3000-2800$ for (sp³) C-H, the δCH_2 and δCH_3 deformations ($\sim 1500-1300\text{cm}^{-1}$), the $\nu C=C$ stretch ($\sim 2200\text{cm}^{-1}$) and the $\nu C=C$ stretch ($\sim 1650\text{cm}^{-1}$). The latter two are very weak and not usually observed; analysis of the other modes gives most of the structural information which can be obtained.

Specific assignments for C_2H_4/Pt at 20°C are:¹⁸⁶

(i) $\sim 3010\text{cm}^{-1}(\text{w})$: PtCH=CHPt

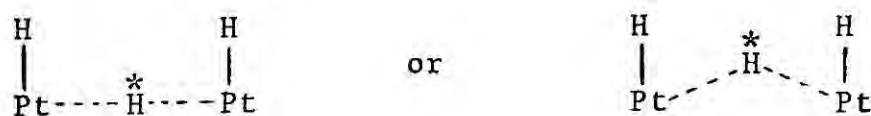
(ii) $\sim 2920\text{cm}^{-1}(\text{m,sh})$: Pt₂CH-CHPt₂

(iii) $\sim 2930\text{cm}^{-1}(\text{m,b})$; $2880\text{cm}^{-1}(\text{s})$ and $2795\text{cm}^{-1}(\text{w})$: PtCH₂-CH₂Pt

All these species co-exist on the Pt surface, but the relative coverages are uncertain because the relative peak intensities cannot

be readily interpreted. Addition of hydrogen at this temperature removes most of the spectrum; however the amount of ethane (and traces of n-butane) observed in the gas phase indicates that there must also exist a substantial amount of completely dehydrogenated ethylene (eg $\text{Pt}_3\text{C-CPt}_3$, $\text{Pt}_2\text{C} = \text{CPt}_2$) in the form of carbidic C_2 residues which do not contribute to the spectrum of adsorbed ethylene. Adsorption of C_2H_4 and hydrogenation at higher temperatures leads to progressive formation of spectra with peaks at $\sim 2960(\text{s})$, $2920(\text{s})$, $2870(\text{m})$ and $2855(\text{m})\text{cm}^{-1}$ attributed to surface butyl groups, $\text{CH}_3(\text{CH}_2)_3\text{Pt}$ ¹⁸⁴⁻¹⁸⁶ and the observation of much n-butane, but little ethane, in the gas phase. Initial adsorption and hydrogenation at -78°C , however, gives¹⁸⁶ bands due to $\text{PtCH}_2\text{-CH}_2\text{Pt}$ and others at 2965cm^{-1} and 2945cm^{-1} . These new bands are assigned to physically adsorbed ethane and (possibly) a labile surface $\text{CH}_3\text{CH}_2\text{Pt}$ species, respectively. Experiments with deuterated ethylenes add strength to the suggestion that the associatively adsorbed C_2H_4 ($\text{PtCH}_2\text{-CH}_2\text{Pt}$) is a major species at room temperature.¹⁸⁶

I.r. spectra have also been observed for chemisorbed H_2 on $\text{Pt}/\text{Al}_2\text{O}_3$ ¹⁸⁷. Two bands occurred at 2105 and 2055cm^{-1} , the former disappeared during evacuation. Using D_2 gave analogous bands in the expected positions. Both bands were ascribed to Pt-H stretches (similar frequencies are found for complex Pt hydrides¹⁸⁸) one form of adsorbed H being more strongly held than the other, e.g.



where H^* is the more strongly adsorbed. However, detailed later work

by Eley and co-workers¹⁸⁹ on H₂ adsorption by Pt/SiO₂ and Pt/Al₂O₃ presented data to support the radically different view that these bands refer to H atoms held on patches of oxide on the supported Pt crystallites. A 2120-2140 cm⁻¹ band was ascribed to H atoms held directly by 'Pt⁴⁺' while a 2040 cm⁻¹ band involved similarly held H atom also hydrogen bonded to adjacent OH⁻ ions formed by H₂O dissociation at anionic defects in the oxide patch. Slight differences in behaviour for the two catalysts could be explained by differing mobilities of -OH groups on the support. This work is discussed further below.

(b) Experimental

The general procedures adopted closely followed those used by Sheppard and co-workers¹⁸⁵⁻¹⁹⁰ except that the 12% Pt/SiO₂ catalyst described above was used directly whereas the latter workers produced the supported metal in situ by reduction of an SiO₂ disc impregnated with H₂PtCl₆. The weight of the Pt/SiO₂ disc was 12-20mg and its area about 0.7 cm².

Two infrared cells were used; both could be connected to a vacuum/gas handling system and had side arms which could be used for disc treatment at up to 650°C. The disc, held in a mount of magnetic material, could be manoeuvred about the glass system by use of external magnets. The first, used for preliminary work, had a path length little greater than the width of disc and holder, the disc being in a well between two KBr windows, and operated at ambient temperature only. The temperature of the disc in the i.r. beam is uncertain, however, and

could reach temperatures as high as 100°C . Because of this a second cell with facilities for heating and cooling between -120°C and 300°C was constructed. The central section of this cell is shown in Fig. 6.11. The area around the disc was wound with wire for resistance heating and also with narrow bore copper tubing through which N_2 could be passed for cooling. A Pt/Rh-Pt thermocouple was positioned so as to touch the disc holder for accurate temperature measurement. The whole of this section of the cell was encased in a refractory cement. The outer KBr windows were affixed with high temperature 'araldite' while flushing the space with dry N_2 , and could themselves be sprayed with warm N_2 to prevent water condensation when the cell was operated at low temperature.

The gases used in this work and the storage methods used were as described in Section (i) above.

In all experiments the Pt/ SiO_2 disc was first thoroughly degassed, in the side-arm, by taking the temperature gradually up to 550°C whilst pumping and maintaining this temperature until a pressure of 10^5 - 10^6 torr was reached. This treatment removed physisorbed water and many surface hydroxyl groups to give a very sharp OH band at $\sim 3740\text{cm}^{-1}$. In each experiment performed before the oxygen cleaning treatment had been discovered (Section (i)) the disc was further treated with 400 torr H_2 at 350°C to remove any Pt contamination - the method of Sheppard et al. After cooling to the desired temperature (or ambient for the simple cell) and evacuating to $< 10^{-5}$ torr, ethylene was bled into the cell up to ~ 20 torr and left for various periods before evacuating, for about 1 min., to remove gas phase and physisorbed

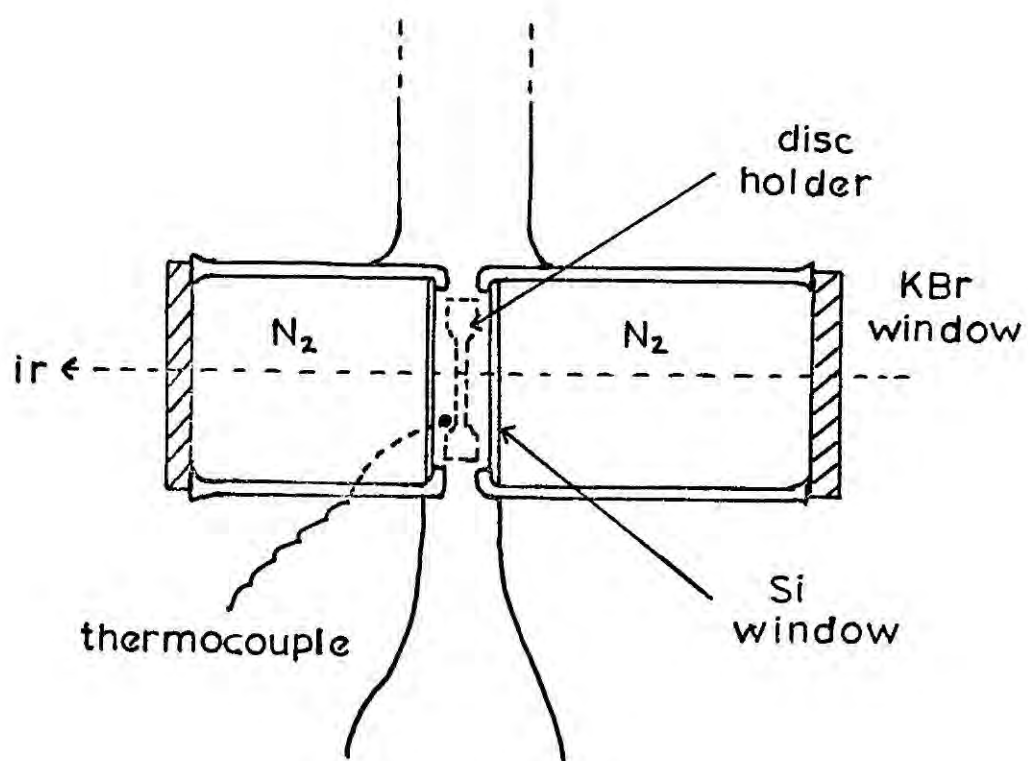


FIGURE 6.11

species. After taking spectra H_2 was added up to 400 torr and left for given periods before similarly evacuating and running spectra.

(c) Results and Discussion.

Preliminary experiments.

Fig. 6.12 shows the ν_{CH} stretch region of the spectra obtained for a disc treated as shown. The high temperature evacuation and subsequent H_2 treatment should produce a 'hydrogen-covered' surface (as opposed to a 'bare' metal surface produced by prolonged evacuation of the H_2 treated sample at high temperature). This differentiation was proposed by Eichens and Pliskin¹⁹¹ who obtained different spectra for C_2H_4 on these two types of Ni surface. Sheppard and co-workers have not been able to reproduce this behaviour on Ni or Pt.¹⁸⁵ There was, however, no evidence of a Pt-H bond in the $2100-2000\text{cm}^{-1}$ region of the present spectrum, nor have the latter workers ever reported one.

The bands produced by adsorbed C_2H_4 occur at 2960, 2920, 2880 and 2860cm^{-1} (w) and possibly at $\sim 2790\text{cm}^{-1}$ (vw). Initially the 2880cm^{-1} band is the most intense but after overnight standing the 2920cm^{-1} seems to have grown at its expense with probable loss of the 2790cm^{-1} band. There is no evidence of a band at 3010cm^{-1} . Evacuation for 1 min. to remove gas phase species (negligible contribution to spectra because of the negligible path length) and physisorbed species produced no basic change. These results could be explained (following Sheppard et al) if species of the type $PtCH_2-CH_2Pt$ and $Pt_2CH-CHPt_2$ slowly reacted with adsorbed H_2 to form some surface n-butyl groups.

Addition of 400 torr H_2 produced a very marked increase in spectral intensities, bands now occurring at 2960, 2930(m) and

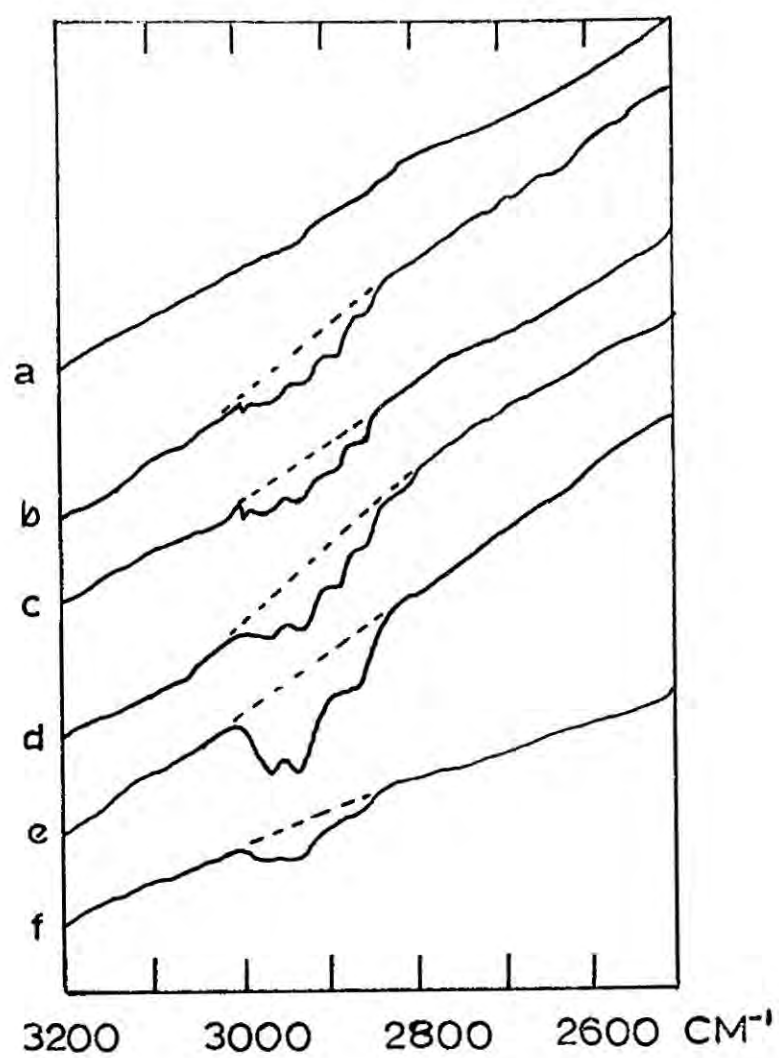


FIGURE 6.12

- (a) After H_2 reduction at 350°C and evacuation for 1 min.
- (b) After addition of 20 torr C_2H_4
- (c) After overnight standing
- (d) After evacuation for 1 min.
- (e) After addition of 400 torr H_2
- (f) After evacuation for 1 min.

2890-2850(w,b). The position of these bands and their relative intensities agree closely with those previously reported for surface n-butyl groups, possibly with a small contribution from physisorbed butane. The spectrum almost entirely disappears on brief evacuation, which would be expected if the disc temperature was $< 60^{\circ}\text{C}$. These results agree very well with those previously reported if it is assumed that the i.r. beam heats the disc to a temperature in the region of 50°C .

Experiments with the variable temperature i.r. cell.

Attempts to repeat these experiments using the more sophisticated variable temperature cell to achieve accurate temperature control were in large measure defeated. When isolated from the vacuum system at high temperature the catalyst disc appeared to pick up large quantities of hydrocarbon contamination which it probably scavenged from the 'araldite' used to seal in the inner windows. Breakdown of the seal led to leakage problems periodically. In one run which did produce results, however, this situation was turned to advantage.

Fig. 6.13 shows the relevant spectra. The large quantity of saturated C-H appeared on a disc which had been pretreated as above. The temperature was adjusted to 125°C and O_2 from a cylinder flowed over the disc for 2.5 hrs. The cell was then evacuated to $\sim 10^{-5}$ torr at 150°C for a similar period and the spectrum then obtained shows that the contamination had been removed. This confirms directly the effect of oxygen treatment noted in Section (i). Addition of H_2 and cooling to 50°C did not alter the C-H region but produced a broad strong band centred on 3460cm^{-1} and a sharp band at 2060cm^{-1} . The former can be attributed to water hydrogen-bonded on the SiO_2 support (probably only

Caption for Fig. 6.13

- (a) Saturated hydrocarbon contamination
- (b) After flowing O_2 treatment for 2.5 hours at $125^\circ C$
and evacuation at $150^\circ C$
- (c) After addition of 400 torr H_2 and cooling to $50^\circ C$
- (d) After standing for 16 hours and evacuation to 5×10^{-4} torr
- (e) After addition of 15 torr C_2H_4 at $-78^\circ C$
- (f) After standing for 25 mins and evacuation for 2 mins.

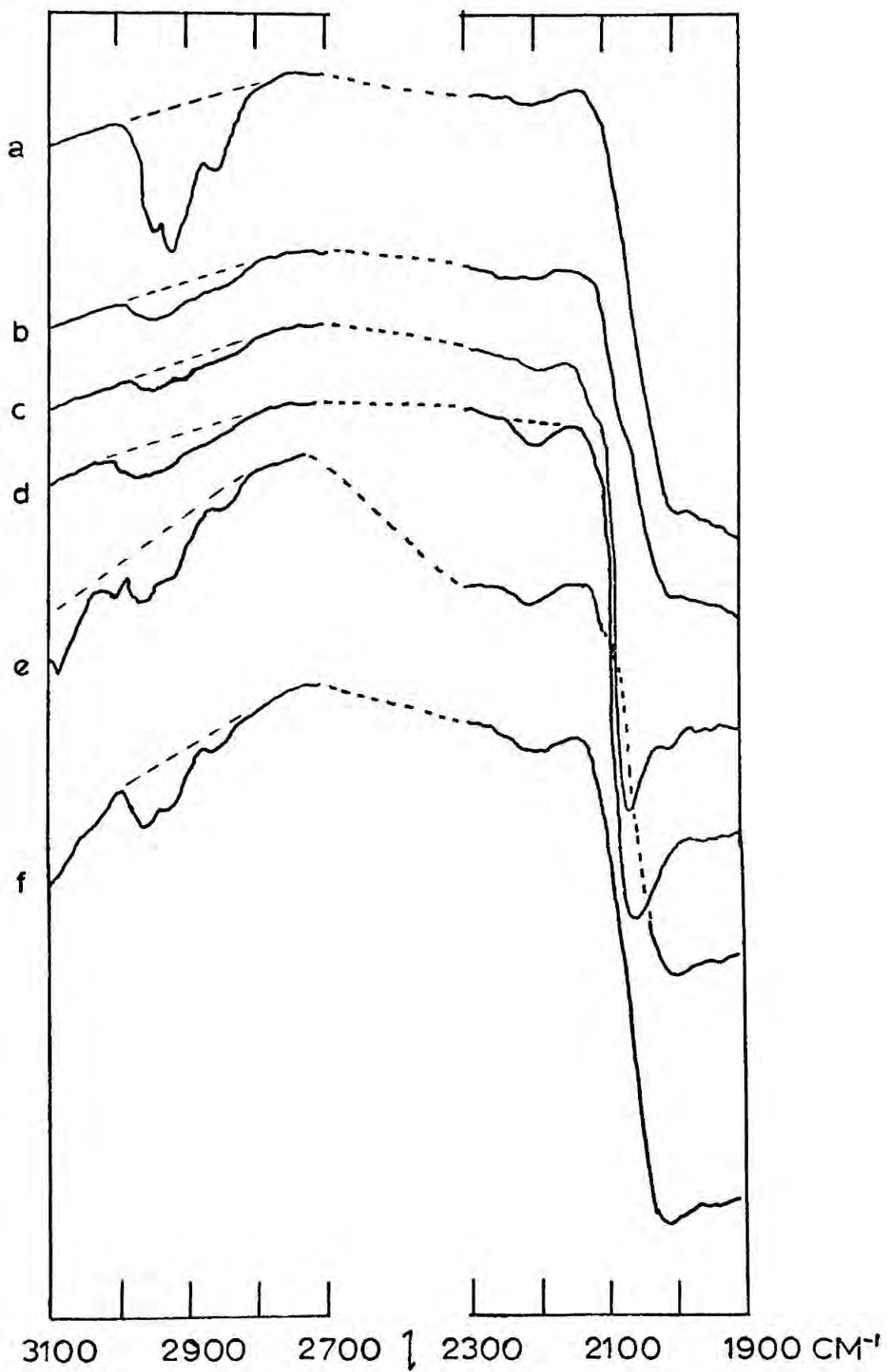


FIGURE 6.13

low coverage) while the latter is in the region of the bands described above for adsorbed H_2 . On standing for 16 hrs. this band increased in breadth and intensity, the peak maximum now appearing at 2040 cm^{-1} , and a weak broad band also appeared at $\sim 2180\text{ cm}^{-1}$. This behaviour exactly combines that reported by Eley et al for Pt/SiO₂ when pretreated with O₂ and evacuated prior to H₂ addition and also when treated with water vapour at 150°C .¹⁸⁹ This data clearly adds weight to the latter workers' interpretations of the 'Pt-H' bands (described above) and indicates that the Pt/Al₂O₃ disc used by Eischens and Pliskin¹⁸⁷ was probably surface oxidised. Since these bands were not seen when the catalyst was pretreated by high temperature degassing and H₂ reduction it can probably be assumed that no oxide patches were present on the Pt crystallites. The above results demonstrate that chemisorbed O₂ does persist on Pt even after high temperature evacuation and that H₂ treatment removes this as H₂O; this is, in fact, the basis of the H₂/Pt-O titration method for measuring Pt surface areas¹⁹² ($3/2H_2 + \text{Pt-O} \rightarrow \text{Pt-H} + H_2O$).

The 'Pt-H' bands were largely removed by ethylene addition at -78°C , presumably by reaction. The weak spectrum in the νCH region had peaks at 3090, 3010, 2960(b), 2920 and 2850 cm^{-1} ; evacuation for 2 mins removed the peak at 3090 cm^{-1} . This peak may be due to weakly bound C₂H₄ on oxidised metal sites, since it has not previously been observed. There is some evidence for the species Pt₂CH=CHPt₂ ($\sim 3010\text{ cm}^{-1}$) not observed at higher temperatures and the other peak positions and intensities in the initial spectrum are reminiscent of the spectrum reported previously¹⁸⁶ for C₂H₄ on Pt after H₂ addition at -78°C .

which possibly inferred the presence of the surface ethyl group, $\text{CH}_3\text{CH}_2\text{Pt}$. After evacuation bands are prominent at 2960cm^{-1} , 2920cm^{-1} with a weak broad band at $2840\text{-}2880\text{cm}^{-1}$ and possibly a weak absorption at 3010 cm^{-1} . The relative intensities of the first three bands are quite different from those observed at higher temperature and are not consistent with n-butyl. The prominence of the 2960cm^{-1} band suggests $-\text{CH}_3$, however, so this spectrum may be due to surface ethyl, $\text{CH}_3\text{CH}_2\text{Pt}$ with contributions from the other C_2 species found in the previous experiment. Assuming that n-butyl and carbidic residues are the catalyst poisons then their apparent non-existence at -78°C is in agreement with the fact that the catalyst does not deactivate when run at this temperature, as discussed above.

In conclusion, it seems as if those species which are postulated as being the reactive intermediates (see next section) are observed by i.r. only at low temperatures (probably $< -50^\circ\text{C}$) while spectra obtained at higher temperatures are indicative of those species which are more likely to be immobile (poisons). Significantly, spectra obtained under flowing catalytic conditions which are claimed¹⁸⁰ to represent those species also observed under static conditions, were observed at -60°C . On the basis of the above results it is suggested that the same experiment performed at room temperature or above would indicate n-butyl-type spectra, if any, even though ethane would remain the sole product.

(v) Conclusions.

It is not proposed here to discuss in detail the mechanism of ethylene hydrogenation; rather to indicate the relevance of the foregoing results to this question. The eventual rationalisation of kinetic and deuterium tracer work up to 1955 (virtually all concerning the reaction over Ni) in terms of an associative rather than a

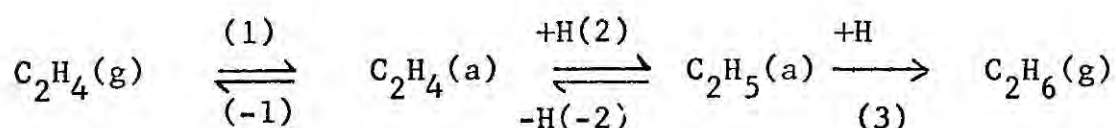
dissociative mechanism has been neatly outlined¹⁷⁷ and the more recent deuteration/exchange work has been reviewed¹⁵⁵ with particular reference to mechanistic interpretations.

Any mechanistic model must fit the observed kinetics, in this connection it can be noted that the route by which ethane is mostly formed probably has the kinetics:

$$d[\text{C}_2\text{H}_6]/dt = k[\text{C}_2\text{H}_4]^0[\text{H}_2]^1$$

the negative orders in C_2H_4 which have been found probably reflect the loss of catalytic sites by poisoning mechanisms - a process which is probably very slow at -80°C , when the above kinetics hold. As has also been shown above, poisoning effects can occur during reductive pretreatments of supported Pt and these markedly affect the observed activation energy. There is a strong case, therefore, for believing that mechanistic studies of hydrocarbon reactions over Pt should be carried out at low temperatures (ideally, -78°C say).

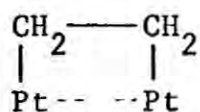
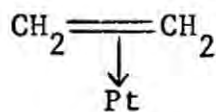
The generally accepted mechanism is based on that originally due to Horiuti and Polyani¹⁹³ (the 'associative' mechanism):



where the origin of H (used generically) was assumed to be dissociatively adsorbed H_2 ($\text{H}_2 \rightarrow 2\text{H}(\text{a})$) but is now thought to involve any hydrogen containing surface species capable of acting as an H donor. The statistical scheme of Kemball¹⁹⁴ based on this model allows the various

probabilities for the reactions of the two types of adsorbed species to be assessed in terms of four parameters. Using this approach Bond and co-workers have obtained computed ethane and ethylene distributions from the D_2 reaction which agree quite well with experimental results.^{154,155,161} The low degree of olefin exchange over Pt (reactions ± 1 , ± 2) has been shown to be due to the desorption step (-1) being very difficult while the production of ethanes d_1 - d_6 results from reactions (± 2) being facile and ethane desorption (3) rate limiting. Hydrogen exchange, which has not been followed in this work, is also accounted for. These considerations have been fully dealt with;^{154,155,161} it is sufficient to add that the above work confirms their conclusions and is significant because the results were obtained from initial distributions using equal partial pressures of reactants.

There is much discussion about the form of the adsorbed ethylene. There are two possibilities:

 σ -diadsorbed π -complex

either of which fits in with the reaction scheme. However, in the i.r. experiments, non-dehydrogenated π -bonded species are not observed, whereas there is evidence for the σ -bonded species. The latter also lends itself more readily to explanation of the production of more dehydrogenated species like PtCH=CHPt and $\text{Pt}_2\text{CH-CHPt}_2$. However, great care must be taken in the interpretation of these data in terms of the reactive intermediates and it has again been indicated above that low temperature work is essential here. I.r. does give a good indication

of the species responsible for catalyst poisoning, however, and confirms the role of O_2 pretreatment in removing carbide residues. It also reveals the possible presence of oxide patches even when this treatment is followed by hydrogen reduction and evacuation at high temperature. This could well account for the fluctuating rates observed for catalysts treated in this way.

Finally, it is satisfying to find that kinetic, i.r. and deuteration work on Pt/SiO_2 reproduces the variety of data observed for Pt used previously in widely different preparations. Different susceptibilities to poisoning may well account for differences in past kinetic results. However, a small but reproducible effect of the support on the $Pt-C_2H_4-H_2$ system has been found though more data needs to be gathered before an explanation can be attempted.

CHAPTER VII

ESCA STUDIES OF THE Pt/SiO₂ CATALYST

(i) Introduction.

During the course of this work there have been two reviews involving the application of electron spectroscopy to studies of surfaces and catalysts. Delgass and co-workers,¹⁹⁵ is an extended series of experiments, attempted surface studies by ESCA in three areas: adsorption, the behaviour of supported metals compared to unsupported metals, and crystalline oxides. Although giving encouraging pointers these experiments were hampered by poor vacuum conditions, lack of sensitivity and inadequate calibration. This work has itself been included in a comprehensive review by Brundle¹⁹⁶ of all aspects of surface studies by electron spectroscopic methods. The existence of the latter article renders any further comparison of these methods unnecessary here.

There have been a number of reports which indicate the usefulness of ESCA in following the composition of the surface layers of catalysts. Wolberg et al¹⁹⁷ have demonstrated the formation of CuO and CuAl_2O_4 phases upon calcination of $\sim 10\%$ $\text{Cu}/\text{Al}_2\text{O}_3$ catalysts depending on the temperature and surface area of the support. Migration of Ca to the metal surface in a supported silver catalyst during γ -irradiation, correlateable with changes in the selectivity for ethylene oxide production, has been demonstrated¹⁹⁸ and preliminary investigations of the chemical state of Mo in olefin disproportionation catalysts (supported $\text{Mo}(\text{CO})_6$) have been reported.¹⁹⁹ Oxygen species on the surface of Pt^{195,200}; Rh²⁰¹; Ni²⁰²; Cu_2O , CuO and NiO ²⁰³ have also been discussed. These studies emphasise the surface sensitivity of ESCA.

The aim of this section of work was to study the state of the metal in the 12% Pt/SiO₂ catalyst, used for the work discussed in the previous chapter, with especial regard to the effect of oxygen and hydrogen pretreatments.

(ii) Experimental.

Two samples were investigated. The first was the 12% Pt/SiO₂ catalyst described previously, the second was the precursor to this - a sample of SiO₂ impregnated with H₂PtCl₆ such as to yield 12% Pt/SiO₂ after reduction. This latter sample was prepared as described previously and dried at 110°C giving a pale brown powder. Both samples were pressed into infrared-type discs and separately investigated mounted on a fixed orientation shaft bolted directly onto the spectrometer housing. This shaft could be heated to 400°C and the obtainable vacuum was somewhat better than could be obtained when the normal sample probe was used. Treatment of the sample with gases was effected in situ by flushing the isolated source region before letting it up to a given pressure of the gas.

(iii) Results and Discussion.

Figure 7.1, shows the Pt4f and Cl2p regions of the spectra for the impregnated sample before and after reduction. The spectra from H₂PtCl₆/SiO₂ (Fig.7.1(a)) indicate the Pt atoms to be in a range of environments (broad peaks). The Cls peak from this sample was reasonably sharp and may be taken to be due to inherent carbonaceous contaminant. Assigning a BE of 285.0 eV to this peak the O1s peak,

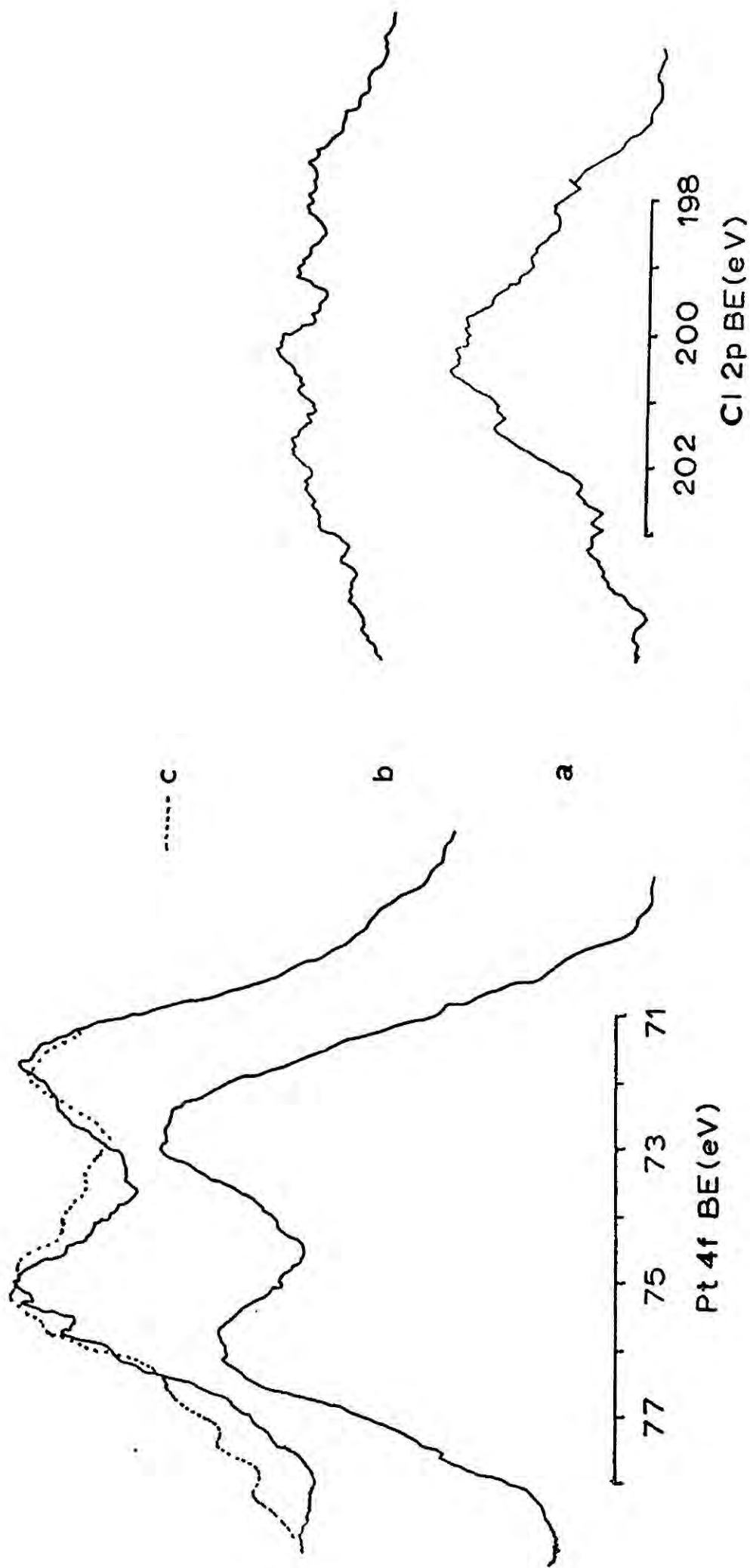


FIGURE 7.1

mainly due to oxide ions in the silica lattice, has a BE of 535.3 eV. All the following BE's have been referenced to the O1s peak from the SiO₂ support at this BE. The average Pt4f_{7/2} BE from the H₂PtCl₆/SiO₂ spectrum is 73.0 eV, ie in the Pt^{II} region. This reduction is oxidation state from Pt^{IV} is doubtless the result of prolonged drying of the catalyst (necessary in order to make sample discs able to withstand high temperature without fracturing) with loss of HCl and/or Cl₂. The area ratio of Cl2p/Pt4f peaks is much lower than would be expected for H₂PtCl₆ which confirms this conclusion.

Reduction under standard conditions (760 torr H₂ for 30 minutes at 150°C) in the spectrometer produced marked spectral changes (see Fig. 7.1(b)). As expected the Cl2p peak shows large loss in intensity but the broad peak remaining indicates that there is residual chlorine- probably incorporated in the support surface layers as Cl⁻ and as Si-Cl, by -OH group replacement on the surface. The Pt4f peak shows a significant drop in both overall intensity and breadth. The latter is expected because Pt⁰ should be the only product while the former can be accounted for in terms of a decrease in the number of observable Pt atoms through their aggregation to form metal crystallites. The doublet is still very broad with a Pt4f_{7/2}/Pt4f_{5/2} ratio apparently less than the usually observed, theoretical value of 1.33. This is a similar result to that reported by Delgass et al¹⁹⁵ for a 5% Pt/SiO₂ catalyst; they explained this in terms of overlap of the Pt4f_{5/2} peak with a 4f_{7/2} contribution from oxidised Pt, the 4f_{5/2} component of which was obscured by noise. The Pt4f_{7/2} maximum occurs at 71.7 eV BE which is a little higher than previously observed for Pt metal (Chapter II).

The sample was further heated in air (~ 400 torr, 150°C) for 30 minutes giving the spectrum shown in Fig. 7.1(c). There is a significant new shoulder on the high BE side of the $\text{Pt}4f_{5/2}$ peak, the $4f_{7/2}$ component of which would also produce the filling up of the valley between the two main peaks. This new addition to the spectrum is most likely to be due to PtO_2 , the estimated $\text{Pt}4f_{5/2}$ BE of which (from the shoulder) is ~ 77.7 eV in agreement with the BE reported for bulk PtO_2 by Kim et al ²⁰⁰ who have also obtained spectra from electrochemically oxidised Pt with components from Pt, PtO(ads), PtO and PtO_2 ($\text{Pt}4f_{7/2}$ BE's 70.7, 71.8, 73.4 and 74.1 eV respectively). Comparison of Pt spectra in Fig. 7.1(b) and (c) with those of Kim et al indicate that in the case of the supported metal the contributions from Pt-O (ads) and Pt-O must be very significant. The oxidation treatment did not, however, have any effect on the Cls peak intensity as might have been anticipated from the discussion in Chapter VI.

Fig. 7.2(a) shows the initial spectrum from the 12% Pt/ SiO_2 catalyst used for the work described in the previous chapter. The $\text{Pt}4f_{5/2}$ and $4f_{7/2}$ peaks are slightly better resolved than in the case of the sample prepared by reduction in situ, but the $\text{Pt}4f_{7/2}$ BE from the peak maximum is the same (71.7eV). Pumping on the sample at $\sim 10^{-6}$ torr for several hours had little effect on the Pt4f or Cls spectra. The sample was heated to 300°C and a low pressure of oxygen maintained in the sample chamber by bleeding gas continuously from a reservoir shaft. This treatment also had little effect on the spectra apart from the slow increase in intensity of the Cls peak and corresponding decrease in intensity of the Pt4f peak. Heating the sample in 500 torr H_2 for several hours at 350°C reversed this trend giving a Pt4f spectrum similar to that obtained initially. Figs. 7.2(b)-(d) show the changes

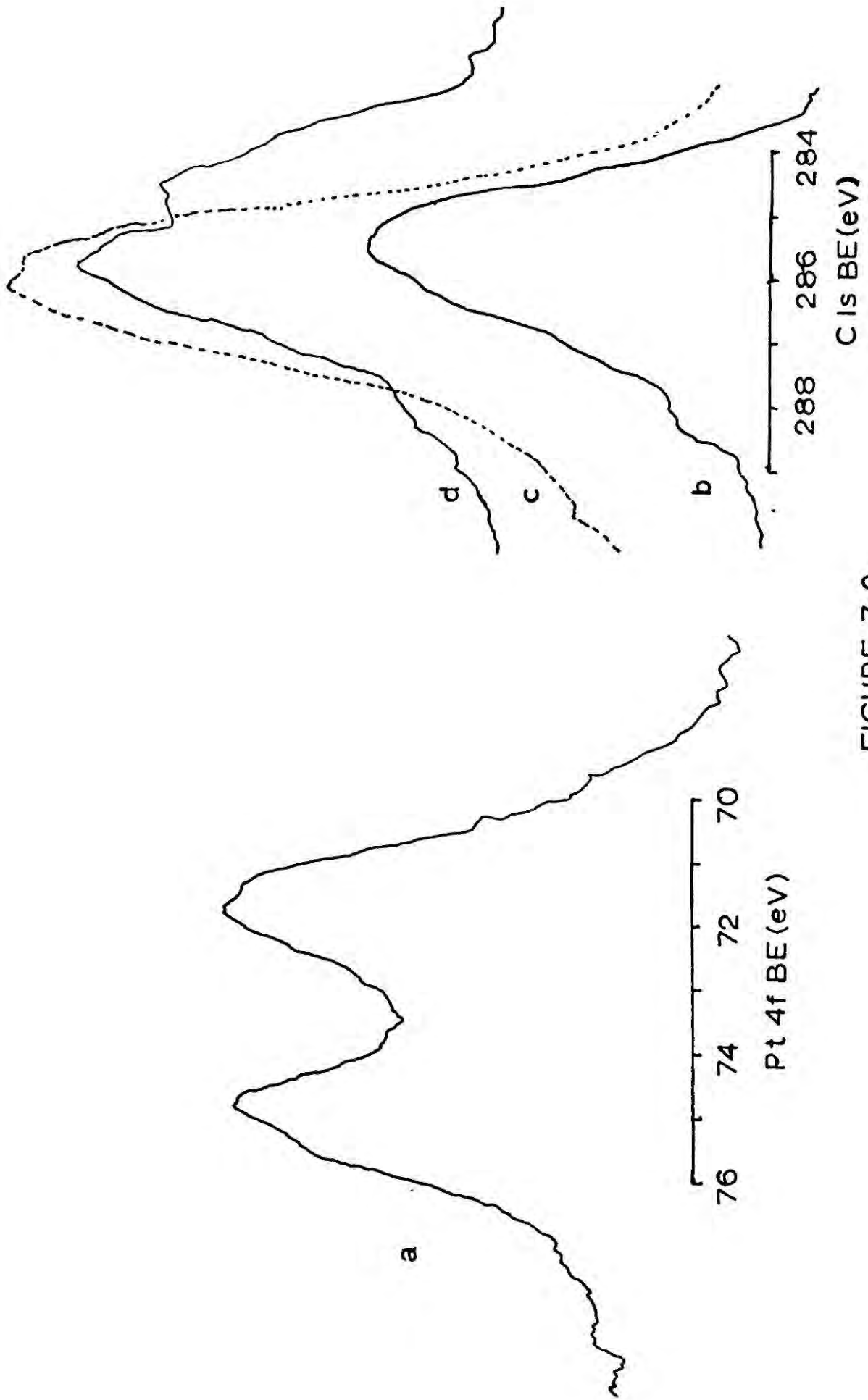


FIGURE 7.2

in Cls spectra during these experiments. While producing a decrease in the Cls peak intensity the hydrogen treatment also appears to enhance a low BE component. This is consistent with the suggestion discussed in Chapter VI that hydrogen treatment at high temperature activates migration of carbonaceous material, primarily held by the support, to the metal where it suffers dehydrogenation to produce 'carbide' residues which poison the catalyst.

The notable inability of prolonged hydrogen treatment at 350°C to produce changes in the Pt4f spectrum is very interesting. Bulk metal Pt readily adsorbs oxygen²⁰⁴ but the contribution of Pt-O (ads) to the Pt4f spectrum is relatively small²⁰⁰ and this species is removeable by hydrogen treatment.¹⁹² PtO is prepared by partial oxidation of Pt foil with O₂ (15 atm) at 300°C.²⁰⁵ If it is assumed that the form of the Pt4f spectrum from Pt/SiO₂ is due to contributions from PtO and possibly PtO₂,²⁰⁰ even when produced by in situ reduction in the spectrometer, then Pt in the form of small supported crystallites must be much more susceptible to surface oxidation than bulk Pt. From the ESCA results the total removal of oxidised centres by traditional reduction methods seems unlikely so the question of what role, if any, these centres play in catalysis arises - especially in view of the fact that oxidation at 300°C (to remove carbonaceous poisons) probably leads to PtO₂ formation and a marked increase in the rate of ethylene hydrogenation. Related to this is the report that the observation by ESCA of high levels of surface oxide on charcoal-supported Rh correlates with high activity for catalytic hydrogenations.²⁰¹ However, the assumption that oxygen adsorbed on supported Pt crystallites can

be removed by hydrogen (the basis of the Pt surface area measurement method noted in Chapter VI) has recently been upheld by calorimetric investigations of the O_2-H_2 titration of Pt/ Al_2O_3 . Thus the possibility that the Pt4f doublet from reduced Pt crystallites of small size is inherently broader than that from bulk Pt metal or Pt complexes cannot be ruled out.

In order to investigate this area further, however, it now seems that ultra-high vacuum conditions will be necessary to allow production of clean surfaces and their controlled reaction.

APPENDIX I

Calculation of turnover number, N_t

1 mole C_2H_2 occupies 22.4 litres (22.4×10^3 ml) at NTP and contains 6.02×10^{23} molecules.

\therefore For 1 torr C_2H_6 in 200 ml at $296^\circ C$ no. of molecules

$$= \frac{200}{22.4 \times 10^3} \times \frac{273}{296} \times \frac{1}{760} \times 6.02 \times 10^{23} = 6.52 \times 10^{18}$$

Assuming 100% dispersion of Pt,

no. of surface atoms = total no. of Pt atoms

1 gm atom of Pt (195 gm) contains 6.02×10^{23} atoms

\therefore no. of Pt atoms in 5 mgms of 12% Pt/SiO₂ diluted 50 times

$$= \frac{5 \times 10^{-3}}{50} \times \frac{12}{100} \times \frac{6.02 \times 10^{23}}{195} = 3.7 \times 10^{16}$$

Rate of ethane production = 0.5 torr/min = $\frac{0.5}{60}$ torr/sec

$$\therefore N_t = \frac{0.5}{60} \times \frac{6.52 \times 10^{18}}{3.7 \times 10^{16}} = 1.47 \text{ molecules/surface atom/sec}$$

This is for initial pressures of 50 torr in C_2H_4 and H_2

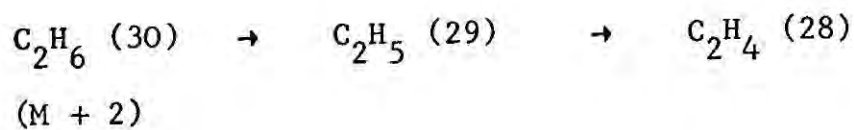
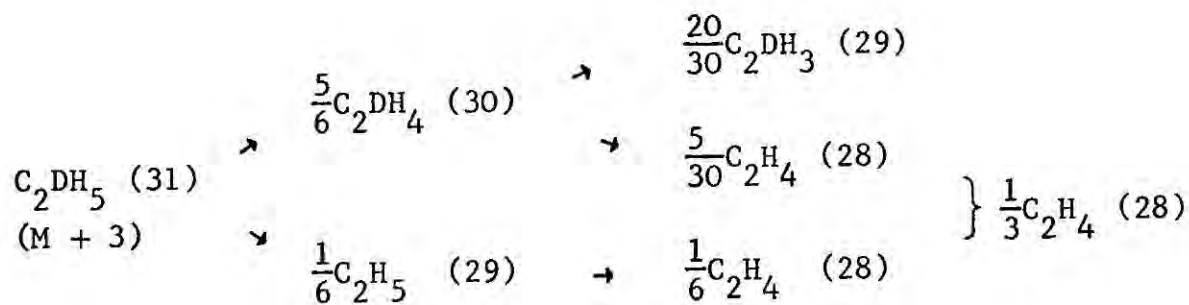
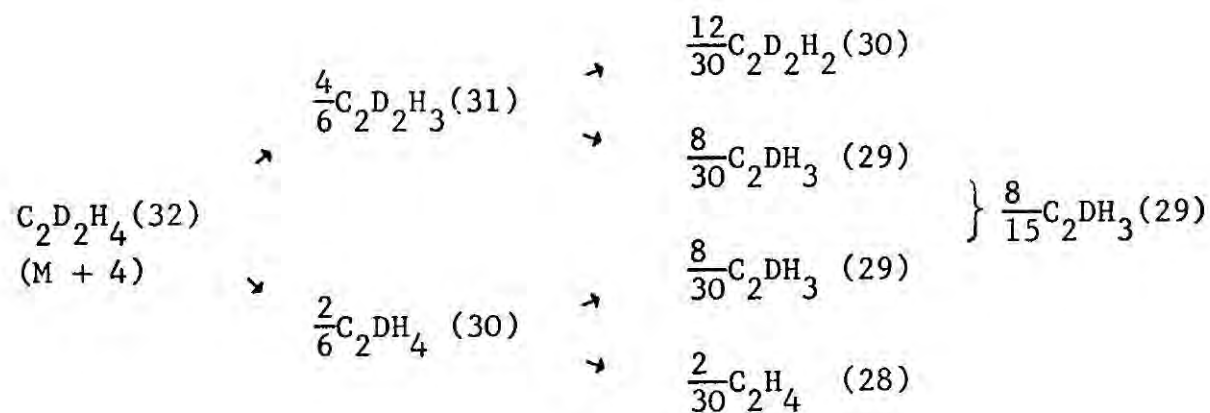
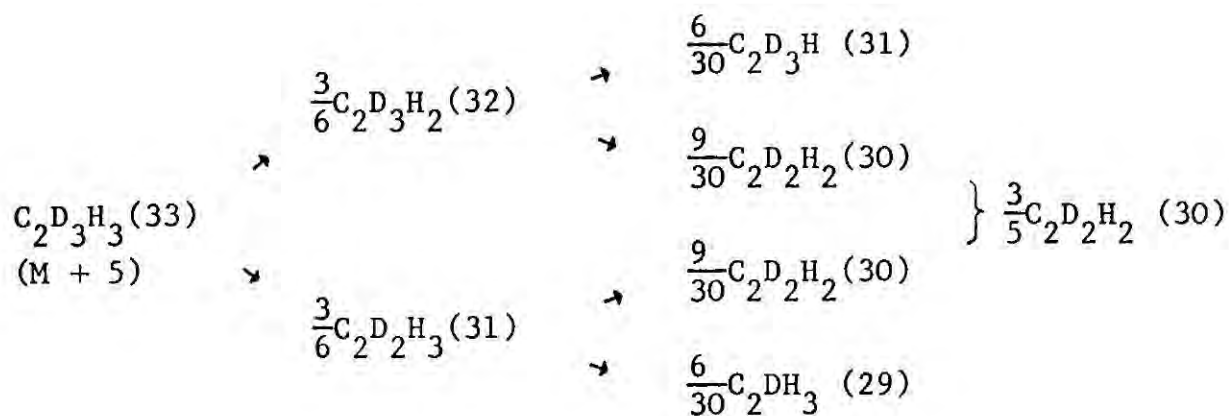
For standard conditions of Schlatter and Boudart (23 torr C_2H_4 , 152 torr H_2) assuming zero order in C_2H_4 and first order in H_2

$$N_t = 1.47 \times \frac{152}{50} = \underline{4.46 \text{ molecules/surface atom/sec.}}$$

In principle N_t can be calculated from knowledge of the mean particle size. Using the relation $\log A + \log r = 3.14$ for Pt²⁰⁶ where r is the crystallite radius (assumed spherical) in Å and A is

the surface area of metal in m^2/gm : For $r = 25\text{\AA}$, $A = 55 \text{ m}^2/\text{gm}$.

Assuming 1.12×10^{15} surface atoms/ cm^2 ,²⁰⁷ the above catalyst has 7.3×10^{15} surface atoms, giving a value for N_t approximately five times the above value, which would be inconsistent with the dispersion to be expected (50-70%). However, the quoted crystallite size (50\AA) was not determined as the statistical mean and the equation used to calculate the metal surface area is necessarily approximate so this value of N_t is somewhat unreliable.



Contributions to each peak in terms of each isomer are then:

peak height	Contributions:
1. 36 =	$(M + 8)$
2. 35 =	$(M + 7)$
3. 34 =	$(M + 6) + \frac{A}{6}(M + 7) + A(M + 8)$
4. 33 =	$(M + 5) + \frac{A}{3}(M + 6) + \frac{5A}{6}(M + 7)$
5. 32 =	$(M + 4) + \frac{A}{2}(M + 5) + \frac{2A}{3}(M + 6) + \frac{B}{15}(M + 6) + \frac{B}{3}(M + 7)$ $+ B(M + 8)$
6. 31 =	$(M + 3) + \frac{2A}{3}(M + 4) + \frac{A}{2}(M + 5) + \frac{B}{5}(M + 5) + \frac{8B}{15}(M + 6)$ $+ \frac{2B}{3}(M + 7)$
7. 30 =	$(M + 2) + \frac{5A}{6}(M + 3) + \frac{A}{3}(M + 4) + \frac{2B}{5}(M + 4) + \frac{3B}{5}(M + 5)$ $+ \frac{2B}{5}(M + 6)$
8. 29 =	$(M + 1) + \frac{A}{6}(M + 3) + \frac{2B}{3}(M + 3) + \frac{8B}{15}(M + 4) + \frac{B}{5}(M + 5)$
9. 28 =	$(M) + \frac{B}{3}(M + 3) + \frac{B}{15}(M + 4)$

Equations (1)-(7) are sufficient to solve for $(M + 8) \rightarrow (M + 2)$ and substituting these values in equations (8) and (9) allows the heights of the 28 and 29 peaks to be calculated.

The programme given below calculates the percentage of each isomer

$C_2D_nH_{6-n}$ ($n = 0-6$) of the total ethane fraction and compares the calculated heights of the 28 and 29 peaks with the measured values. A and B are taken from a standard ethane fragmentation pattern, remeasured following each experiment on deuterated samples.

```

DIMENSION H(36),E(36),EP(36),R(10)
10 READ (2,500)A,B
500 FORMAT (2F12.5)
   IF(A)20,70,20
20 READ (2,502)(H(I),I=28,36)
502 FORMAT (9F7.3)
   E(7)=H(36)
   E(6)=H(35)
   E(5)=H(34)-A*(E(6)/6.+E(7))
   E(4)=H(33)-A*(E(5)/3.+5*E(6)/6.)
   E(3)=H(32)-A*(E(4)/2.+2*E(5)/3.)-B*(E(5)/15.+E(6)/3.+E(7))
   E(2)=H(31)-A*(2*E(3)/3.+E(4)/2.)-B*(E(4)/5.+8*E(5)/15.+2*E(6)/3.)
   E(1)=H(30)-A*(5*E(2)/6.+E(3)/3.)-B*(2*E(3)/5.+3*E(4)/5.+2*E(5)/5.)
   R(1)=A*(E(1)+E(2)/6.)+B*(2*E(2)/3.+8*E(3)/15.+E(4)/5.)
   R(2)=B*(E(1)+E(2)/3.+E(3)/15.)
   SUM=0.
   DO 30 I=1,7
   SUM=SUM+E(I)
30 CONTINUE
   DO 40 I=1,7
   EP(I)=E(I)*100./SUM
40 CONTINUE
   DO 50 K=1,7
   I=K+29
   E(I)=E(K)
   EP(I)=EP(K)
50 CONTINUE
   WRITE(3,503)
503 = FORMAT(50X,'ETHANE DISTRIBUTIONS'////////)
   WRITE(3,504)
504 = FORMAT(4X,'MASS',7X,'PEAK HT.',5X,'PARENT',5X,'D.NUMBER',6X,
1'PERCENT')
   DO 60 I=1,7
   M=I+29
60 WRITE(3,505) M,H(M),E(I),EP(I)
505 = FORMAT(5X,I2,5X,2F12.5,17X,F12.5//)
   WRITE(3,506)
506 = FORMAT(8X,'PEAK HT.',10X,'RESIDUAL')
   WRITE(3,507) H(29),R(1)
507 = FORMAT(2(5X,F12.5))
   WRITE(3,507) H(28),R(2)
   GO TO 10
70 CALL EXIT
END

```

REFERENCES

1. K. Siegbahn, C. Nordling, A. Fahlman, R. Nordbert, K. Hamrin, J. Hedman, G. Johansson, T. Bergmark, S.E. Karlsson, J. Lidgren, and B. Lindberg, 'ESCA - atomic, molecular and solid state structure studied by means of electron spectroscopy'. Uppsala (1967).
2. K. Siegbahn, C. Nordling, G. Johansson, J. Hedman, P.F. Heden, K. Hamrin, U. Gelius, T. Bergmark, L.O. Werme, R. Manne and Y. Baer, 'ESCA applied to free molecules' North Holland, Amsterdam (1969).
3. D.W. Turner, C. Baker, A.D. Baker and C.R. Brundle, 'Molecular Photoelectron Spectroscopy' Wiley - Interscience (1970).
4. D.E. Eastman, 'Photoemission Spectroscopy of Metals', in 'Techniques in Metal Research VI', ed. E. Passaglia, Wiley-Interscience (1972).
5. T.W. Haas, G.J. Dooley, A.G. Jackson and M.P. Hooker, 'Progress in Surface Science', Vol 1(2), Pergamon (1971).
6. (a) H. Robinson and W.F. Rawlinson, *Phil. Mag.*, 28, 277 (1914).
(b) H. Robinson, *Proc. Roy. Soc. A*, 104, 455 (1923).
(c) H. Robinson, *Phil. Mag.*, 50, 241 (1925).
7. M. de Broglie, *Compt. Rend.*, 172, 274 (1921).
8. J.A. Van Akker and E.C. Watson, *Phys. Rev.*, 37, 1631 (1931).
9. M. Farence Jr., *Phys. Rev.*, 51, 720 (1937).
10. A. Bazin, *Zhurnal Eksperimental noi i Teoreticheskoi Fiziki*, 14, 23 (1944).
11. R.G. Steinhardt Jr., F.A.D. Granados and G.I. Post, *Anal. Chem.*, 27, 1046 (1955).
12. B.L. Henke, Tech. Report No. 6, Contract No. AF49 (638)-394, Air Force Office of Scientific Research (1962).

13. K. Siegbahn and K. Edvarrson, *Nucl. Phys.*, 1, 137 (1956).
14. A.M. Lindh, 'Handbuch der Experimentalphysik', Bd 24 Teil 4, ed. W. Wien and F. Harnes, Leipzig (1930).
15. H.W.B. Skinner and J.E. Johnston, *Proc. Roy. Soc. A*, 161, 420 (1937).
16. C. Nordling, E. Sokolowski and K. Siegbahn, *Arkiv. Fys*, 13, 483 (1958).
17. S. Hagstrom, C. Nordling and K. Siegbahn, *Phys. Lett.*, 9, 235 (1964).
18. C. Nordling, S. Hagstrom and K. Siegbahn, *Z. Physik*, 178, 433, 439 (1964).
19. C.R. Brundle, *Appl. Spectroscopy*, 25, 8 (1971).
20. M.I. Al-Joboury and D.W. Turner, *J. Chem. Soc.* 5154 (1963); 4434 (1965).
21. D.W. Turner, *Proc. Roy. Soc. (London)*, A307, 15 (1968).
22. (a) A.L. Hughes and V. Rojansky, *Phys. Rev.*, 34, 284 (1929).
(b) A.L. Hughes and H. McMillan, *ibid*, 34, 293 (1929).
23. J.D.H. Eland and C.J. Danby, *J. Sci. Instrum*, 1, 406 (1968).
24. F.W. Aston, *Phil. Mag.*, 38, 710 (1919).
25. H. Hafner, J.A. Simpson and C.E. Kuyatt, *Rev. Sci. Instrum.*, 39, 33 (1968).
26. G. Atelson, K. Hamrin, A. Fahlman, C. Nordling and B.J. Lindberg, *Spectrochim. Acta*, 23A, 2015 (1967).
27. E.M. Purcell, *Phys. Rev.*, 54, 818 (1938).
28. J.A. Simpson, *Rev. Sci. Instrum*, 35, 1968 (1964).

29. G.E. Lee-Whiting, 'Uniform Magnetic Fields', At. Energy Can., Ltd., Chalk River Report CRT-673, Chalk River, Ont. (1957).
30. D.M. Hercules, Anal. Chem., 42, 20 (1970).
31. J.C. Helmer and N.H. Weichert, Appl. Phys. Lett., 13, 266 (1968).
32. K. Siegbahn, D. Hammond, H. Fellner-Feldegg and E.F. Barnett, Science, 176, 245 (1972).
33. K. Siegbahn, Uppsala Univ. Inst. Phys. Report No. 793, presented at the Third International Conference on Atomic Physics, Univ. of Colorado, Boulder, Colorado, Aug. 1972.
34. D. Kilcast and D.T. Clark, personal communication.
35. A. Hammett and A.F. Orchard in 'Electronic Structure and Magnetism of Inorganic Compounds' Vol. 1, Chem. Soc. London (1972).
36. D.M. Hercules, Anal. Chem. 44, 106 (1972).
37. H. Basch, Chem. Phys. Lett, 5, 337 (1970).
38. W.E. Swartz, Jr., and D.M. Hercules, Anal. Chem. 43, 1066 (1971).
- 39a. K. Siegbahn and U. Gelius, Discuss. Farad., 54, (1972) (in press).
- 39b. D.T. Clark and D. Kilcast, J. Chem.Soc. (A), 1971, 3286.
R.E. Block, J. Magn. Resonance, 5, 155 (1971).
40. D.T. Clark, D. Briggs and D.B. Adams, J.C.S. (Dalton), 1973, 169
41. M. Barber, P. Swift, D. Cunningham and M.J. Frazer, Chem. Comm., 1970, 1338.
42. D. Buchanan, M. Robbins, H. Guggenheim, G.K. Wertheim and V.G. Lambrecht, Jr., Solid State Comm., 9, 583 (1971).
43. I. Adams, J.M. Thoms, G.M. Bancroft, K.D. Butler and M. Barber, Chem. Comm. 1972, 751.

44. A. Fahlman, R. Carlsson and K. Siegbahn, *Ark. Kemi*, 25, 301 (1966).
45. L. Hulet and T. Carlson, *Appl. Spectrosc.* 25, 33 (1971).
46. C.S. Fadley, S.B.M. Hagstrom, M.P. Klein and D.A. Shirley, *J. Chem. Phys.*, 48, 3779, (1968).
47. D.N. Hendrickson, J.M. Hollander and W.L. Jolly, *Inorg. Chem.*, 9, 612 (1970).
48. *ibid*, 8, 2642 (1969).
49. R. Nordberg, H. Brecht, R.G. Albridge, A. Fahlman, J.R. Van Wazer
Inorg. Chem., 9, 2469 (1970).
50. M. Pelain, D.N. Hendrickson, J.M. Hollander and W.L. Jolly,
J. Phys. Chem., 74, 1116 (1970).
51. W.J. Stec, W.E. Morgan, R.G. Albridge and J.R. Van Wazer,
Inorg. Chem., 11, 219 (1972).
52. W.E. Swartz Jr., and D.M. Hercules, *Anal. Chem.*, 1774 (1971).
53. M.V. Zeller and R.G. Hayes, *Chem. Phys. Lett*, 10, 610 (1971).
54. T.C. Carner, G.K. Sweitzer and T.A. Carlson, *J. Chem. Phys.*,
57, 973 (1972).
55. L. Kramer and M. Klein, *J. Chem. Phys.*, 51, 3620 (1969).
56. D.C. Frost, A. Ishitani and C.A. McDowell, *Mol. Phys.*, 24, 861
(1972).
57. C.K. Jorgenson, *Chimica*, 25, 213 (1971).
58. D.T. Clark, D.B. Adams and D. Briggs, *Chem. Comm.*, 1971, 602
59. W.E. Moddeman, J.R. Blackburn, G. Kumar, K.A. Morgan, R.G.
Albridge and M.M. Jones, *Inorg. Chem.*, 11, 1715 (1972).
60. G. Kumar, J.R. Blackburn, R.G. Albridge, W.E. Moddeman and
M.M. Jones, *ibid*, 11, 296 (1972).

61. W.M. Riggs, *Anal. Chem.*, 44, 830 (1972).
62. V.I.N. Nefedov, M.A. Porai-Kochito, I.A. Zakhorova, J.A. Kohomitov, and N.N. Kuzmina, *Isv. Akad. Nauk, S.S.S.R. Ser. Fiz*, 36, 381 (1972).
63. D. Leibfritz and W. Bremser, *Chem. Ztg., Chem. App.*, 94, 982 (1970).
64. G. Wertheim and A. Rosenewaig. *J. Chem. Phys.* 54, 3235 (1971).
65. M.F. Farona, J.G. Grasselli, H. Grossman and W.M. Ritchey, *Inorganica Chimica Acta*, 3, 495 (1969).
66. W.E. Morgan, W.J. Stec, R.G. Albridge and J.R. Van Wazer, *Inorg. Chem*, 10, 926 (1971).
67. J.R. Blackburn, R. Nordberg, F. Stevie, R.G. Albridge and M.M. Jones, *ibid*, 9, 2374 (1970).
68. D.T. Clark and D.B. Adams, *Chem. Comm.* 1971, 74.
69. M. Barber, T.A. Connor, I.H. Hillier and V.R. Saunders, *Chem. Comm.*, 1971, 682.
70. G.J. Leigh, J.N. Murrel, W. Bremser and W.G. Proctor, *Chem. Comm.*, 1970, 1661.
71. P. Finn and W.L. Jolly, *Inorg. Chem.*, 11, 1434 (1972).
72. W.E. Swartz. Jr., J.K. Ruff and D.M. Hercules, *J. Amer. Chem. Soc*, 94, 5227 (1972).
73. C.S. Fadley and D.A. Shirley, *Phys. Rev. A*, 2, 1109 (1970).
74. G.K. Wertheim, A. Rosenewaig, R.L. Cohen and H.J. Guggenheim, *Phys. Rev. Lett.*, 27, 505 (1971).
75. D.T. Clark and D.B. Adams, *Chem. Phys. Lett.* 10, 121 (1971).

76. D.C. Frost, C.A. McDowell and I.S. Woolsey, *Chem. Phys. Lett.*, 17, 320 (1972).
77. S. Kono, T. Ishii, T. Sagawa and T. Kobayasi, *Phys. Rev. Lett.*, 28, 1385 (1972).
78. K. Hamrin, G. Johansson, U. Gelius, C. Nordling and K. Siegbahn, *Phys. Lett.*, 29, 178 (1969).
79. R. Prins and T. Novakov, *Chem. Phys. Lett.*, 9, 593 (1971).
80. J.A. Connor, I.H. Hiller, V.R. Saunders and M. Barber, *Mol. Phys.*, 23, 81 (1972).
81. J.A. Connor, I.H. Hiller, V.R. Saunders, M.H. Wood and M. Barber, *ibid*, 497 (1972).
82. R.E. Davis, D.L. Rousseau and R.D. Board, *Science*, 171, 167 (1971).
83. J.P. Collman and J.W. Kang, *J. Amer. Chem. Soc.*, 89, 844 (1967).
84. (a) M.J.S. Dewar, *Bull. Soc. Chim. Fr.*, 18c, 79 (1951).
(b) J. Chatt and L.A. Duncanson, *J. Chem. Soc.*, 1953, 2939.
85. J.H. Nelson, K.S. Wheelock, L.C. Cusaks and H.B. Johanssen, *J. Amer. Chem. Soc.*, 91, 7005 (1969).
86. A.C. Blizzard and D.P. Santry, *ibid*, 90, 5749 (1968).
87. D.T. Clark and D. Briggs, *Nature Phys. Sci.*, 237, 15 (1972).
88. C.D. Cook, K.Y. Wan, U. Gelius, K. Hamrin, G. Johansson, E. Olsson, H. Siegbahn, C. Nordling and K. Siegbahn, *J. Amer. Chem. Soc.*, 93, 1904 (1971).
89. R. Mason, D.M.P. Mingos, G. Rucci and J.A. Connor, *J.C.S. Dalton*, 1972, 1729.
90. P.T. Cherg, C.D. Cook, S.C. Nyburg and K.Y. Wan, *Inorg. Chem.*, 10, 2210 (1971).
91. G. Bombieri, E. Forsellini, C. Panattoni, R. Graziana and E. Bandoli, *J. Chem. Soc. (A)*, 1970, 1313.

92. J.N. Francis, A. McAdam and J.A. Ibers, *J. organometal. Chem.*, 29, 131 (1971).
93. V. Albano, P.L. Bellon and V. Scatturin, *Chem. Comm.*, 1966, 507.
94. J.O. Granville, J.M. Stewart and S.O. Grim, *J. Organometal. Chem.*, 81, 18 (1959).
95. A.D. Walsh, *J. Chem. Soc.*, 1953, 2260.
96. C.D. Cook and K.Y. Wan, *J. Amer. Chem. Soc.*, 92, 2595 (1970).
97. K.S. Wheelock, J.H. Nelson, L.C. Cusacks and H.B. Johansen, *ibid*, 95, 5110 (1970).
98. E.O. Greaves, C.J.L. Lock and P.M. Maitlis, *Con. J. Chem.*, 46, 3879 (1968).
99. T.A. Carlson, M.O. Krause and W.E. Modderman, *J. Physique C*, 4, 76 (1971).
100. U. Gelius, C.J. Allan, D. Allison, H. Siegbahn and K. Siegbahn, *Chem. Phys. Lett.*, 11, 224 (1971).
101. G.K. Wertheim and A. Rossewaig, *Phys. Rev. Lett*, 26, 1179 (1971).
102. J.H. Thomas, I. Adams and M. Barber, *Solid State Comm.*, 9, 1571 (1971).
103. T. Novakov, *Phys. Rev. B*, 3, 2693 (1971).
104. T. Novakov and R. Prins, *Solid State Comm.*, 9, 1975 (1971).
105. J.E. Castle, *Nature Phys. Sci.*, 234, 93 (1971).
106. A. Rossewaig, G.K. Wertheim and H.J. Guggenheim, *Phys. Rev. Lett.*, 27, 479 (1971).
107. C.S. Fadley and D.A. Shirley, *Phys. Rev. A*, 2, 1109 (1970).
108. C.S. Fadley and D.A. Shirley, *Phys. Rev. Lett.*, 26, 1179 (1971).

109. M. Barber, J.A. Connor and I.H. Hiller, *Chem. Phys. Lett.*, 9, 570 (1971).
110. S. Pignataro, *Z. Naturforsch.*, 279, 816 (1972).
111. M. Barber, J.A. Connor, M.F. Guest, M.B. Hall, I.H. Hiller and W.N.E. Meredith, *Farad. Discuss.*, 54, (1972) (in press).
112. I. Ikemeto, J.M. Thomas and H. Kurōda, *ibid.*, (in press).
113. G.W. Parshall, *J. Amer. Chem. Soc.*, 86, 5367 (1964).
114. R.V. Lindsay Jr., G.W. Parshall and U.G. Stolberg, *ibid.*, 87, 658 (1965).
115. D.T. Clark and D. Kilcast, *J. Chem. Soc. (A)*, 1971, 3286.
116. C.W. Fryer and J.A.S. Smith, *J. Chem. Soc. (A)*, 1970, 1029.
117. C.W. Fryer, unpublished results.
118. C.W. Fryer, *Chem. Comm.*, 1970, 902.
119. C.H. Townes and B.P. Dailey, *J. Chem. Phys.*, 17, 782 (1949).
120. M. Kubo and D. Nakamura, *Adv. Inorg. Chem. Radiochem.*, 8, 257 (1966).
121. W. von. BronsWyk and R.S. Nyholm, *J. Chem. Soc. (A)*, 1968, 204.
122. Y.K. Syrkin, *Bull. Acadm. Sci., USSR, Classe Sci. chim.*, 1948, 69.
123. L.M. Venanzi, *Chem. Brit.*, 4, 162 (1968).
124. P.R.H. Alderman, P.G. Owston and J.M. Rowe, *Acta Cryst.*, 13, 149 (1960).
125. J.A.J. Jarvis, B.T. Kilbourn and P.G. Owston, *ibid.*, B27, 366 (1971).
126. R.H.B. Mais, P.G. Owston and A.M. Wood, *ibid.*, B28, 393 (1972).
127. A.F. Schreiner and T.B. Brill, *Theoret. chim. Acta*, 17, 323 (1970).
128. T.L. Brown, *Discuss. Farad. Soc.*, 47, 200 (1969).

129. T.L. Brown and T.P. Yesinowski, *Inorg. Chem.*, 10, 1097 (1971).
130. D. Nakamura and M. Kubo, *J. Phys. Chem.*, 68, 2986 (1964).
131. W.J. Bland and R.D.W. Kemmitt, *J. Chem. Soc. (A)*, 1968, 1278.
132. W.J. Bland, J. Burgess and R.D.W. Kemmitt, *J. Organometal. Chem.*, 14, 201 (1968).
133. W.J. Bland, J. Burgess and R.D.W. Kemmitt, *ibid*, 18, 199 (1969).
134. J.D. Jones, personal communication (1971).
135. W.J. Bland, J. Burgess and R.D.W. Kemmitt, *J. Organometal. Chem.*, 15, 217 (1968).
136. W.J. Bland and R.D.W. Kemmitt, *J. Chem. Soc. (A)*, 1969, 2062
137. (a) J.D. Jones, Ph.D. Thesis (U.C. London) p.46 (1971).
(b) J. Lewis, B.F.G. Johnson, K.A. Taylor and J.D. Jones, *J. Organometal. Chem.*, 32, c62 (1971).
138. R. Nordberg, R.G. Albridge, T. Bergmark, U. Ericson, J. Hedman, C. Nordling, K. Siegbahn and B.J. Lindberg, *Arkiv Kemi*, 28, 257 (1968).
139. M. Kilner and J.N. Pinkney, *J. Chem. Soc. (A)*, 1971, 2887.
140. K. Farmery, M. Kilner and C. Midcalf, *ibid*, 1970, 2279.
141. D.T. Clark and D. Kilcast, *Chem. Comm.*, 1971, 516.
142. H.R. Keable and M. Kilner, unpublished results.
143. M. Kilner and C. Midcalf, *Chem. Comm.*, 1970, 552.
144. M. Kilner and C. Midcalf, *J. Chem. Soc. (A)*, 1971, 292.
145. H.M.M. Shearer and J.D. Sowerby, personal communication.
146. R. Snaith, C. Summerford, K. Wade and B.K. Wyatt, *J. Chem. Soc. (A)*, 1970, 2635.
147. J.B. Farmer and K. Wade, personal communication.
148. T. Inglis and M. Kilner, unpublished results.

149. H.R. Keable and M. Kilner, J.C.S. Dalton, 1972, 153.
150. T.G. Hewitt and J.J. De Boer, J. Chem. Soc. (A), 1971, 817.
151. C. Panattoni, G. Bombieri, U. Belluco and W.H. Baddley,
J. Amer. Chem. Soc., 90, 798 (1968).
152. H.R. Keable and M. Kilner, J.C.S. Dalton, 1972, 1535.
153. P.W. Selwood, 'Adsorption and Collective Paramagnetism',
Academic Press, New York (1962).
154. G.C. Bond, 'Catalysis by Metals', Academic Press, London (1962).
155. G.C. Bond and P.B. Wells, Advan. Catalysis, 15, 91 (1964).
156. P.B. Wells in 'Surface and Defect Properties of Solids', ed J.M.
Thomas and M.W. Roberts, The Chemical Society, London, (1972).
157. B.A. Morrow and N. Sheppard, Proc. Roy. Soc. A. 311, 391 (1969).
158. T.A. Dorling, M.J. Eastlake and R.L. Moss, J. Catalysis, 14,
23 (1969).
159. T.A. Dorling, B.W.J. Lynch and R.L. Moss, J. Catalysis, 20, 190
(1971).
160. G.C. Bond, Trans. Farad. Soc., 52, 1235 (1956).
161. G.C. Bond, J.J. Phillipson, P.B. Wells and J.M. Winterbottom,
ibid, 60, 1847 (1964).
162. J.C. Schlatter and M. Boudart, J. Catalysis, 24, 482 (1972).
163. J.H. Sinfelt and P.J. Lucchesi, J. Amer. Chem. Soc., 85, 3365
(1963).
164. G.C.A. Shint and L.L. Van Reijen, Adv. Catalysis, 10, 242 (1958).
165. D. Cormack, S.J. Thomson and G. Webb, J. Catalysis, 5, 224 (1966).
166. G.F. Taylor, S.J. Thomson and G. Webb, ibid., 12, 191 (1968).
167. J.A. Altham and G. Webb, ibid., 18, 133 (1970).
168. A. Farkas, L. Farkas and E.K. Rideal, Proc. Roy. Soc. (London)
A146, 630 (1934).

169. G.H. Twiggs and E.K. Rideal, *ibid*, A171, 55 (1939).
170. G.K.T. Conn and E.M. Twigg, *ibid*, A171, 70 (1939).
171. J. Turkevich, F. Bonner, D. Schissler and P. Irsa, *Discuss. Farad. Soc.*, 8, 352 (1950).
172. J.N. Wilson, J.W. Otvos, D.P. Stevenson and C.D. Wagner, *Ind. Eng. Chem.*, 45, 1480 (1953).
173. G.C. Bond and J. Turkevich, *Trans. Farad. Soc.*, 49, 281 (1953).
174. C. Kemball, *J. Chem. Soc.*, 1956, 735.
175. C. Kemball, *Catalysis Rev.*, 5, 33 (1971).
176. M. Boudart, A. Aldag, J.E. Benson, N.A. Dougharty and C.G. Harkins, *J. Catalysis*, 6, 92 (1966).
177. L.H. Little, 'Infrared Spectra of Adsorbed Species', New York, Academic Press (1966).
178. M.L. Hair, 'Infrared Spectroscopy in surface Chemistry', ed. Arnold (London) and Marcel Dekker (New York), (1967).
179. N. Sheppard, N.R. Avery, M. Clark, B.A. Morrow, R. St.C. Smart, T. Takenaka and J.W. Ward in 'Molecular Spectroscopy', Institute of Petroleum, 1968, 97.
180. N. Sheppard, N.R. Avery, B.A. Morrow and R.P. Young, presented to the symposium on Chemisorption and Catalysis (Hydrocarbon Research Group, Institute of Petroleum), October 1970.
181. R.P. Eischens, S.A. Francis and W.A. Pliskin, *J. Chem. Phys.*, 22, 1786 (1954).
182. W.A. Pliskin and R.P. Eischens, *ibid*, 24, 482 (1956).
183. L.H. Little, N. Sheppard and D.J.C. Yates, *Proc. Roy. Soc.*, A259, 242 (1960).
184. J. Erkelens and Th.J. Liefkens, *J. Catalysis*, 8, 36 (1967).
185. B.A. Morrow and N. Sheppard, *J. Phys. Chem.*, 70, 2406 (1966).

186. B.A. Morrow and N. Sheppard, Proc. Roy. Soc., A311, 391 (1969).
187. W.A. Pliskin and R.P. Eischens, Z. Physik. Chem., 24, 11 (1960).
188. J. Chatt, L.A. Duncanson and B.L. Shaw, Proc. Chem. Soc., 1957, 343.
189. D.D. Eley, D.M. Moran and C.H. Rochester, Trans. Farad. Soc., 64, 2168 (1968).
190. N. Sheppard and J.W. Ward, J. Catalysis, 15, 50 (1969).
191. R.P. Eischens and W.A. Pliskin, Adv. Catalysis, 10, 1 (1958).
192. J.E. Benson and M. Boudart, J. Catalysis, 4, 704 (1965).
193. J. Horiuti and M. Polyani, Trans. Farad. Soc., 30, 1164 (1934).
194. C. Kemball, J. Chem. Soc., 1956, 735.
195. W.N. Delgass, T.R. Hughes and C.S. Fadley, Catalysis Rev., 4, 179 (1970).
196. C.R. Brundle in 'Surface and Defect Properties of Solids', ed. J.M. Thomas and M.W. Roberts, The Chemical Society (London), p.171(1972).
197. A. Wolberg, J.L. Ogilvie and J.F. Roth, J. Catalysis, 19, 86 (1970).
198. J.J. Carberry, G.C. Kuczynski, E. Martinez and A. Susu, Nature Phys. Sci., 235, 55 (1972).
199. D.A. Whan, M. Barber and P. Swift, Chem. Comm., 1972, 198.
200. K.S. Kim, N. Winograd and R.E. Davis, J. Amer. Chem. Soc., 93, 6296 (1971).
201. J.S. Brinen and A. Melera, J. Phys. Chem., 76, 2525 (1972).
202. G. Schon and S.T. Lundin, J. Electron Spectrosc., 1, 105 (1972).
203. T. Robert, M. Bartel and G. Offergeld, Surface Science, 33, 123 (1972).

204. D.O. Hayward and D.M.W. Trapnell, 'Chemisorption', Butterworths, London (1964).
205. P. Grandadam, Ann. Chim., 4, 83 (1935).
206. J.M. Basset, A. Theolier, M. Primet and M. Prettre, paper 65 in 'Proceedings of the Fifth International Congress on Catalysis', North Holland, Amsterdam (1972).
207. G.C. Bond, paper 67 presented to The Fourth International Congress on Catalysis, Moscow, 1968.
208. T.A. Dorling and R.L. Moss, J. Catalysis, 5, 111 (1966).

This is not the end
It is not even the beginning of the end
But it is, perhaps, the end of the beginning.

Winston Churchill.

